Interfacial phenomena in hard-rod fluids

Interfacial phenomena in hard-rod fluids

Grensvlak verschijnselen in suspensies van harde staafjes

(met een samenvatting in het Nederlands)

PROEFSCHRIFT

ter verkrijging van de graad van doctor aan de Universiteit Utrecht, op gezag van de Rector Magnificus, Prof. dr. W.H. Gispen, ingevolge het besluit van het College voor Promoties in het openbaar te verdedigen op maandag 24 Mei 2004 des namiddags te 16.15 uur

door

Kostyantyn Yevgenyevich Shundyak

geboren op 14 maart 1974,
te Odessa, Oekraine

Promotor: Prof. dr. M.H. Ernst

Copromotor: Dr. R.H.H.G. van Roij

Instituut voor Theoretische Fysica
Faculteit Natuur- en Sterrenkunde
Universiteit Utrecht

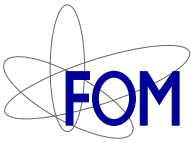

The work described in this thesis is part of the research program of the "Stichting voor Fundamenteel Onderzoek der Materie" (FOM), which is financially supported by the "Nederlandse Organisatie voor Wetenschappelijk Onderzoek" (NWO). It was carried out at the Institute of Theoretical Physics, Utrecht University.

ISBN 90-393-3716-0

Every man has been made by God
in order to acquire knowledge and contemplate

Pythagoras

This thesis is partially based on the following papers:

- K.Shundyak and R. van Roij, *Isotropic-nematic interfaces of hard-rod fluids*, J. Phys.: Condens. Matter **13**, 4789 (2001).
- K.Shundyak and R. van Roij, *Entropy-driven triple point wetting in hard-rod mixtures*, Phys. Rev. Lett. **88**, 205501 (2002).
- K. Shundyak and R. van Roij, *Free planar isotropic-nematic interfaces in binary hard-rod fluids*, Phys. Rev. E **68**, 061703 (2003).
- K. Shundyak and R. van Roij, *Restricted-orientation models of hard-rod fluids*, Proceedings of the International School of Physics "Enrico Fermi", 2003.
- K. Shundyak and R. van Roij, *Isotropic-nematic transition in hard-rod fluids: relation between continuous and restricted-orientation models*, Phys. Rev. E. **69**, 0417XX (2004).
- K. Shundyak and R. van Roij, *Ordering near a "soft" wall*, in preparation.
- K. Shundyak, R. van Roij and P. van der Schoot, *Phase behavior and interfacial properties of nonadditive hard-rod mixtures*, in preparation.

Contents

Chapter 1

Introduction

To explain all nature is too difficult a task for any one man or even for any one age. 'Tis much better to do a little with certainty, and leave the rest for others that come after you, than to explain all things.

Newton

1.1 Liquid crystals

One of the first classifications of nature that we learn is the concept of three basic states of matter: solid, with a definite volume and shape; liquid, with a definite volume, but with the shape of the containing vessel; and gaseous, with neither a definite shape nor volume. Despite the rough nature of such a classification, it reflects the fundamental symmetries, characterizing the structure of these states on the atomic level. The presence of short- and long-range atomic order is typical for crystals, the long-range disorder, combined with the short-range quasi-crystalline order, is common of liquids, and the quasi-uncorrelated structure characterizes gases. This idea of adopting symmetries to distinguish different states of matter is central in modern physics.

Specific symmetries can be associated not only with the positions of atoms or molecules, but also with orientations of magnetic moments in magnets, with charge of excitations in semiconductors, with properties of wave functions of electrons in superconductors etc. In this thesis we will consider some properties of materials in which the building blocks are anisotropic entities (of which an example is shown in Fig. 1.1). Hence, symmetries of their states are determined by the positions and orientations of the constituent particles. It turns out that in addition to common gas, liquid and crystal phases these materials exhibit a whole variety of orientationally and/or partially spatially ordered states, called mesophases (mesomorphic or mesogenic phases), or *liquid crystals*.

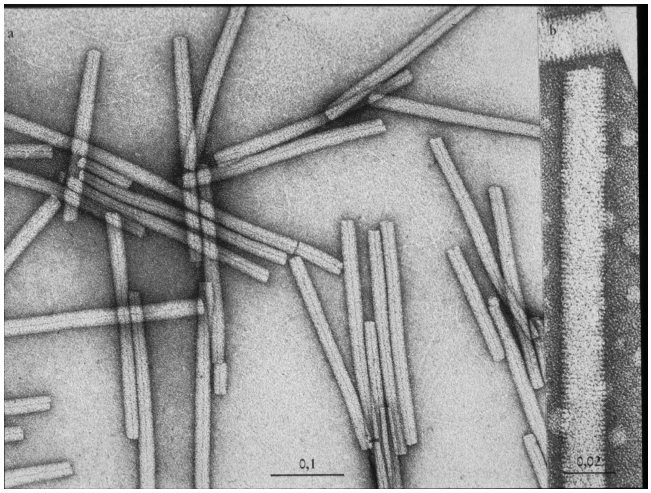

Figure 1.1: left) Electron micrograph picture of Tobacco Mosaic Virus (TMV), which is a rod 300 nm in length and 18 nm in diameter. It has a hollow core that shows up as a dark line because it is filled with the negative stain used in this EM picture. right) Magnified image of one TMV rod. TMV is composed of identical protein subunits arranged in a helical fashion [1].

Liquid crystals (LC's) occupy some intermediate position between the fully disordered liquid state and the completely ordered crystal state. The existence of a certain degree of crystalline order in mesophases might be demonstrated through X-ray diffraction experiments, whereas some of the liquid-like disorder is evident from its flow properties. One can roughly estimate the amount of order in a liquid crystalline state through the value of the latent heat ΔQ released at the phase transition. For many common mesophases it is on the order of $\Delta Q \sim 200 - 300$ J/g at the solid-liquid crystal transition, which is similar to the release at the transition from solid to isotropic liquid. This indicates that most of the crystalline order is lost when it transforms to a mesophase. Note that the latent heat release in a liquid crystal to isotropic liquid transition is typically much smaller (~ 5 J/g). This suggests that in order to understand the physical properties of the mesomorphic phases we need to explore extensions of the theory of liquids.

The anisotropy of the particles of a liquid crystalline material can be present either in their shape such that one axis is very different from the other two or, in some cases, different parts of the molecules can have very different solubility properties. Several classifications of mesogenic materials were put forward. From the molecular structure they can be divided into the calamitic LCs, which consist of rod-like molecules, the discotic LCs, derived from the disc-like species, and intermediate polycatenar LCs, which occurs in materials of lath-like molecules. In general, in order to produce interactions that favor alignment, the mesogenic molecules need to be fairly rigid for

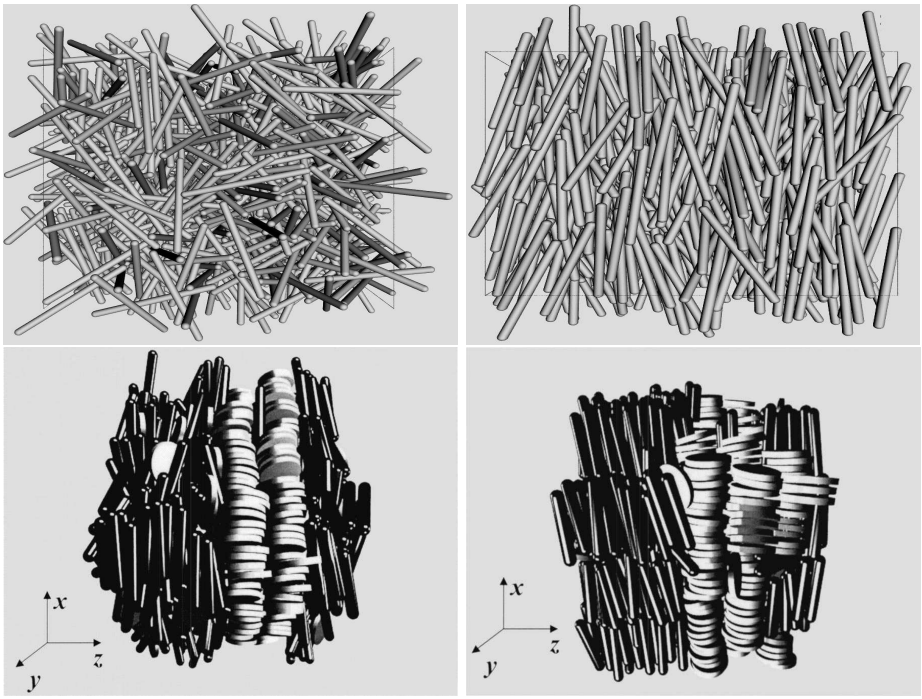

Figure 1.2: $\left(\frac{a|b}{c|d}\right)$ Several liquid crystalline phases observed in computer simulations of monodisperse hard-rod fluids or mixtures of hard rods and plates. Illustrations represent an isotropic phase (a) and uniaxial nematic phase (b) (courtesy of S. Savenko), biaxial nematic phase in contact with columnar phase (c) and smectic phase S_A in contact with columnar phase (d) [2].

at least some portion of the length. Another classification is based on the way the transitions to the mesophases are brought about. Liquid crystals obtained by thermal driving are called thermotropics, whereas those obtained by the influence of solvents are known as lyotropics, although there are materials which form thermotropic as well as lyotropic mesophases. Every member in these classifications is represented by a vast number of substances, and only symmetry properties characterize differences between various liquid crystalline states. We describe several common mesophases, formed in suspensions of rod-like colloidal particles, the main subject of this thesis. For the full classification the interested reader is referred to the literature [3–6].

The symmetries of the mesophases can be classified in terms of orientational and translational degrees of freedom. Following the nomenclature as proposed originally by Friedel [7], the liquid crystals of non-chiral calamitic molecules can be generally divided into two types: nematics and smectics. The nematic phase is the simplest liquid crystal phase, in which the molecules maintain a preferred orientational direc-

tion as they diffuse throughout the sample, but no long-range positional order exists. Several nematic phases can be distinguished, and Fig. 1.2 shows some examples from computer simulations (courtesy of S. Savenko and from Ref. [2]). Whereas an isotropic liquid possesses full translational and orientational symmetry $T(3) \times O(3)$ (Fig. 1.2(a)), at the isotropic liquid-nematic (IN) transition the rotational symmetry is broken. In the simplest case the group $O(3)$ is replaced by one of the uniaxial symmetry groups D_∞ or $D_{\infty h}$, and the resulting phase is called the uniaxial nematic phase N_u (Fig. 1.2(b)). The average orientation of the molecules can be represented by a unit vector $\hat{n}$ called a *director*. Another nematic phase, which is referred to as biaxial, N_b, may appear upon further breaking of the rotational symmetry of the system around the director $\hat{n}$. In this phase different symmetry groups, namely orthorhombic, triclinic, hexagonal or cubic, which are subgroups of $O(3)$, are in principle allowed. Fig. 1.2(c) illustrates the biaxial nematic phase existing in a mixture of calamitic and discotic molecules. In this phase the free rotation around a certain direction is possible for one component but strongly hindered for the other. All known biaxial nematics are either mixtures of rod-like and plate-like molecules or systems of lath-like particles [8, 9].

When the crystalline translational order is lost in two of the three dimensions, one obtains essentially stacks of two-dimensional liquids: such systems are called smectics. The smectic liquid crystals have layered structures, with a well-defined interlayer spacing which can be measured by means of X-ray diffraction. In most smectics the molecules are mobile within the layers and can rotate about their long axis. Since the interlayer interactions are weak compared to the lateral forces between the molecules, the layers can easily slide over one another. This gives rise to a fluid-like behavior with a higher viscosity than in nematics. A smectic can be identified by its periodicity in one spatial direction and by its point group symmetry. A priori no point group is forbidden, which results in an infinite number of allowed smectic phases. One of the simplest is the smectic-A (S_A) phase, with symmetry $T(2) \times D_{\infty h}$, demonstrated in Fig. 1.2(d). In this phase the average molecular axis is normal to the smectic layers. In both figures 1.2(c,d) the aforementioned phases are shown in contact with the so-called columnar phase which occurs in discotic materials and is characterized by the symmetry group $D_{6h} \times T(1)$. There are many more different liquid crystal phases which are not described here. The interested reader is referred to the literature [3–6].

1.2 Interactions

So far, we have been concentrating on the microscopic and macroscopic structure of the various mesogenic materials. However, the interparticle interactions determine the stability of a liquid-crystalline phase against destructive thermal fluctuations. One might speculate that attractive forces are required in order to maintain a long-range orientational ordering as observed in nematic and smectic LC's. However, it turns out that properties of some mesogenic substances can be understood on the basis of purely

repulsive interactions. The aforementioned suspensions of colloidal rod-like particles represent an example of such systems. Their experimental studies were pioneered by Bawden who was first to observe the isotropic-nematic transition in a suspension of the tobacco mosaic virus (TMV, see Fig. 1.1) in 1936 [10]. The experimental studies were complemented by Onsager [11], who, on the basis of a model fluid of hard needles, was able to explain the isotropic-nematic (IN) transition in terms of competition between orientational and packing entropies, i.e. by a purely *entropic* argument. In the 1980's computer simulations, and later theory and experiments (again on TMV solutions), showed that the mere presence of short-ranged repulsive interactions between rod-like particles can also be responsible for the formation of the smectic phase. One may point out a similar situation in simple fluids, where the structure to a large extent is determined by purely repulsive interactions [12]. Although in the low molecular weight liquid crystals the situation is much more difficult due to the complexity of the molecular structure and interactions, studies of hard-rod fluids represent a unique possibility to quantify the role of repulsive interactions in establishing liquid-crystalline order.

In many practical situations the thermodynamic state of the system is determined not only by the bulk thermodynamic variables, but also by the imposed boundary conditions. The corresponding interfacial problems have then to be considered. This thesis contributes to the understanding of interfacial phenomena in hard-rod fluids.

1.3 Interfaces

Several major interfacial effects can be distinguished in mesogenic materials [13]. The interaction of liquid crystal molecules with a substrate or interface leads to the formation of a boundary layer of thickness ξ with an ordering different from the bulk. When the system is far from any bulk phase transition, ξ is of order of a few molecular lengths. However, upon approach to the transition point such a layer can transform into a thick wetting film of another (yet metastable) bulk phase. Similar to wetting phenomena in other systems, complete or partial wetting can be distinguished upon approach to coexistence, and critical or first-order wetting transitions at coexistence [14]. The interplay between surface and bulk ordering also leads to another surface effect specific for liquid-crystalline materials. In many cases, close to the interface the mesogenic molecules take a fixed mean orientation which is called the anchoring direction of the liquid crystal at the interface. For orientationally ordered bulk phases (in absence of any other ordering field) the orientation of the bulk director becomes fixed by this preferred direction at the interface. This phenomenon is called anchoring.

Since an interface reduces the translational symmetry group of the bulk mesophase, the parameters that characterize the liquid-crystalline order start to depend on the spatial coordinates. This complicates the theoretical studies significantly. Similar to problems of the liquid-crystalline ordering in bulk, the interfacial phenomena can be described by purely phenomenological models of Landau-de Gennes type [3] or through the specifications of microscopic interactions and the construction of appro-

priate molecular models. Phenomenological theories treat an interface as a specific boundary condition, characterized by its own symmetry properties. But the coupling between orientational and translational degrees of freedom in the interfacial region requires specification of many material constants, which makes the classification of various phenomena rather complex. These theories allow one to reproduce the general structures of the surface phase diagrams and can be considered as a standard tool in physics of molecular liquid crystals, where experimental resolution is not enough to address molecular details. However, recent progress in experimental techniques and simulations, aimed at characterizing surfaces on the nanoscale, certainly motivates the development of molecular theories. Microscopic models are also frequently used in studies of interfaces in colloidal liquid crystals, where the microscopic structure can be probed by various means. And, similar to bulk ordering, it is highly desirable to quantify the role of various interactions in interfacial phenomena separately. Studies of interfaces in fluids of hard rods represent such a possibility for repulsive interactions.

1.4 Summary

This thesis addresses questions of interfacial ordering in hard-rod fluids at coexistence of the isotropic and nematic phases and in their contact with simple model substrates. It is organized as follows.

Chapter 2 provides some background information about the relation between the statistical mechanical and thermodynamical level of descriptions of bulk hard-rod fluids, as well as introduces the asymptotically exact Onsager model, and some basic facts of interfacial thermodynamics.

Chapter 3 represents studies of the simplest free IN interface in a fluid of monodisperse Onsager hard rods. For the analysis of this system we develop an efficient perturbative method to determine the (biaxial) one-particle distribution function in inhomogeneous systems.

Studies of the free planar isotropic-nematic interfaces are continued in Chapter 4, where they are considered in binary mixtures of hard rods. For sufficiently different particle shapes the bulk phase diagrams of these mixtures exhibit a triple point, where an isotropic (I) phase coexists with two nematic phases (N_1 and N_2) of different composition. For all explored mixtures we find that upon approach of the triple point the IN_2 interface shows complete wetting by an intervening N_1 film. We compute the surface tension of isotropic-nematic interfaces, and find a remarkable increase with fractionation.

These studies are complemented by an analysis of bulk phase behavior and interfacial properties of nonadditive binary mixtures of thin and thick hard rods in Chapter 5. The formulation of this model was motivated by recent experiments in the group of Fraden, who explored the phase behavior of a mixture of viruses with different effective diameters. In our model, species of the same types are considered as interacting with the hard-core repulsive potential, whereas the excluded volume

for dissimilar rods is taken to be larger (smaller) then for the pure hard rods. Such a nonadditivity enhances (reduces) fractionation at the isotropic-nematic (IN) coexistence and may induce (suppress) a demixing of the high-density nematic phase into two nematic phases of different composition (N_1 and N_2). Studies of their interfaces show an increase of the surface tension with fractionation at the IN interface, and complete wetting of the IN_2 interface by the N_1 phase upon approach of the triple point coexistence. In all explored cases bulk and interfacial properties of the nonadditive mixtures exhibit a surprising similarity with the properties of additive mixtures of larger diameter ratio.

In Chapter 6 we consider properties of a monodisperse hard-rod fluid in contact with the single wall (W). Studies of surface properties of a fluid of Onsager hard rods represent significant numerical difficulties, therefore we consider a simpler model fluid of hard rods with a restricted number of allowed orientations. Within this model, known as the Zwanzig model, we explore the thermodynamic properties of a fluid of monodisperse hard rods in contact with a model substrate represented by a hard wall with a short-ranged attractive or repulsive "tail". The attraction enhances the orientational ordering near the wall in both isotropic and nematic phases, and shifts the transition from uniaxial (U) to biaxial (B) symmetry in the isotropic surface layer to lower chemical potentials, whereas the wetting properties of the substrate remain similar to those of the pure hard wall. The soft repulsion reduces the density in the surface layer, which leads to the shift (or even suppression) of the UB transition, and strong modification of wetting properties. At the WI interface one always finds the wetting transition at sufficiently large repulsion, whereas a drying transition at the WN interface is observed only for sufficiently long-ranged potentials.

In Chapter 7 we explore some limitations of models of hard-rod fluids with a finite number of allowed orientations. Within Onsager's second virial theory we construct their bulk phase diagrams. For a one-component fluid, we show that the discretization of the orientations leads to the existence of an artificial (almost) perfectly aligned nematic phase, which coexists with the (physical) nematic phase if the number of orientations is sufficiently large, or with the isotropic phase if the number of orientations is small. Its appearance correlates with the accuracy of the sampling of the nematic orientation distribution within its typical opening angle. For a binary mixture this artificial phase also exists, and a much larger number of orientations is required to shift it to such high densities that it does not interfere with the physical part of the phase diagram.

Chapter 2

Theoretical background

Everything should be made as simple as possible, but not simpler.

A.Einstein

In this Chapter we briefly discuss the foundation on which the theoretical description of the bulk and surface phase behavior of hard rod fluids is based. Section 2.1 describes the standard connections between statistical mechanics and thermodynamics and recalls relevant thermodynamic relations. Section 2.2 focuses on the form of the grand potential of the fluid within a low-density virial expansion. Section 2.3 briefly introduces the formalism of density functional theory and generalizes the second virial approximation of the grand potential to inhomogeneous and anisotropic systems. Section 2.4 describes the bulk phase behavior of a fluid of monodisperse hard rods and discusses the validity of the second virial approximation. Finally, Section 2.5 of this Chapter is concerned with important basic concepts of surface thermodynamics.

2.1 Statistical mechanics

Statistical mechanics provides a systematic link between the macroscopic level of phenomenological thermodynamics, where the system in equilibrium is fully characterized by a small number of experimentally controlled state variables, and a microscopic level of description, which requires specification of coordinates and momenta of all particles at any instant of time. Here we simply collect several facts from standard courses on statistical mechanics [15, 16] in order to make a self-contained presentation.

Consider an isolated system of N identical classical *rod-like* particles in a three-dimensional volume V. Since each particle i has three translational and three orientational degrees of freedom $q_i = \{r_i, \hat{\omega}_i\}$, the microscopic state of the system is fully characterized by the $6N$ generalized coordinates $q^N = \{q_1, \ldots, q_N\}$, and the $6N$ conjugate generalized momenta $p^N = \{p_1, \ldots, p_N\}$ of the particles. The values of

these variables define a phase point $\Gamma \equiv (q^N, p^N)$ in a $12N$-dimensional phase space. The Hamiltonian $H(\Gamma)$ of the system can be written as

$$H(\Gamma) = \sum_{i=1}^{N} K_i(p_i) + \Phi(q^N), \tag{2.1}$$

where $K_i(p_i)$ denotes the kinetic energy of particle i, which includes contributions of translational and rotational degrees of freedom, and $\Phi(q^N)$ is the potential energy of the system. The time evolution of the phase point Γ is governed by the Hamilton equations

$$\dot{q_i} = \frac{\partial H}{\partial p_i}, \tag{2.2}$$

$$\dot{p_i} = -\frac{\partial H}{\partial q_i}, \tag{2.3}$$

together with $12N$ initial conditions.

The statistical description is based on the definition of an ergodic ensemble of macroscopically identical systems that only differ by their position in phase space. At a given time t the ensemble is characterized by a set of phase points distributed with a probability density $f(\Gamma, t)$, such that $f(\Gamma, t)d\Gamma$ is the probability to find the system in the infinitesimal volume element $d\Gamma = dq^N dp^N$ around Γ.

The equilibrium properties of a closed ergodic system with fixed energy E, volume V, and number of particles N can be described through the *microcanonical* ensemble, which is characterised by the phase space distribution

$$f_m(\Gamma) = \frac{\delta(E - H(\Gamma))}{\int d\Gamma \delta(E - H(\Gamma))}, \tag{2.4}$$

where δ is the Dirac delta function. The connection with thermodynamics is established through the Boltzmann relation

$$S(E, V, N) = k_B \ln \frac{\int d\Gamma \Theta\left(E - H(\Gamma)\right)}{N! h^{6N}}, \tag{2.5}$$

where k_B is the Boltzmann constant, h is Planck's constant, $\Theta(x)$ is the Heaviside function, and the factor $N!$ ensures extensivity of the entropy S. The inverse temperature of the microcanonical ensemble (E, V, N) can be identified as

$$\beta(E, V, N) = \left(\frac{\partial \ln \left[\int d\Gamma \Theta\left(E - H(\Gamma)\right) \right]}{\partial E} \right)_{N,V} = \frac{1}{k_B T}, \tag{2.6}$$

with T the temperature.

However, in many practical situations it is certainly more convenient to consider an ensemble with fixed temperature T instead of energy E. Transformation to the

new variables (N, V, T) defines the set of systems in contact with a heat bath at temperature T, which is called the *canonical* ensemble. The canonical probability distribution of a system of volume V, number of particles N, at temperature T can be written as

$$f_c(\Gamma) = \frac{\exp[-\beta H(\Gamma)]}{N! h^{6N} Z(N, V, T)}, \tag{2.7}$$

with the canonical partition function

$$Z(N, V, T) = \frac{1}{N! h^{6N}} \int d\Gamma \exp[-\beta H(\Gamma)]. \tag{2.8}$$

The link with thermodynamics can be established through the definition of the Helmholtz free energy

$$F(N, V, T) \equiv -k_B T \ln Z(N, V, T) = E - TS. \tag{2.9}$$

The function $F(N, V, T)$ generates the full thermodynamics of a system with fixed (N, V, T), just like $S(E, V, N)$ does for a system with fixed (E, V, N). Specifically we have for the internal energy

$$E = \int d\Gamma f_c(\Gamma) H(\Gamma) = -\frac{\partial \ln Z(N, V, T)}{\partial \beta} = \frac{\partial \beta F(N, V, T)}{\partial \beta}, \tag{2.10}$$

and for the pressure and chemical potential, respectively,

$$p = -\left(\frac{\partial F}{\partial V}\right)_{N,T}, \qquad \mu = \left(\frac{\partial F}{\partial N}\right)_{V,T}. \tag{2.11}$$

The kinetic energy contribution can be factorized from $Z(N, V, T)$. The integral over the conjugate momenta p^N can be carried out analytically, and the partition function can be represented as

$$Z(N, V, T) = \frac{Q(N, V, T)}{N! \nu^N}, \tag{2.12}$$

where the configurational integral is defined as

$$Q(N, V, T) = \int dq^N \exp[-\beta \Phi(q^N)], \tag{2.13}$$

and the thermal volume of a particle

$$\nu = \Lambda^3 \times \frac{h^3}{((2\pi k_B T)^3 I_1 I_2 I_3)^{1/2}}, \tag{2.14}$$

depends on the thermal (De Broglie) wavelength $\Lambda = h/(2\pi m k_B T)^{1/2}$ and the principal moments of inertia I_1, I_2, I_3 . The calculation of the configurational integral

$Q(N,V,T)$ is difficult and can only be performed by making approximations, or by resorting to computer simulations.

Although many physical systems can be characterised by fixed (N,V,T), and therefore by the canonical ensemble, in some cases the number of particles N can fluctuate because of permeability of walls or surfaces of the system. The ensemble of systems that can exchange energy and particles with their environment is called the *grand canonical* ensemble. It is characterized by the grand canonical probability distribution of a system of volume V, at temperature T with chemical potential μ, and can be written as

$$f_g(\Gamma,N) = \frac{1}{N!h^{6N}\Xi(\mu,V,T)} \exp[-\beta H(\Gamma) + \beta\mu N] \tag{2.15}$$

with the so-called grand canonical partition function

$$\begin{aligned}\Xi(\mu,V,T) &= \sum_{N=0}^{\infty} \frac{\exp[\beta\mu N]}{N!h^{6N}} \int d\Gamma \exp[-\beta H(\Gamma)] \\ &= \sum_{N=0}^{\infty} \exp[\beta\mu N] Z(N,V,T).\end{aligned} \tag{2.16}$$

The grand canonical ensemble can be regarded as a linear combination of canonical ensembles with different numbers of particles. Similarly one can regard the canonical ensemble as a linear combination of microcanonical ensembles with different energies.

The corresponding thermodynamic potential is the grand potential defined as

$$\Omega(\mu,V,T) \equiv -k_B T \ln \Xi(\mu,V,T), \tag{2.17}$$

and the average number of particles in the system is given by

$$\langle N \rangle = -\frac{\partial \beta\Omega(\mu,V,T)}{\partial \beta\mu}. \tag{2.18}$$

All these expressions can be readily generalized to the case of mixtures of several species α by substitution $N \to N_\alpha$, $\mu \to \mu_\alpha$ and proper summations over α.

2.2 Virial expansion

Assume that no external forces act on the particles in the system (except for the forces due to the walls that confine the particles in a volume V) and that the interactions are pairwise additive, thus

$$\Phi_N(q^N) = \sum_{i<j}^{N} \phi(q_i, q_j). \tag{2.19}$$

The grand partition function of a gas of rod-like particles in a volume V at temperature T and chemical potential μ (or fixed fugacity $z = \exp[\beta\mu]/\nu$) takes the form

$$\Xi(\mu, V, T) = \sum_{N=0}^{\infty} \frac{\exp[\beta\mu N]}{N!\nu^N} \int dq^N \exp[-\beta \sum_{i<j}^{N} \phi(q_i, q_j)]$$
$$= \sum_{N=0}^{\infty} \frac{z^N}{N!} Q(N, V, T) = 1 + zQ(1, V, T) + \frac{1}{2}Q(2, V, T)z^2 + \ldots, \tag{2.20}$$

where the configurational integral $Q(N, V, T)$ was defined in Eq.(2.13). Using a Taylor expansion in terms of z, we write the grand potential as

$$\beta\Omega(\mu, V, T) = -\mathcal{A}\left(z + \frac{z^2}{2}\left(Q(2, V, T) - Q^2(1, V, T)\right) + \ldots\right) \tag{2.21}$$

with $\mathcal{A} = 4\pi V$ (or $8\pi^2 V$) the one-particle configurational volume of a uniaxial (or biaxial) particle, respectively. Since in the isotropic phase the density of particles in unit volume with orientation $\hat{\omega}$ (uniform one-particle distribution function) can be determined as

$$\rho = \frac{\langle N \rangle}{\mathcal{A}} = \beta \frac{z}{\mathcal{A}} \frac{\partial \Omega}{\partial z}, \tag{2.22}$$

the grand potential functional can be written in the form of an expansion in powers of the density

$$\beta\Omega(\mu, V, T) = -\mathcal{A}(\rho + \frac{\rho^2}{2}(Q(2, V, T) - Q^2(1, V, T)) + \ldots, \tag{2.23}$$

which is known as the *virial expansion*. Since we keep in the expansion density terms up to second order, it is commonly referred as a *second virial approximation*. It turns out to be convenient to single out the ideal gas contribution $Q(N, V, T) = \mathcal{A}^N$. Since $\beta\Omega_{id}(\mu, V, T) = \mathcal{A}\rho(\ln[\rho\nu] - 1 - \beta\mu)$, it yields

$$\beta\Omega(\mu, V, T) = \mathcal{A}\rho(\ln[\rho\nu] - 1 - \beta\mu) - \frac{\rho^2}{2} \int dq_1 dq_2 f_M(q_1, q_2) + \mathcal{O}(\rho^3), \tag{2.24}$$

where we used translational invariance of the pair interaction, ignored surface effects and introduced the Mayer function

$$f_M(q_i, q_j) = \exp[-\beta\phi(q_i, q_j)] - 1. \tag{2.25}$$

We have now expressed the lowest-order correction to the ideal-gas pressure in terms of the pair interaction $f_M(q_1, q_2)$. The coefficient

$$B_2 = -\frac{1}{2\mathcal{A}} \int dq_1 dq_2 f_M(q_1, q_2) \tag{2.26}$$

is commonly called the second virial coefficient. For further details we refer the reader to the existing literature. For the hard-core pair potential

$$f_M(q_i, q_j) = \begin{cases} -1 & \text{if overlap} \\ 0 & \text{otherwise,} \end{cases} \tag{2.27}$$

and the virial contribution is independent of temperature. The only nontrivial temperature dependence in Ω comes from the thermal volume ν of the particle. However, it is irrelevant for the phase behavior, determined by the minimum of the grand potential. Since $\beta\Omega = \beta E - S/k_B - \beta\mu N$ and the average internal energy can be calculated with Eq. (2.10) as $\beta E = \beta(\partial\beta\Omega/\partial\beta)_{\mu,V} = 3\mathcal{A}\rho$, the minimum of $\beta\Omega$ corresponds to a maximum entropy for a given μ, V and T. As the temperature dependence of ν is irrelevant anyway, one can choose ν to be an arbitrary (but convenient) volume, for instance $\nu = L^2 D$ for rods of length L and diameter D.

2.3 Density functional theory

The virial expansion as written in Eq.(2.24) is valid only in a homogeneous isotropic phase, where all possible orientations and positions are equally probable for any particle. A theoretical framework that is capable of describing inhomogeneous and anisotropic phases is density functional theory. Here we give only a brief account of the most important ingredients of this framework, and refer the interested reader to the existing literature [17]. A key element of the theory is the proof of the existence of a functional $\Omega[\rho]$ of the one-particle distribution $\rho(q)$, with the properties that

1. $\Omega[\rho]$ is unique for a given pair-potential ϕ.
2. $\Omega[\rho]$ is a function of the volume V, temperature T and chemical potential μ.
3. $\Omega[\rho_{eq}] \leq \Omega[\rho]$, where ρ_{eq} is the equilibrium one-particle distribution for given μ, V, T.
4. $\Omega[\rho_{eq}] = \Omega_{eq}(\mu, V, T)$, where $\Omega_{eq}(\mu, V, T)$ is the equilibrium grand potential of the system.

It follows from these properties that for a given type of particles the full thermodynamics can be obtained by means of a variational principle. The main problem is that density functional theory only proves the existence of a unique and exact functional $\Omega[\rho]$, but provides no explicit recipe for constructing it. Therefore, approximations are inevitable.

The direct generalization of the grand potential of Eq. (2.24) can be written as

$$\begin{aligned} \beta\Omega[\rho(q)] &= \int dq\rho(q)\left(\ln(\rho(q)\nu) - 1 - \beta\mu\right) \\ &\quad -\frac{1}{2}\int dq_1 dq_2 f_M(q_1, q_2)\rho(q_1)\rho(q_2) + \mathcal{O}(\rho^3). \end{aligned} \tag{2.28}$$

The present second virial approximation is equivalent to setting the direct correlation function $c^{(2)}(q_1, q_2) = -\delta^2(\beta\Omega[\rho(q)] - \beta\Omega_{id}[\rho(q)])/\delta\rho(q_1)\delta\rho(q_2)$ equal to the Mayer function [18], and its range of validity is limited usually to the low-density regime. It was shown by Onsager, however, that this approximation becomes exact for bulk isotropic and nematic phases of rods of length L and diameter D in the limit $L/D \to \infty$. For this reason one expects the functional of Eq. (2.28) to be accurate, at least qualitatively correct, for inhomogeneous fluids of long hard rods.

2.4 Onsager model

Onsager modelled a TMV suspension as a fluid of long spherocylinders of length L and diameter D with the aspect ratio $L/D \to \infty$ [11]. Since the bulk one-particle distribution function is translationally invariant, i.e. $\rho(r, \hat{\omega}) = \rho(\hat{\omega})$, one can rewrite the grand potential as

$$\begin{aligned} \frac{\beta\Omega[\rho(\hat{\omega})]}{V} &= \int d\hat{\omega}\rho(\hat{\omega})\left(\ln(\rho(\hat{\omega})\nu) - 1 - \beta\mu\right) \\ &\quad + \frac{1}{2}\int d\hat{\omega}_1 d\hat{\omega}_2 E(\hat{\omega}_1, \hat{\omega}_2)\rho(\hat{\omega}_1)\rho(\hat{\omega}_2), \end{aligned} \tag{2.29}$$

where

$$E(\hat{\omega}_1, \hat{\omega}_2) = -\frac{1}{V}\int dr_1 dr_2 f_M(q_1, q_2) \tag{2.30}$$

is the (excluded) volume which is denied to particle 2 by the presence of particle 1, and v.v. It can be expressed analytically as

$$E(\hat{\omega}_1, \hat{\omega}_2) = 2L^2 D|\sin\varphi(\hat{\omega}_1, \hat{\omega}_2)| + 2\pi D^2 L + 4\pi D^3/3, \tag{2.31}$$

as a function of the angle $\varphi(\hat{\omega}_1, \hat{\omega}_2) = \arccos(\hat{\omega}_1 \cdot \hat{\omega}_2)$ between the cylinders [11]. The last two terms represent end corrections which can be neglected in the limit $L/D \to \infty$. Onsager also argued the second virial approximation in Eq. (2.29) to be exact in this limit through an estimate of the scaling behavior of the third virial coefficient in the isotropic phase, which describes simultaneous overlap of three rods. More recently, his results were confirmed by a combination of analytical and numerical work of Straley [19], and similar conclusions for higher virial coefficients were made by Frenkel [20] on the basis of Monte Carlo simulations. Fortunately, all these results are also valid in the nematic phase in the same limit $L/D \to \infty$ [20].

Since the bulk number density can be determined as $n_b = \int d\hat{\omega}\rho(\hat{\omega})$, we can define the orientational distribution function $\psi(\hat{\omega}) = \rho(\hat{\omega})/n_b$ which gives the probability to find a particle with an orientation $\hat{\omega}$. Let us also introduce a dimensionless concentration $c = (\pi/4)L^2 D n_b$. In these variables the grand potential of the fluid can be written (up to a constant C) as

$$\frac{\beta\Omega[\rho(\hat{\omega})]}{N} \simeq \ln(c) + \sigma(\psi) + c\eta(\psi) + C, \tag{2.32}$$

where $\sigma(\psi)$ is related to an orientational entropy

$$S_{or} = -Nk_B\sigma(\psi) = -Nk_B \int d\hat{\omega}\psi(\hat{\omega}) \ln(\psi(\hat{\omega})), \tag{2.33}$$

and $\eta(\psi)$ is a measure for the excluded volume,

$$\eta(\psi) = \frac{4}{\pi} \int d\hat{\omega}_1 d\hat{\omega}_2 |\sin\gamma(\hat{\omega}_1, \hat{\omega}_2)| \psi(\hat{\omega}_1)\psi(\hat{\omega}_2), \tag{2.34}$$

and hence determines the entropy of packing. The isotropic-nematic transition originates from the competition between the orientational entropy (maximal in the isotropic phase) and the packing entropy (maximal in the nematic phase). Since no closed analytical form of the orientational distribution function $\psi_N(\hat{\omega})$ in the nematic phase is known, one might consider a trial function with some variational parameters, and then minimize the grand potential with respect to them. Onsager proposed a trial function of the form

$$\psi(\hat{\omega}) = \frac{\alpha \cosh(\alpha \cos\theta)}{4\pi \sinh\alpha}, \tag{2.35}$$

with θ the polar angle of $\hat{\omega}$ with respect to the director $\hat{n}$. Some others forms of $\psi(\hat{\omega})$ were used later [19, 21]. Direct numerical schemes [22, 23] verified their findings and give the following coexisting concentrations

$$c_I = 3.290, \quad c_N = 4.191, \tag{2.36}$$

which can be compared with Onsager's results $c_I = 3.340, c_N = 4.486$, and the value of the uniaxial nematic order parameter at the transition

$$S = \frac{\int d\hat{\omega}\psi(\hat{\omega}) P_2(\hat{\omega}\cdot\hat{n})}{\int d\hat{\omega}\psi(\hat{\omega})} = 0.7922 \tag{2.37}$$

with $P_2(\hat{\omega}\cdot\hat{n})$ the second Legendre polynomial of the cosine of the angle between $\hat{\omega}$ and nematic director $\hat{n}$, and Onsager's result $S = 0.848$. Although variational methods turn out to be rather effective in the analysis of the bulk IN transition, it is much more difficult to control their validity in interfacial problems, where the coupling between orientational and translational degrees of freedom is present. Therefore, in subsequent Chapters only purely numerical schemes will be used for determination of the one-particle distribution function $\rho(\hat{\omega})$. But, before we start to consider interfacial problems, let us discuss some general facts about surface thermodynamics.

2.5 Surface thermodynamics

Consider a fluid mixture of hard rods of several types $i = 1, \ldots, s$ in contact with a reservoir at fixed temperature T and chemical potentials $\{\mu_i\}$. Assume that the

system shows a coexisting isotropic (I) and nematic (N) phase with a planar interface between them localized near $z = 0$, which can be brought about by means of an infinitesimal field that makes negligible contributions otherwise. Coexistence of the two phases requires fulfilment of conditions of chemical, mechanical, and thermal equilibrium, respectively:

$$\begin{aligned} \mu_{iI} &= \mu_{iN} = \mu_i, \\ p_I &= p_N = p, \\ T_I &= T_N = T. \end{aligned}$$

As we have already seen in Section 2.2, T plays no role in the thermodynamic behavior of hard-rod fluids, and can be simply regarded as constant. However, for generality we will keep the temperature dependence in all subsequent expressions. The presence of the interface introduces an additional work term γdA so that a change in the grand potential is given by

$$d\Omega = -pdV - SdT - \sum_{i=1}^{s} N_i d\mu_i + \gamma dA, \tag{2.38}$$

and the surface tension of the IN interface is

$$\gamma = (\partial\Omega/\partial A)_{V,T,\mu}\,.$$

Surface excess quantities can be defined by constructing a Gibbs dividing surface. This is a mathematical surface located somewhere in the interfacial region. The total volume is then divided into subvolumes V_I and V_N: $V = V_I + V_N$. Away from the dividing surface each phase will take on its bulk number density ρ_{iI} and ρ_{iN}. Extensive properties of the bulk I phase are defined via

$$N_{iI} = \rho_{iI} V_I, \quad \Omega_I = \omega_I V_I, \quad S_I = s_I V_I,$$

and similarly for the bulk nematic phase. The surface excess quantities can be defined by writing

$$\begin{aligned} N_i &= N_{iI} + N_{iN} + N_i^{ex}, \\ \Omega &= \Omega_I + \Omega_N + \Omega^{ex}, \\ S &= S_I + S_N + S^{ex}. \end{aligned} \tag{2.39}$$

Evidently, N_i^{ex}, Ω^{ex} and S^{ex} depend upon the choice of the dividing surface. For a one-component system this can be chosen such that $N^{ex} = 0$, i.e. corresponding to the equimolar surface, and Ω_{ex} and S_{ex} are proportional to A. In a mixture no choice is possible that makes all N_i^{ex} vanish. Since the grand potential Ω is an extensive quantity one can integrate Eq. (2.38) to obtain

$$\Omega = -pV + \gamma A \tag{2.40}$$

for the whole system, and

$$\Omega_I = -pV_I, \quad \Omega_N = -pV_N$$

for the bulk phases so that

$$\gamma = \Omega^{ex}/A \tag{2.41}$$

irrespective of the choice of dividing surface. The surface excess quantities refer to differences between the properties of the whole (inhomogeneous) system and those of the two bulk phases in contact at the dividing surface. It must be remembered that the actual interface is not sharp.

From Eqs. (2.39) and the corresponding equations for the bulk phases it follows that

$$d\Omega^{ex} = d(\Omega - \Omega_I - \Omega_N) = -S^{ex}dT + \gamma dA - \sum_{i=1}^{s} N_i^{ex} d\mu_i.$$

However, Eq. (2.41) implies $d\Omega^{ex} = \gamma dA + Ad\gamma$ so that

$$S^{ex}dT + \sum_{i=1}^{s} N_i^{ex} d\mu_i + Ad\gamma = 0.$$

Dividing through by A we obtain

$$sdT + \sum_{i=1}^{s} \Gamma_i d\mu_i + d\gamma = 0, \tag{2.42}$$

with $\Gamma_i \equiv N_i^{ex}/A$ the excess adsorption (number of atoms per unit area), and $s \equiv S^{ex}/A$ the excess entropy per unit area. Equation (2.42) is the Gibbs adsorption equation. For isothermal processes it allows to determine the excess adsorption of the component i as

$$\Gamma_i = \left(\frac{\partial \gamma}{\partial \mu_i}\right).$$

These relations represent the basic surface thermodynamics that is applied in the subsequent Chapters.

We have a habit in writing articles published in scientific journals to make the work as finished as possible, to cover up all the tracks, to not worry about the blind alleys or describe how you had the wrong idea first, and so on. So there isn't any place to publish, in a dignified manner, what you actually did in order to get to do the work.

R. Feynman, Nobel Lecture, 1966.

Chapter 3

The free isotropic-nematic interface of a monodisperse hard-rod fluid

Within the Onsager theory we consider the free planar isotropic-nematic interface of a fluid of monodisperse hard rods. Using a perturbative method for the interfacial biaxiality we calculate the one-particle distribution function $\rho(\mathbf{r}, \hat{\omega})$. Profiles of the density and the uniaxial order parameter are found to be monotonic, whereas the biaxial order parameter exhibits non-monotonic behavior. The bulk correlation lengths of the coexisting phases and the surface tensions are determined.

3.1 Introduction

A fluid of monodisperse hard rods of number density n exhibits an interface between the coexisting isotropic phase (at density n_I) and nematic phase (at density n_N) when $n_I < n < n_N$. Several authors [24–32] considered a generalization of Onsager's theory to include inhomogeneities in order to study the isotropic-nematic interface. An important issue that appears in these studies involves the numerical value of the surface tension as a function of the angle between the interface normal $\hat{z}$ and the (imposed) nematic director $\hat{n}$ far from the interface. Another issue concerns the equilibrium profile of the total density and the orientation order parameters as a function of the spatial coordinate z running across the interface. In particular Chen's work in 1993 [27] seems to settle that (i) the lowest interfacial tension is obtained when $\hat{n} \perp \hat{z}$, (ii) the density and uniaxial order parameter profile are monotonic functions of z, (iii) the biaxial order parameter profile is small in magnitude and ignoring it (in order to reduce the computational cost) hardly affects the numerical value of the tension. Some of these findings, however, were challenged in Ref. [28], where it was

argued that the equilibrium profiles are non-monotonic and that the tension is higher, by about 50%, than reported by Chen [27]. This is one of the reasons why we revisit the problem. The other reason why we study the inhomogeneous pure hard-rod fluid is due to its role as a stepping stone towards the study of interfacial phenomena in *binary mixtures* of hard rods, considered in Chapter 4.

Although the density functional formalism we adopt does not differ from that in other studies, our numerical implementation does differ somewhat. In particular our perturbative treatment of the biaxiality that occurs in the interface is supposed to be rather efficient. We calculate the equilibrium profiles and the tension of the free isotropic-nematic interface for $\hat{n} \perp \hat{z}$ and $\hat{n} \parallel \hat{z}$.

3.2 Density functional

Consider a fluid of monodisperse hard spherocylinders of length L and diameter D in a macroscopic volume V at temperature T and chemical potential μ. The grand potential functional $\Omega[\rho]$ of the system with the one-particle distribution function $\rho(\mathbf{r}, \hat{\omega})$, where $\mathbf{r}$ denotes the center-of-mass coordinate of the rods and $\hat{\omega}$ the orientation of the long axis, in the absence of an external potential is given by

$$\begin{aligned} \beta\Omega[\rho] &= \int d\mathbf{r} d\hat{\omega} \rho(\mathbf{r}, \hat{\omega}) \Big(\ln[\rho(\mathbf{r}, \hat{\omega}) L^2 D] - 1 - \beta\mu \Big) \\ &- \frac{1}{2} \int d\mathbf{r} d\hat{\omega} d\mathbf{r}' d\hat{\omega}' f(\mathbf{r}, \hat{\omega}; \mathbf{r}', \hat{\omega}') \rho(\mathbf{r}, \hat{\omega}) \rho(\mathbf{r}', \hat{\omega}'), \end{aligned} \tag{3.1}$$

with $\beta = 1/k_B T$, and f the Mayer function which equals -1 if the rods overlap and 0 otherwise [11, 33]. Although the functional of Eq.(3.1) is a second virial approximation, i.e. cubic and higher-order terms in ρ are being ignored, it is supposed to give accurate results for rods in the "needle" limit $L/D \to \infty$ [11, 33]. The minimum condition on the functional, $\delta\Omega[\rho]/\delta\rho(\mathbf{r}, \hat{\omega}) = 0$, leads to the nonlinear integral equation

$$\ln[\rho(\mathbf{r}, \hat{\omega}) L^2 D] - \int d\mathbf{r}' d\hat{\omega}' f(\mathbf{r}, \hat{\omega}; \mathbf{r}', \hat{\omega}') \rho(\mathbf{r}', \hat{\omega}') = \beta\mu, \tag{3.2}$$

to be solved for the equilibrium distribution $\rho(\mathbf{r}, \hat{\omega})$. Once $\rho(\mathbf{r}, \hat{\omega})$ has been determined, it can be inserted into the functional to obtain the minimum value

$$\beta\Omega_{min} = \int d\mathbf{r} d\hat{\omega} \rho(\mathbf{r}, \hat{\omega}) \Big(-1 + \frac{1}{2} \ln[\rho(\mathbf{r}, \hat{\omega}) L^2 D] - \frac{1}{2} \beta\mu \Big). \tag{3.3}$$

and the interface tension $\gamma(\mu) = (\Omega_{min} + pV)/A$ (see Eq. (2.40)), with p the bulk fluid pressure.

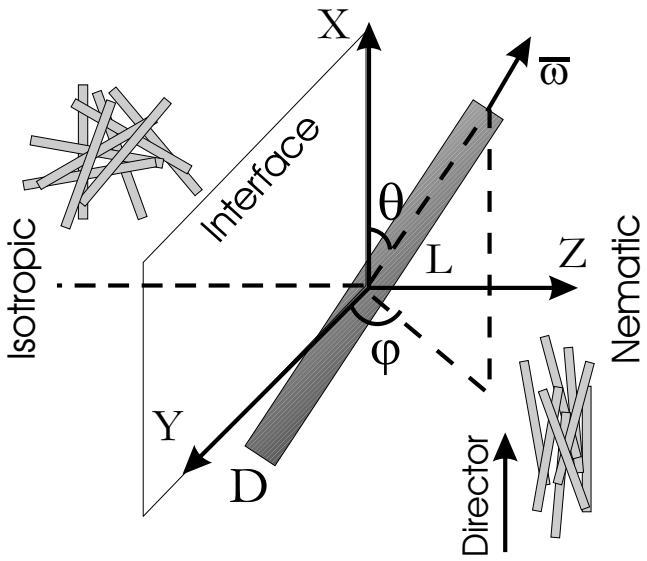

Figure 3.1: Geometry of the interface between the coexisting isotropic and nematic bulk phases and the corresponding coordinate system.

3.3 The free isotropic-nematic interface

We assume the interface between the coexisting isotropic and nematic phase to be planar, with surface normal $\hat{z}$, as illustrated in Fig. 3.1. The one-particle distribution, which in this geometry depends on the coordinate $z = \mathbf{r} \cdot \hat{z}$ and the orientation $\hat{\omega}$, is a solution of the stationarity equation (3.2), with $\mu = \mu_{IN}$,

$$\ln[\rho(z,\hat{\omega})L^2 D] + \int dz' d\hat{\omega}' K(z-z';\hat{\omega},\hat{\omega}')\rho(z',\hat{\omega}') = \beta\mu_{IN}, \tag{3.4}$$

subject to the boundary conditions

$$\begin{array}{ll} \rho(z,\hat{\omega}) = \rho_I(\hat{\omega}) & (z \to -\infty), \\ \rho(z,\hat{\omega}) = \rho_N(\hat{\omega}) & (z \to \infty), \end{array} \tag{3.5}$$

with $\rho_I(\hat{\omega})$ and $\rho_N(\hat{\omega})$ the one-particle distribution function of the bulk isotropic and nematic phase, respectively, and $\hat{n}$ is a fixed nematic director at $z \to \infty$. In Eq.(3.4) we defined the kernel K as

$$K(z-z',\hat{\omega},\hat{\omega}') = -\int dx' dy' f(\mathbf{r},\hat{\omega};\mathbf{r}',\hat{\omega}'), \tag{3.6}$$

which was calculated explicitly for hard spherocylinders of arbitrary L/D earlier [34]. In the limit $L/D \to \infty$ of interest here the results obtained in Ref. [34] can be written

as

$$K(z_{12},\hat{\omega}_1,\hat{\omega}_2) = \begin{cases} 0 & |z_{12}| > |A| + |B| \\ \dfrac{E(\hat{\omega}_1,\hat{\omega}_2)}{4|AB|}(|A| + |B| - |z_{12}|) & |A| - |B| \leq |z_{12}| \leq |A| + |B| \\ \dfrac{E(\hat{\omega}_1,\hat{\omega}_2)}{2|A|} & |z_{12}| \leq |(|A| - |B|)| \end{cases}, \tag{3.7}$$

with the excluded volume E defined in Eq.(2.31), and $A = \frac{L}{2}\max(\hat{\omega}_1 \cdot \hat{z}, \hat{\omega}_2 \cdot \hat{z})$ and $B = \frac{L}{2}\min(\hat{\omega}_1 \cdot \hat{z}, \hat{\omega}_2 \cdot \hat{z})$.

Note that the profiles that satisfy Eqs.(3.4)-(3.6) depend nontrivially on $\hat{n} \cdot \hat{z}$. In all cases where $\hat{n}$ is not parallel to $\hat{z}$, the uniaxial symmetry about $\hat{n}$ is broken in the interface, i.e. the distribution is a nontrivial function of the spatial coordinate z, the polar angle θ *and* the azimuthal angle φ of the orientation $\hat{\omega}$ with respect to $\hat{n}$. Taking into account inhomogeneity and biaxiality simultaneously is computationally demanding, and therefore approximations that simplify or discard either one or both of these features have often been made. Instead of solving the Euler-Lagrange equations (3.4)-(3.6) some authors treated the problem variationally by e.g. imposing a step function for the total density [24], or a wider class of variational smooth profiles with a finite width [25, 26]. It was argued and shown by Chen and Noolandi [26], and by Chen [27], who did solve the full Euler Lagrange equations (3.4)-(3.6) numerically on a (z, θ, φ) grid, that the biaxiality of the interface profile is small and that it does not affect the numerical value of the surface tension γ within the numerical accuracy. The results of Ref. [27] seem to settle that the lowest tension is obtained when $\hat{n} \perp \hat{z}$, that its numerical value is given by $\beta\gamma LD = 0.183 \pm 0.002$, and that the profile of the total density and the uniaxial nematic order parameter are monotonic functions of the spatial variable z. Very recently, however, it was argued by Koch and Harlen [28] that a refinement of the z-grid yields a non-monotonic density profile, and a significantly higher surface tension than determined in Ref. [27]. This is one of the reasons why we revisit the problem here, as already stated in the introduction.

Since there is no disagreement in the literature on the conclusion that the surface tension is minimal when $\hat{n} \perp \hat{z}$, we take this for granted here, and thus consider the geometry where $\hat{n} \perp \hat{z}$. We define the polar and azimuthal angle θ and φ of $\hat{\omega}$ by $\cos\theta = \hat{n} \cdot \hat{\omega}$ and $\sin\theta\sin\varphi = \hat{z} \cdot \hat{\omega}$. This choice for the angles θ and φ is identical to that in Ref. [27], and is such that the one-particle distribution can exactly be written as the $N \to \infty$ limit of

$$\rho(z,\theta,\varphi) = \sum_{j=0}^{N} \rho_j(z,\theta)\cos(2j\varphi). \tag{3.8}$$

The distribution is thus characterised by the functions $\rho_j(z,\theta)$. On the basis of the small biaxiality reported by Chen [27] we expect that $|\rho_j(z,\theta)|$ decreases rapidly with increasing j, so that accurate distributions are obtained for small N. Insertion of the

parametrization (3.8) into the stationarity condition (3.4) yields, after multiplication of Eq. (3.4) by $\cos(2k\varphi)$ and integration from $\varphi = 0$ to $\varphi = 2\pi$, that

$$\begin{aligned}\beta\mu_{IN}\delta_{k0} &= \frac{1}{2\pi}\int_0^{2\pi} d\varphi \cos(2k\varphi)\ln[\sum_{j=0}^{N}\rho_j(z,\theta)\cos(2j\varphi)L^2D] \\ &+ \int dz'\int d\theta'\sin\theta'\sum_{m=0}^{N}K_{km}(z-z',\theta,\theta')\rho_m(z',\theta') \qquad (3.9)\\ &\quad (k=0,1,\cdots N),\end{aligned}$$

where the doubly azimuthally integrated kernels K_{km}, with $k, m = 0, 1, \cdots N$, are given by

$$K_{km}(z-z',\theta,\theta') = \frac{1}{2\pi}\int_0^{2\pi} d\varphi \int_0^{2\pi} d\varphi' \cos(2k\varphi)\cos(2m\varphi')K(z-z',\hat{\omega},\hat{\omega}'). \quad (3.10)$$

For a given value of N Eq. (3.10) constitutes $N+1$ coupled nonlinear integral equations for the $N+1$ unknowns $\rho_k(z,\theta)$, $(k = 0, 1, \cdots N)$. This set of equations can be solved numerically on a (z,θ) grid, for instance by iteration. Note that the numerical determination of the K_{km}'s, on a $(z-z',\theta,\theta')$ grid, need be performed only once, as it does not depend on $\rho_j(z,\theta)$.

By setting $N = 0$ we ignore any biaxiality in the interface, i.e. only the term $j = 0$, which is independent of φ, contributes in Eq. (3.8). The resulting equilibrium distribution $\rho_0(z,\theta)$ is, from Eq. (3.10), the solution of

$$\beta\mu_{IN} = \ln[\rho_0(z,\theta)L^2D] + \int dz'\int d\theta'\sin\theta' K_{00}(z-z',\theta,\theta')\rho_0(z',\theta'). \qquad (3.11)$$

This is, essentially, the equation solved by Chen and Noolandi in Ref. [26] on an equidistant grid (z_i,θ_j), with $N_z = 40$ points $z_i \in [-5L, 5L]$ and $N_\theta = 41$ points $\theta \in [0,\pi/2]$, i.e. the resolution is such that $z_{i+1} - z_i = L/4$ and $\theta_{j+1} - \theta_j = \pi/80$. The profiles reported in Ref. [26] are monotonic, and the surface tension γ for the case of interest here, $\hat{n} \perp \hat{z}$, is given by $\beta\gamma LD = 0.183 \pm 0.002$ [26, 27].

In our calculations we have used a nonequidistant θ-grid, with half of the N_θ points distributed in the angle $[0,\pi/4]$ and the other half in the rest, in order to improve resolution close to the orientation of the nematic director $\hat{n}$. It will be demonstrated in Chapter 7 that the accuracy of the orientational discretization may influence significantly the resulting bulk orientation distributions: a rough θ grid promotes the appearance of an artificial (almost) perfectly aligned nematic phase. This is not particularly relevant for the present calculations performed with $N_\theta = 50$, since even a uniform angular grid provides significant accuracy at the densities where the IN coexistence takes place. However, in order to use our results in calculations of binary mixtures of hard rods, presented in the next Chapter, we stick to such a nonuniform grid.

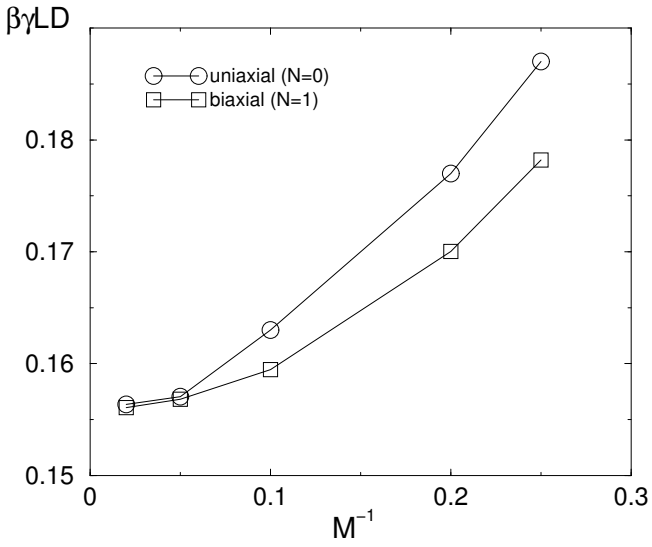

Figure 3.2: Surface tension γ of the free planar isotropic-nematic interface of hard rods of length L and diameter $D \ll L$ as a function of M^{-1}, where M is the number of spatial grid-points per L (see text). For both curves the bulk nematic director is perpendicular to the interface normal. The interface biaxiality is ignored in the $N = 0$ curve ($\circ$), and taken into account to lowest order in the $N = 1$ curve ($\Box$). The significant levelling of the two curves for $M \geq 20$ indicates good convergence for the $M = 50$ grid.

When we solve Eq. (3.11) on approximately the same grid as that of Refs. [26,27], i.e. with $N_\theta = 50$ and $N_z = 40$, we obtain the value $\beta\gamma LD = 0.187 \pm 0.001$, where the uncertainty is estimated on the basis of the accuracy of the numerical φ integrations in the calculation of K_{00}. A refinement of the θ-grid, i.e. increasing N_θ, does not change the value of γ within the numerical accuracy. However, gradually increasing N_z from 40 to 500 (with the same interval $z_i \in [-5L, 5L]$) lowers γ systematically. This can be seen in Fig. 3.2, where we plot γ as a function of $1/M$ with fixed $N_\theta = 50$, where $M = N_z/10$ is the number of grid points per rod length L (in the interval $z_i \in [-5L, 5L]$).

On the basis of this figure we conclude that the calculation with $M = 50$ has converged, and yields $\beta\gamma LD = 0.156 \pm 0.001$, which is about 15% lower than the estimate given in Ref. [26, 27]. The uniaxially symmetric profiles are monotonic, in agreement with Refs. [26, 27]. However, these findings are in disagreement with the claims in Ref. [28], where a refinement of the spatial grid yields a higher value for γ and a non-monotonic density profile.

In Fig. 3.3 we present the profiles of the density $c(z) = n(z)L^2D(\pi/4)$ and the uniaxial order parameter $S(z)$, for $M = 20$. One might conventionally define the center of the profile as the position in the interface at which the profile decreases

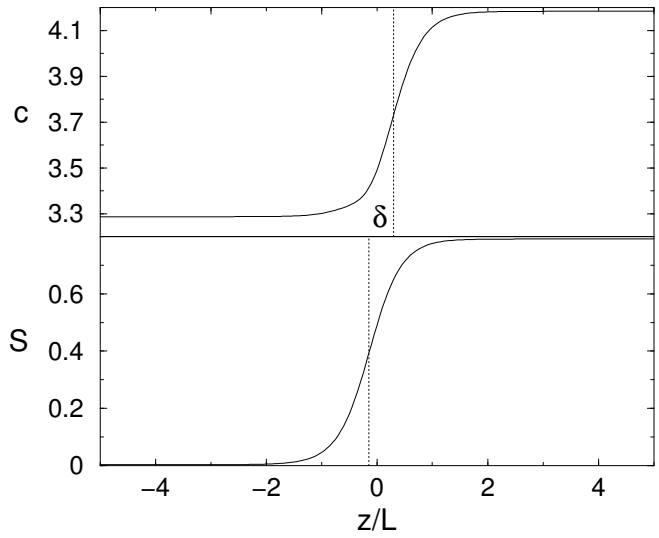

Figure 3.3: Density profile $c(z) = n(z)L^2D(\pi/4)$ and uniaxial order parameter profile $S(z)$ for $M = 20$ and $N = 0$ (uniaxial). The dotted lines mark the relative shift $\delta \simeq 0.45L$ between the centers of the profiles.

half of the bulk-value difference from the nematic value. Similar to the findings in Ref. [26], the profiles are shifted with respect to each other by a distance $\delta \simeq 0.45L$. The interpretation is that it takes approximately one rod length for isotropic rods to interact with the ordered ones.

Another interesting point is related to the monotonicity of the density and uniaxial order parameter profiles across the interface, evident from Fig. 3.3. From a general point of view a hard-rod fluid can be considered as a mixture of rods of various orientations, with the total number of rods in the system conserved. The different components of the mixture may change differently across the interface, which in turn could lead to non-monotonic changes in the total density. In Fig. 3.4 we present profiles of the one-particle distribution function $\rho(z, \theta)$ for several values of θ. Although we observe non-monotonic variations of the density of some components (i.e. some θ's), it turns out that densities of rods with orientations close to the nematic director are high enough to screen these modulations in the profiles of the total density $n(z)$ and the uniaxial order parameter $S(z)$. In contrast, this effect was observed in binary mixtures, as will be shown in the next Chapter.

Different variations of densities of rods with distinct orientations across the interface do not imply that one needs to introduce several correlation lengths. Similar to hard-sphere mixtures [35] a unique correlation length ξ_b governs the decay of all components of the one-particle distribution function to their bulk values. Introducing the deviation from the bulk distribution $\rho_b(\hat{\omega})$ as $\delta\rho(z, \hat{\omega}) = \rho(z, \hat{\omega}) - \rho_b(\hat{\omega})$, it turns

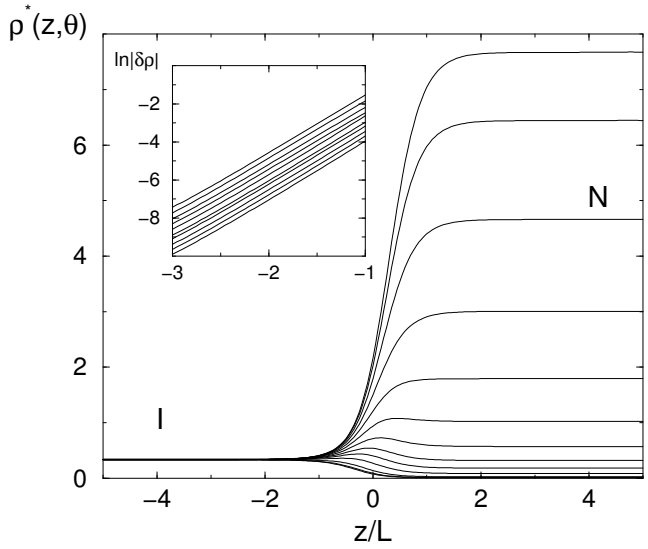

Figure 3.4: The dimensionless one-particle distribution function $\rho^*(z,\theta) = \rho(z,\theta)L^2D$ for several values of θ. The system is isotropic at $z \to -\infty$, and nematic at $z \to \infty$. The Inset shows $\ln|\delta\rho(z,\theta)|$ for several values of θ at the I side of the IN interface. For clarity, curves were shifted in a vertical direction.

out that

$$\delta\rho(z,\hat{\omega}) = A_{\pm}(\hat{\omega})\exp(-|z|/\xi_{\pm}), \quad z \to \pm\infty, \tag{3.12}$$

where the only orientation dependence is in the decay amplitude $A_{\pm}(\hat{\omega})$. This is illustrated in the Inset in Fig. 3.4, where dependence of $\delta\rho(z,\hat{\omega})$ upon approach to the bulk I phase is presented on a logarithmic scale. All curves (representing different θ's) are parallel, and the correlation length $\xi_I = 0.335 \pm 0.005$ follows from the (common) slope of these curves. Analogously, the correlation length of the bulk nematic phase at the IN coexistence density is equal to $\xi_N = 0.322 \pm 0.005$.

In order to study the effect of interfacial biaxiality we consider the Euler-Lagrange equations (3.10) for $N = 1$, which we write as

$$\begin{aligned}
\beta\mu_{IN} &= \ln[\rho_0(z,\theta)L^2D] + I_0\Big(\frac{\rho_1(z,\theta)}{\rho_0(z,\theta)}\Big) \\
&+ \int dz'd\theta' \sin\theta' \Big(K_{00}(z-z',\theta,\theta')\rho_0(z',\theta') + K_{01}(z-z',\theta,\theta')\rho_1(z',\theta')\Big), \\
0 &= I_1\Big(\frac{\rho_1(z,\theta)}{\rho_0(z,\theta)}\Big) + \int dz'd\theta' \sin\theta' \Big(K_{10}(z-z',\theta,\theta')\rho_0(z',\theta') + \\
&\quad K_{11}(z-z',\theta,\theta')\rho_1(z',\theta')\Big),
\end{aligned} \tag{3.13}$$

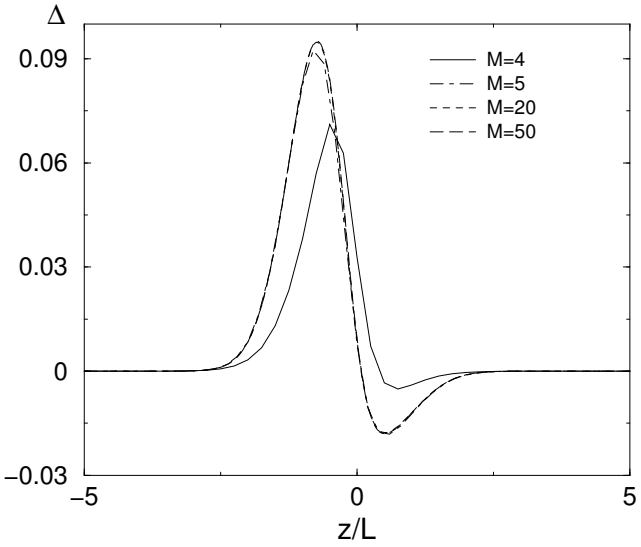

Figure 3.5: Profile of the biaxial order parameter Δ as a function of the spatial coordinate z running across the isotropic-nematic planar interface for several values of M, the number of grid points per L. The system is isotropic for $z \to -\infty$, and nematic at $z \to \infty$. The $M = 4$ grid is clearly too coarse, and comparing the $M = 20$ and $M = 50$ grid reveals good convergence.

where $I_0(x)$ and $I_1(x)$ are defined, for $|x| < 1$, as

$$I_0(x) = \frac{1}{2\pi}\int_0^{2\pi} d\varphi \ln\big(1 + x\cos(2\varphi)\big) = \ln\frac{1+\sqrt{1-x^2}}{2}$$

$$I_1(x) = \frac{1}{2\pi}\int_0^{2\pi} d\varphi \cos(2\varphi)\ln\big(1 + x\cos(2\varphi)\big) = \frac{1-\sqrt{1-x^2}}{x}. \qquad (3.14)$$

Equations (3.13), with the boundary conditions given in Eq. (3.5), can be solved iteratively on a (z, θ) grid. Note that the boundary conditions given in Eq. (3.5) imply that $\rho_1(z, \theta) \to 0$ for $|z| \to \infty$.

From the solution of Eq. (3.13) we construct the profile of the total density $n(z) = \int d\hat{\omega}\rho(z, \hat{\omega})$, the uniaxial nematic order parameter $S(z) = \frac{1}{2}\langle 3\cos^2\theta - 1\rangle(z)$, and the biaxiality $\Delta(z) = \langle \frac{3}{2}\sin^2\theta\cos 2\varphi\rangle(z)$. Note that the latter coincides with Chen's definition of biaxiality in Ref. [27]. Combining this with our $N = 1$ parametrization of the distribution we obtain

$$\Delta(z) = \frac{\int d\hat{\omega}\rho(z,\hat{\omega})\frac{3}{2}\sin^2\theta\cos(2\varphi)}{\int d\hat{\omega}\rho(z,\hat{\omega})} = \frac{3}{4}\frac{\int_0^{\pi/2} d\theta \sin^3\theta\rho_1(z,\theta)}{\int_0^{\pi/2} d\theta\sin\theta\rho_0(z,\theta)}. \qquad (3.15)$$

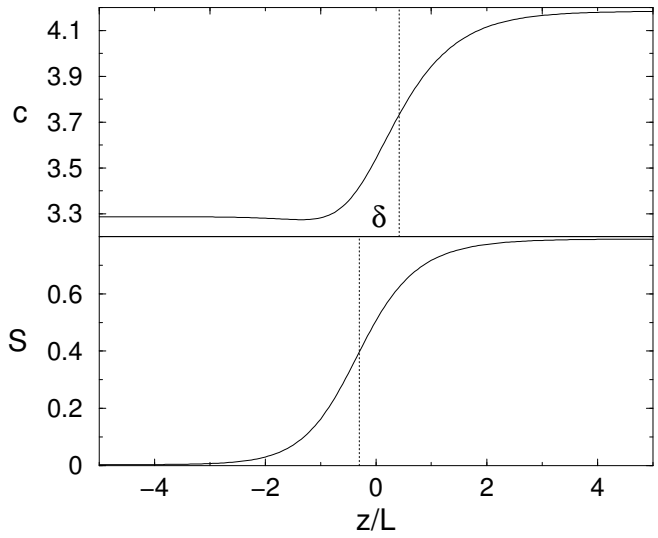

Figure 3.6: Profiles of the density $c(z) = n(z)L^2D(\pi/4)$, the nematic order parameter $S(z)$ as a function of the spatial coordinate z running accross the isotropic-nematic planar interface for $\hat{n} \parallel \hat{z}$. The system is isotropic at $z \to -\infty$, and nematic at $z \to \infty$.

The profiles $n(z)$ and $S(z)$ are almost identical to the ones obtained with the uniaxially symmetric profile (Fig. 3.3). The resulting biaxiality profiles $\Delta(z)$ are shown in Fig. 3.5 for several choices of the z-grid parameter M. It is seen that $\Delta(z)$ is non-monotonic, with a positive value at the isotropic side of the interface, a negative value at the nematic side, and a decay to zero in the two bulk phases.

The structure of $\Delta(z)$ we obtain is very similar to that obtained by Chen in Ref. [27]. The negative dip is basically identical, whereas the positive peak in $\Delta(z)$ is a factor of about two smaller than the result in Ref. [27]. Refining the z-grid from $M = 4$ to $M = 5$ yields a substantial change in $\Delta(z)$, while further refinement to $M = 20$ and 50 hardly changes the biaxiality (although it does change the resulting surface tension, see Fig. 3.2). These results provide support for truncating the expansion in Eq. (3.8) at $N = 1$ without loss of quantitative accuracy. The IN surface tension that follows from the biaxial $N = 1$ profiles is also plotted in Fig. 3.2. It is seen that γ obtained from the biaxial profiles are substantially smaller than the corresponding uniaxial ones in the case of the cruder grids with $M < 20$. The difference becomes vanishingly small, however, in the case of the $M = 20$ and $M = 50$ grid points. We conclude therefore that $\beta\gamma LD = 0.156 \pm 0.001$ for the Onsager model, and that the total density and uniaxial order-parameter profiles are monotonic.

For the sake of completeness, we consider the IN interface with $\hat{n} \parallel \hat{z}$, i.e. the orientation of the nematic director in the bulk is fixed perpendicular to the interface by external means. The polar and azimuthal angles θ and φ of $\hat{\omega}$ can be conveniently

redefined as $\cos\theta = \hat{n}\cdot\hat{\omega}$ and $\sin\theta\sin\varphi = \hat{z}\cdot\hat{\omega}$. Since the whole formalism does not change upon the rotation of the coordinate system, we just present the results. The density profile $n(z)$ exhibits some non-monotonicity at the isotropic side, although small, whereas the profile of $S(z)$ remains monotonic, as shown in Fig. 3.6. The convergence of the values of the surface tension is achieved again for $M \geq 20$ and gives $\beta\gamma_{\|}LD = 0.295 \pm 0.001$, which is comparable with the value $\beta\gamma_{CN}LD = 0.29$ extracted from Chen and Noolandi's paper [26].

3.4 Summary

We calculated the structure and the surface tension of the planar free interface between the coexisting isotropic and nematic phase of a hard-rod fluid in the Onsager limit. We restricted attention mainly to the case where $\hat{n} \perp \hat{z}$ (as a thermodynamically favorable geometry for the free interface), with $\hat{n}$ the bulk nematic director and $\hat{z}$ the interface normal. However, some results for the case $\hat{n} \parallel \hat{z}$ were also provided. We showed that the surface tension γ of the one-component system is given by $\gamma = (0.156 \pm 0.001)kT/(LD)$, where L and D denote the length and diameter of the rods, respectively. This value is lower by about 15% than a previous estimate by Chen [27], and we argued that the difference is due to the finer spatial grids used in the present study. This conclusion is in contrast with that of Ref. [28], where a finer grid is argued to yield a higher surface tension than that of Ref. [27]. The profiles we obtain for the total density and uniaxial order parameter are monotonic, whereas the biaxiality profile has a richer structure (see Fig.2). These findings are in good agreement with those of Ref. [27], even though we treat the biaxiality perturbatively here in order to reduce the computational cost. The monotonic density and uniaxial order parameter profiles are in disagreement with the recent claims in Ref. [28].

Chapter 4

Free planar isotropic-nematic interfaces in binary hard-rod fluids

Within the Onsager theory we consider free planar isotropic-nematic interfaces in binary mixtures of hard rods. For sufficiently different particle shapes the bulk phase diagrams of these mixtures exhibit a triple point, where an isotropic (I) phase coexists with two nematic phases (N_1 and N_2) of different composition. For all explored mixtures we find that upon approach of the triple point the IN_2 interface shows complete wetting by an intervening N_1 film. We compute the surface tensions of isotropic-nematic interfaces, and find a remarkable increase with fractionation.

4.1 Introduction

Whereas the original Onsager theory [11] addressed the isotropic-nematic (IN) transition in a fluid of monodisperse hard rods, it was also extended to describe bulk *mixtures* of colloidal rods. For the case of binary mixtures of longer and shorter rods, it was found that the IN transition is accompanied by strong fractionation, such that the coexisting nematic phase contains a relatively large fraction of the longer rods [21,22]. Later theoretical work on long-short mixtures also showed the possibility of nematic-nematic (N_1N_2) demixing (driven by a peculiar competition between orientation entropy and ideal mixing entropy), and an isotropic-nematic-nematic (IN_1N_2) triple point in the phase diagram [23, 36–38] of mixtures with a length ratio more extreme than about 1:3. Later, also binary mixtures of thin and thick hard rods were considered. These were shown to have phase diagrams similar to those of long-short mixtures, i.e., with strong fractionation at IN coexistence and with N_1N_2 and IN_1N_2 coexistence for diameter ratios exceeding 1:3.8 [23,38–40], but with an additional possi-

bility for isotropic-isotropic (I_1I_2) phase coexistence due to the depletion effect [39–41] if the diameter ratio is more extreme than about 1 : 8. Interestingly, thin-thick mixtures have recently been realized experimentally by mixing "bare" fd virus particles (length 1μm) with ones that are "coated" with polyethyleneglycol (PEG) [43]. The diameter ratio of these systems can be tuned by varying the ionic strength of the solvent: due to an increasing salt concentration the effective diameter of the (charged) bare rods shrinks because of enhanced screening, whereas that of the PEG-coated rods is not (or hardly) affected because of the steric nature of PEG. Exploiting this effect allowed for the experimental study of diameter ratios up to about 1:4.5, and IN_1, IN_2, N_1N_2 as well as IN_1N_2 triple coexistence were actually observed [43].

The present study is devoted to the planar interfaces that exist between the coexisting bulk phases in binary mixtures of colloidal rods, with a focus on the calculation of both thermodynamic and structural properties of these interfaces. The main thermodynamic quantity of interest is the surface tension γ, and the structural properties we will investigate are the profiles of the density and the order parameters. It is known from the study of the IN interface of pure (one-component) suspensions of rods that γ depends on the angle between the interface normal $\hat{z}$ and the director $\hat{n}$ of the nematic phase asymptotically far from the interface [24–26]. The studies of Refs. [26,27] showed that γ is minimal when $\hat{n} \perp \hat{z}$, and on this basis (and on the basis of some test calculations) we assume this to be the case for mixtures as well. It was already demonstrated in Chapter 3 and in Refs. [26,27,44] that (i) the density profile and the nematic order parameter profile of the IN interface of the pure hard needle fluid change monotonically from their values in the isotropic bulk phase to those in the nematic phase, (ii) the interface thickness is of the order of the length L of the rods, and (iii) the interfacial biaxiality is small and non-monotonic. In this Chapter we will show that the density profiles in mixtures of rods are *not* always monotonic, and that the interface thickness is not always of order L due to the formation of macroscopically thick wetting films close to the bulk triple points. Moreover, we will show that the surface tension in mixtures of rods tends to be substantially higher than that of the pure systems of their components.

This Chapter is organized as follows. In Sec. 4.2 we introduce the Onsager functional and the basic Euler-Lagrange equation. In Sec. 4.3 we solve this equation for bulk geometries, and present a few typical bulk phase diagrams. In Sec. 4.4 we generalize a method of Chapter 3 to solve the Euler-Lagrange equation for interfaces with small biaxiality in mixtures, and study IN_1, N_1N_2 and IN_2 interfaces, the latter in particular in the vicinity of the bulk IN_1N_2 triple point. A summary and some discussion of the results are given in Sec. 4.5.

4.2 Density functional

Consider a fluid of hard cylinders of two different species $\sigma = 1, 2$ of length L_σ and diameter D_σ in a macroscopic volume V at temperature T and chemical potentials μ_σ. The thermodynamic properties and the structure of the system can be determined

from the grand potential functional $\Omega[\{\rho_\sigma\}]$ of the one-particle distribution functions $\rho_\sigma(\mathbf{r},\hat{\omega})$, where $\mathbf{r}$ denotes the center-of-mass coordinate of the rod of species σ and $\hat{\omega}$ the orientation of the long axis. The functional $\Omega[\{\rho_\sigma\}]$ is such that (i) it is minimized, for given $(\{\mu_\sigma\},V,T)$, by the equilibrium one-particle distributions $\rho_\sigma(\mathbf{r},\hat{\omega})$, and (ii) the minimal value of the functional is the equilibrium grand potential Ω [45].

Within the second virial approximation and in the absence of external potentials, the functional $\Omega[\{\rho_\sigma\}]$ can be written [11,33] as

$$\begin{aligned}\beta\Omega[\{\rho_\sigma\}] &= \sum_\sigma \int dq \rho_\sigma(q)\Big(\ln[\rho_\sigma(q)L_\sigma^2 D_\sigma] - 1 - \beta\mu_\sigma\Big) \\ &\quad -\frac{1}{2}\sum_{\sigma\sigma'}\int dq dq' f_{\sigma\sigma'}(q;q')\rho_\sigma(q)\rho_{\sigma'}(q'),\end{aligned} \tag{4.1}$$

with $\beta=(k_BT)^{-1}$ the inverse temperature and $f_{\sigma\sigma'}(q;q')$ the Mayer function of the $\sigma\sigma'$-pair of rods with coordinates $q=\{\mathbf{r},\hat{\omega}\}$ and $q'=\{\mathbf{r}',\hat{\omega}'\}$. For hard rods, the focus of this study, $f_{\sigma\sigma'}(q;q')$ equals -1 if the rods overlap and vanishes otherwise. Onsager argued that the second virial approximation is accurate for long rods, and becomes even exact for isotropic and nematic bulk fluids in the limit of vanishing diameter-to-length ratio [11]. We shall adopt this limit throughout this Chapter, i.e., we consider $D_\sigma/L_{\sigma'}\to 0$ for any $\sigma\sigma'$ pair. Therefore, the relative shape of the rods is only characterized by the ratios $l=L_2/L_1$ and $d=D_2/D_1$ of the lengths and the diameters, respectively.

The minimum conditions $\delta\Omega[\{\rho_\sigma\}]/\delta\rho_\sigma(q)=0$ on the functional lead to the set of nonlinear integral equations

$$\ln[\rho_\sigma(q)L_\sigma^2 D_\sigma] - \sum_{\sigma'}\int dq' f_{\sigma\sigma'}(q;q')\rho_{\sigma'}(q') = \beta\mu_\sigma \tag{4.2}$$

to be solved for the equilibrium distributions $\rho_\sigma(q)$. Once determined, they can be inserted into the functional to obtain the equilibrium value of the grand potential

$$\beta\Omega = \frac{1}{2}\sum_\sigma \int dq \rho_\sigma(q)\Big(\ln[\rho_\sigma(q)L_\sigma^2 D_\sigma] - 2 - \beta\mu_\sigma\Big). \tag{4.3}$$

Note that $\Omega=-pV$ for a bulk system in a volume V, with $p=p(\{\mu_\sigma\},T)$ the pressure. In the presence of a planar surface or interface of area A we have $\Omega=-pV+\gamma A$ with $\gamma=\gamma(\{\mu_\sigma\},T)$ the surface or interface tension.

4.3 Bulk phase diagrams

The bulk thermodynamic properties of binary hard-rod fluids were studied extensively within Onsager theory. The minimization of the functional was either performed variationally [23, 36–38, 41, 42] or through a fully numerical solution [22, 40, 44]. We

adopt the latter approach as it can be easily generalized for inhomogeneous systems. For clarity we briefly repeat the essential points of the method and summarize the available results.

The bulk distribution functions of the isotropic and nematic phase are translationally invariant, i.e., $\rho_\sigma(\mathbf{r},\hat{\omega}) = \rho_\sigma(\hat{\omega})$, which allows to reduce Eq. (4.2) to

$$\ln[\rho_\sigma(\hat{\omega})L_\sigma^2 D_\sigma] + \sum_{\sigma'} \int d\hat{\omega}' E_{\sigma\sigma'}(\hat{\omega},\hat{\omega}')\rho_{\sigma'}(\hat{\omega}') = \beta\mu_\sigma, \tag{4.4}$$

with $E_{\sigma\sigma'}$ the excluded volume of a pair of cylinders of species σ and σ' given by [33]

$$\begin{aligned} E_{\sigma\sigma'}(\hat{\omega},\hat{\omega}') &= -\int d\mathbf{r}' f_{\sigma\sigma'}(\mathbf{r},\hat{\omega};\mathbf{r}',\hat{\omega}') \\ &= L_\sigma L_{\sigma'}(D_\sigma + D_{\sigma'})|\sin\varphi| \end{aligned} \tag{4.5}$$

in terms of the angle φ between $\hat{\omega}$ and $\hat{\omega}'$, i.e., $\varphi = \arccos(\hat{\omega}\cdot\hat{\omega}')$. Note that additional $O(LD^2)$ terms are being ignored in Eq. (4.4), in line with the needle limit ($D_\sigma/L_{\sigma'} \to 0$) of interest here.

At sufficiently low $\{\beta\mu_\sigma\}$ the only stable solution of Eq. (4.4) is the isotropic distribution $\rho_\sigma^I(\hat{\omega}) = n_\sigma/(4\pi)$, with $n_\sigma = \int d\hat{\omega}\rho_\sigma(\hat{\omega})$ the bulk number density of species σ. As μ_σ are high enough, one or possibly two sets of stable uniaxial solutions $\rho_\sigma^N(\hat{\omega}) = \rho_\sigma(\theta)$ exist, with $\theta = \arccos(\hat{\omega}\cdot\hat{n})$ the angle between $\hat{\omega}$ and the nematic director $\hat{n}$. These distributions have "up-down" symmetry, $\rho_\sigma(\theta) = \rho_\sigma(\pi-\theta)$, hence $\rho_\sigma(\theta)$ needs only to be determined for $\theta \in [0,\pi/2]$. In our calculations we use a nonequidistant θ-grid, with the $3N_\theta/4$ points distributed in the interval $[0,\pi/4]$ and the other $N_\theta/4$ in the rest, in order to improve resolution close to the orientation of the nematic director $\hat{n}$. It will be demonstrated in Chapter 7 that the accuracy of the orientational discretization may significantly influence the resulting bulk orientation distributions: a rough θ grid promotes the appearance of an artificial (almost) perfectly aligned nematic phase. We have checked in particular that our numerical schemes do not induce such artefacts within the studied range of parameters. Using the θ-grid of $N_\theta = 30$ points $\theta_i \in [0,\pi/2]$, where $1 \le i \le N_\theta$, we iteratively solve Eq. (4.4) for the set of $2N_\theta$ equations in order to find $\rho_\sigma(\theta_i)$ numerically. The integral in Eq. (4.4) is calculated with the trapezoidal rule. Coexistence of different phases $\{I, N_1, N_2\}$ can be determined by imposing conditions of mechanical and chemical equilibrium.

In order to gauge the accuracy of the chosen θ-grid we calculate the resulting densities of the coexisting isotropic and nematic phase of the one-component system. We find $n^I L^2 D(\pi/4) = 3.281\pm0.001$, $n^N L^2 D(\pi/4) = 4.172\pm0.001$; the nematic order parameters of the two coexisting phases are $S^I = 0.008\pm0.001$ and $S^N = 0.791\pm0.001$, and the pressure $(\pi/4)\beta p L^2 D = 14.045 \pm 0.001$. These data, based on $N_\theta = 30$, differ by less then a percent from the most accurate results available in the literature [33], which we can reproduce with $N_\theta \ge 80$, and they are identical to the results presented in Chapter 3. In order to have consistency between bulk and interfacial results we

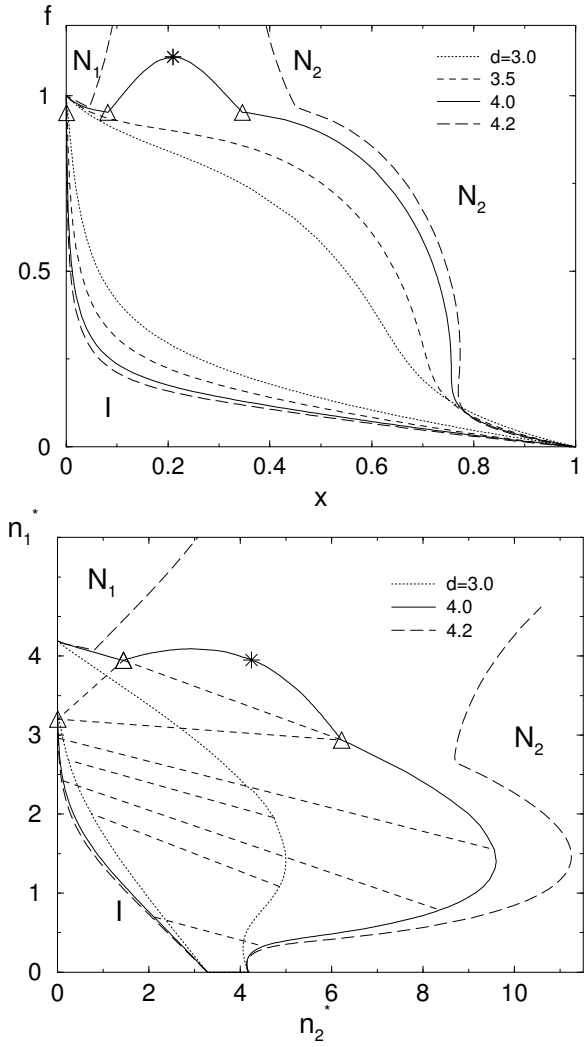

Figure 4.1: (a) Bulk phase diagrams of binary thin-thick mixtures for different diameter ratios d in the $f - x$ representation, with $f = (p - p_{thick})/(p_{thin} - p_{thick})$ the dimensionless shifted pressure, and x the mole fraction of the thicker rods. We distinguish the fully symmetric isotropic phase (I) and orientationally ordered nematic phases (N_1 and N_2). For the diameter ratio $d = 4.0$ the IN_1N_2 triple phase coexistence is marked by ($\triangle$), and the N_1N_2 critical point by ($*$). (b) The same phase diagrams in density-density representation, where $n_1^* = n_1 L D_1^2(\pi/4)$ and $n_2^* = n_2 L D_2^2(\pi/4)$ are the dimensionless bulk number densities of thin and thick rods, respectively. The tie-lines connect coexisting state points.

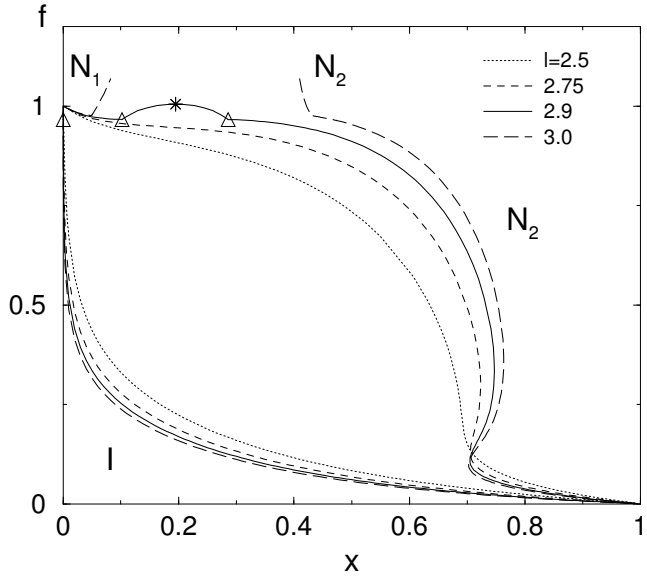

Figure 4.2: Bulk phase diagrams of binary long-short mixtures for different length ratio l in the $f-x$ representation (see caption to Fig. 4.1). The IN_1N_2 triple phase coexistence is marked by ($\triangle$), and ($*$) marks the N_1N_2 critical point for $l = 2.9$.

take $N_\theta = 30$ in most of the calculations. The exception is the case of long-short mixtures in the nematic phase, which requires $N_\theta = 50$ for acceptable accuracy.

In Fig. 4.1 we show both pressure-composition (a) and density-density (b) representations of bulk phase diagrams of thin-thick binary mixtures ($L_\sigma = L, D_2 > D_1$) for several diameter ratios $d \equiv D_2/D_1$. In Fig. 4.1(a) the composition variable $x = n_2/(n_1+n_2)$ denotes the mole fraction of thick rods and $f = (p-p_{thick})/(p_{thin}-p_{thick})$ is a dimensionless shifted pressure which takes the values $f = 1$ and 0 at isotropic-nematic coexistence of the pure-thin ($x = 0$) and pure-thick ($x = 1$) systems, respectively. Note that $(\pi/4)\beta p_{thin}L^2D_1 = (\pi/4)\beta p_{thick}L^2D_2 = 14.045$, i.e., $p_{thick} = p_{thin}/d$, and that the tie-lines connecting coexisting phases are horizontal in the $f-x$ representation of Fig. 4.1(a).

At low pressures (or low densities) the phase diagrams show an isotropic (I) phase and at higher pressures (or densities) one ($d = 3.0, 3.5$) or two ($d = 4.0, 4.2$) nematic phases (N_1 and N_2). For diameter ratios $d = 3.0, 3.5$ the phase diagram is spindle-like, and the only feature is a strong fractionation at coexistence, such that the nematic phase is relatively rich in thick rods and the isotropic phase in thin ones. The reason behind this fractionation is the relatively large excluded-volume interactions of the thick rods, which makes them more susceptible to orientational ordering [22, 23, 40]. The fractionation at isotropic-nematic coexistence becomes stronger for increasing d. For $3.8 < d < 4.29$ the bulk phase diagram develops nematic-nematic (N_1N_2)

coexistence in a pressure regime $p_t < p < p_c$, with p_t the triple-point pressure and p_c the critical (consolute) pressure. For $d = 4.0$ the consolute point is indicated by $(*)$ in Fig. 4.1. The mechanism of this demixing transition was spelled out in detail in Refs. [37, 40], and involves a competition between orientational entropy (favoring demixing) and entropy of mixing (favoring mixing). Interestingly, the width of the fractionation gap $\Delta x = x_{N_1} - x_{N_2}$ for the triple point N_1 and N_2 phases scales linearly with the triple-point pressure p_t. The critical pressure of the N_1N_2 transition diverges as $d \to 4.29$ [37, 40]. For $d > 3.8$ the lower bound of the N_1N_2 coexistence is an IN_1N_2 triple point, indicated by triangles ($\triangle$) in Fig. 4.1 for $d = 4.0$. With increasing d the triple point I and N_1 phases approach the pure-thin bulk coexistence (i.e., $x_{I,N_1} \to 0$), whereas the composition of the triple point N_2 phase shifts to a pure-thick phase ($x_{N_2} \to 1$).

The $f - x$ representation is convenient for the present analysis, whereas the densities (volume fractions) of thin and thick rods are the natural experimental parameters [46]. For this reason the same phase diagrams of thin-thick binary mixtures are shown in Fig. 4.1(b) in density-density representation, with $n_1^* = n_1 L D_1^2(\pi/4)$ and $n_2^* = n_1 L D_2^2(\pi/4)$ being the dimensionless bulk number densities of thin and thick rods, respectively. In this representation the tie-lines are no longer horizontal.

In Fig. 4.2 a set of bulk phase diagrams for long-short binary mixtures ($D_\sigma = D, L_2 > L_1$) for several length ratios $l \equiv L_2/L_1$ is presented. Here $x = n_2/(n_1 + n_2)$ denotes the fraction of long rods and $f = (p - p_{long})/(p_{short} - p_{long})$ with $p_{long} = p_{short}/l^2$. All characteristic features of the phase diagrams are the same as in thin-thick mixtures. The fractionation of the coexisting IN_2 and N_1N_2 phases has a strong dependence on l, and limits the values accessible for calculations to $l \leq 3.1$ for the chosen grids and the required accuracy. The main reason is that the nematic ordering in the triple point N_2 phase is very pronounced, requiring a fine grid [40].

4.4 Free interfaces

We now turn to the thermodynamics and the structure of the free interfaces between the coexisting phases. We assume that the interfaces are planar, with surface normal $\hat{z}$. The nematic director $\hat{n}$ of the asymptotic nematic bulk phase(s) can, in general, have a nontrivial tilt angle $\theta_t = \arccos(\hat{n} \cdot \hat{z})$ with respect to the interface normal. In the present calculations we restrict attention to $\theta_t = \pi/2$, i.e., $\hat{n} \perp \hat{z}$. This geometry is known to be thermodynamically favorable because of its minimal surface tension [26, 32].

The equilibrium distribution functions $\rho_\sigma(z, \hat{\omega})$ depend on the spatial coordinate $z = \hat{z} \cdot \mathbf{r}$, and angular coordinates $\hat{\omega} = (\theta, \varphi)$ defined by $\cos\theta = \hat{n} \cdot \hat{\omega}$ and $\sin\theta \sin\varphi = \hat{z} \cdot \hat{\omega}$. These functions are solutions of the Euler-Lagrange equations (4.2) at the coexisting chemical potentials $\beta\mu_\sigma = \beta\mu_\sigma^{coex}$, with boundary conditions $\rho_\sigma(z \to \pm\infty, \hat{\omega}) = \rho_\sigma^{(\pm)}(\theta)$ being the two coexisting bulk distributions (labelled by $(+)$ and $(-)$ here for brevity).

The planar symmetry, i.e., the independence of $\rho_\sigma(z,\hat{\omega})$ of the in-plane coordinates x and y, allows for a reduction of the numerics, since the "excluded slab" $\mathcal{K}_{\sigma\sigma'}(z,\hat{\omega},z',\hat{\omega}') = -\int dx'dy' f_{\sigma\sigma'}(\mathbf{r},\hat{\omega};\mathbf{r}',\hat{\omega}')$ can be calculated analytically [34, 44]. This reduces the Euler-Lagrange equations to

$$\begin{aligned}\beta\mu_\sigma^{coex} &= \ln[\rho_\sigma(z,\hat{\omega})L_\sigma^2 D_\sigma] \\ &\quad + \sum_{\sigma'}\int dz' \int d\hat{\omega}' \mathcal{K}_{\sigma\sigma'}(|z-z'|,\hat{\omega},\hat{\omega}')\rho_{\sigma'}(z',\hat{\omega}'). \end{aligned} \tag{4.6}$$

The expression for $\mathcal{K}_{\sigma\sigma'}(|z|,\hat{\omega},\hat{\omega}')$ is taken from Ref. [34] in the limit $D_\sigma/L_\sigma \to 0$. In terms of $A = \frac{1}{2}\max(L_\sigma\hat{\omega}\cdot\hat{z}, L_{\sigma'}\hat{\omega}'\cdot\hat{z})$, $B = \frac{1}{2}\min(L_\sigma\hat{\omega}\cdot\hat{z}, L_{\sigma'}\hat{\omega}'\cdot\hat{z})$ and the excluded volume $E_{\sigma\sigma'}(\hat{\omega},\hat{\omega}') = L_\sigma L_{\sigma'}(D_\sigma + D_{\sigma'})|\sin(\arccos(\hat{\omega}\cdot\hat{\omega}'))|$, it can be written as

$$\mathcal{K}_{\sigma\sigma'}(|z|,\hat{\omega},\hat{\omega}') = \begin{cases} 0, & |z| > |A|+|B|, \\ \dfrac{E_{\sigma\sigma'}(\hat{\omega},\hat{\omega}')}{4|AB|}(|A|+|B|-|z|), & |A|-|B| \le |z| \le |A|+|B|, \\ \dfrac{E_{\sigma\sigma'}(\hat{\omega},\hat{\omega}')}{2|A|}, & |z| \le |(|A|-|B|)|. \end{cases} \tag{4.7}$$

In principle one could now solve Eq. (4.6) on a (z,θ,φ) grid. However, the numerical effort can be further reduced if one realizes that the biaxiality, i.e., the φ-dependence, is weak [27, 44]. In that case the truncated expansion

$$\rho_\sigma(z,\theta,\varphi) = \sum_{m=0}^{M} \rho_{\sigma,m}(z,\theta)\cos(2m\varphi) \tag{4.8}$$

is expected to be accurate for small M, and hence only a few "coefficients" $\rho_{\sigma,m}(z,\theta)$ ($m \le M$) need to be determined on a (z,θ)-grid. It is important to realize, however, that Eq. (4.8) assumes implicitly that the nematic director $\hat{n}$ does not vary in space. The coefficients $\rho_{\sigma,m}(z,\theta)$ follow from an insertion of Eq. (4.8) into Eq. (4.6), multiplication by $\cos(2m\varphi)$, and integration over φ ($0 \le \varphi \le 2\pi$). For $M = 0$ this yields

$$\begin{aligned}\beta\mu_\sigma^{coex} &= \ln[\rho_{\sigma,0}(z,\theta)L_\sigma^2 D_\sigma] \\ &\quad + \sum_{\sigma'}\int dz'd\theta' \sin\theta' \mathcal{K}^{00}_{\sigma\sigma'}(z-z',\theta,\theta')\rho_{\sigma',0}(z',\theta'), \end{aligned} \tag{4.9}$$

where $\mathcal{K}^{00}_{\sigma\sigma'}(z-z',\theta,\theta') = (2\pi)^{-1}\int_0^{2\pi}\int_0^{2\pi} d\varphi d\varphi' \mathcal{K}_{\sigma\sigma'}(z-z',\hat{\omega},\hat{\omega}')$ is the doubly azimuthally integrated excluded slab, which we determine numerically once on an appropriate grid.

The lowest-order correction that takes into account biaxiality results from $M = 1$, and yields $\rho_{\sigma,m}(z,\theta)$, $(m = 0, 1)$ from the coupled set of equations

$$\begin{aligned}
\beta\mu_\sigma^{coex} &= \ln[\rho_{\sigma,0}(z,\theta)L_\sigma^2 D_\sigma] + I_0\left(\frac{\rho_{\sigma,1}(z,\theta)}{\rho_{\sigma,0}(z,\theta)}\right) \\
&\quad + \sum_{\sigma'}\int dz'd\theta' \sin\theta' \Big(\mathcal{K}^{00}_{\sigma\sigma'}(z-z',\theta,\theta')\rho_{\sigma',0}(z',\theta') \\
&\quad + \mathcal{K}^{01}_{\sigma\sigma'}(z-z',\theta,\theta')\rho_{\sigma',1}(z',\theta')\Big), \\
0 &= I_1\left(\frac{\rho_{\sigma,1}(z,\theta)}{\rho_{\sigma,0}(z,\theta)}\right) + \sum_{\sigma'}\int dz'd\theta' \sin\theta' \Big(\mathcal{K}^{10}_{\sigma\sigma'}(z-z',\theta,\theta')\rho_{\sigma',0}(z',\theta') \\
&\quad + \mathcal{K}^{11}_{\sigma\sigma'}(z-z',\theta,\theta')\rho_{\sigma',1}(z',\theta')\Big), \qquad (4.10)
\end{aligned}$$

with $\mathcal{K}^{km}_{\sigma\sigma'}(z-z',\theta,\theta') = (2\pi)^{-1}\int_0^{2\pi}\int_0^{2\pi} d\varphi d\varphi' \cos(2k\varphi)\cos(2m\varphi')\mathcal{K}_{\sigma\sigma'}(z-z',\hat{\omega},\hat{\omega}')$, $k, m = \{0, 1\}$, again to be determined numerically only once, with

$$\begin{aligned}
I_0(x) &= \frac{1}{2\pi}\int_0^{2\pi} d\varphi \ln\big(1 + x\cos(2\varphi)\big) = \ln\frac{1+\sqrt{1-x^2}}{2}, \\
I_1(x) &= \frac{1}{2\pi}\int_0^{2\pi} d\varphi \cos(2\varphi)\ln\big(1 + x\cos(2\varphi)\big) = \frac{1-\sqrt{1-x^2}}{x},
\end{aligned}$$

for $|x| < 1$.

Note that the boundary conditions imply that $\rho_{\sigma,1}(z,\theta) \to 0$ for $|z| \to \infty$. In general, the solutions $\rho_{\sigma,0}(z,\theta)$ for $M = 0$ are not identical to $\rho_{\sigma,0}(z,\theta)$ for $M = 1$, but the difference is small in most cases since $|\rho_{\sigma,1}(z,\theta)L_\sigma^2 D_\sigma| \ll 1$. In the remainder of this Chapter we shall mainly concentrate on solutions of Eq. (4.9), although some results of Eqs. (4.10) will be discussed.

By iteration of Eq. (4.9) (or Eqs. (4.10)) with the appropriate boundary conditions we calculated the equilibrium distributions $\rho_{\sigma,0}(z,\theta)$ (and $\rho_{\sigma,1}(z,\theta)$) for a number of state points μ_σ^{coex} on the IN_1, IN_2 and N_1N_2 binodals. We used an equidistant spatial grid of $N_z = 200$ points $z_i \in [-5L, 5L]$, an angular grid of $N_\theta = 30$ points $\theta_j \in [0, \pi/2]$ for thin-thick mixtures or an angular grid of $N_\theta = 50$ points $\theta_j \in [0, \pi/2]$ for long-short mixtures. From the equilibrium distributions $\rho_{\sigma,0}(z,\theta)$ we calculated the local density and the nematic order parameter profiles

$$\begin{aligned}
n_\sigma(z) &= 4\pi\int_0^{\pi/2} d\theta \sin\theta\rho_{\sigma,0}(z,\theta) \\
S_\sigma(z) &= 4\pi\int_0^{\pi/2} d\theta \sin\theta P_2(\cos\theta)\rho_{\sigma,0}(z,\theta)/n_\sigma(z),
\end{aligned}$$

with $P_2(x) = (3x^2 - 1)/2$ the second Legendre polynomial. In the case of iterating

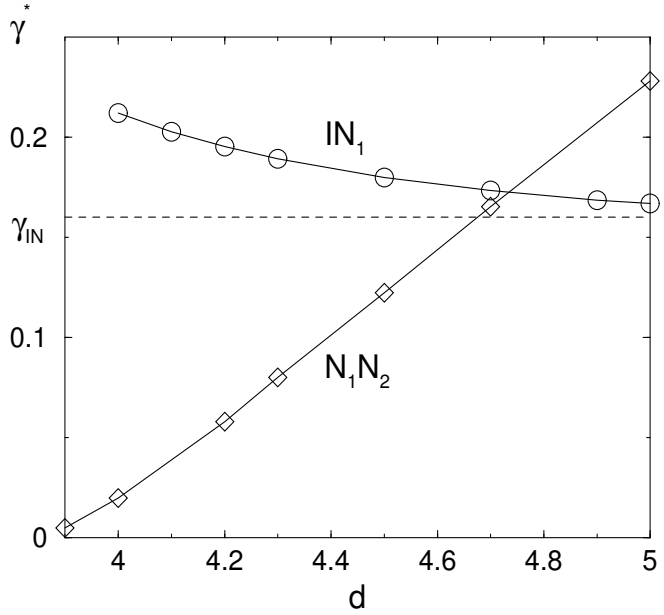

Figure 4.3: Dimensionless surface tension $\gamma^* = \beta\gamma LD_1$ of IN_1 ($\circ$) and N_1N_2 ($\diamond$) interfaces at triple phase coexistence ($p = p_t$) for different diameter ratio d of thin-thick mixtures. The dashed line corresponds to the surface tension of the one-component IN interface for which $\gamma^*_{IN} = 0.156 \pm 0.001$, as it was demonstrated in Chapter 3 and in Ref. [44].

Eqs. (4.10) the biaxiality is defined as [27, 44]

$$\begin{aligned} \Delta_\sigma(z) &= \left\langle \frac{3}{2}\sin^2\theta\cos 2\varphi \right\rangle_\sigma \\ &= \frac{3}{4n_\sigma(z)}\int_0^{\pi/2} d\theta \sin^3\theta \rho_{\sigma,1}(z,\theta). \end{aligned}$$

The interface thickness t is defined as $t = |z_+ - z_-|$ where $z_\pm$ are solutions of ${n_1}'''(z) = 0$, where a prime denotes differentiation with respect to z. As this equation has a set of solutions in every interfacial region, we choose $(z_\pm)$ to be the outermost ones, i.e., the nearest to the bulk phases. This criterion provides a single measure for the thickness of both monotonic and non-monotonic profiles, with and without a thick film in between the asymptotic bulk phases at $z \to \pm\infty$. Also thin (or short) rods have a smaller excluded volume and a non-vanishing concentration in both coexisting phases, so their density is a convenient representation of structural changes within the interface. The interfacial width for the one-component IN interface is, with the present definition, given by $t/L = 0.697$. We have checked that other definitions of the thickness lead to similar results.

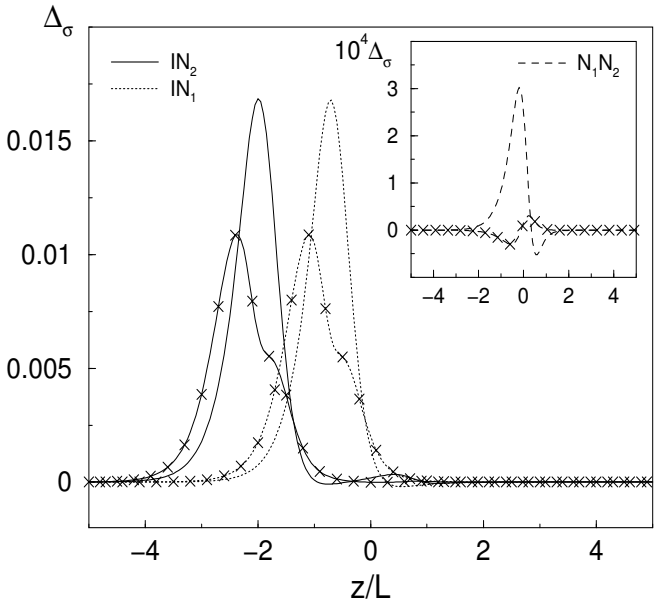

Figure 4.4: Biaxiality profiles $\Delta_\sigma(z)$ of the thin (without symbols) and thick (marked by $\times$) rods in the IN_1 and IN_2 (at undersaturation $\epsilon = 5 \cdot 10^{-4}$) interfaces for the diameter ratio $d = 4.0$. The inset shows the same quantity for the N_1N_2 interface.

4.4.1 IN_1 and N_1N_2 interfaces

The IN_1 interfaces exist only in a small pressure regime $p_{thin} \geq p \geq p_t$ for mixtures with the diameter ratio $d > 3.8$ or length ratio $l > 2.75$. They closely resemble the IN interface of the pure hard-rod fluid, i.e., the profiles of the order parameters $S_\sigma(z)$ and the densities $n_\sigma(z)$ change monotonically from the bulk values in the I phase to those in the N_1 phase. The thickness of the IN_1 interface is of order L which is similar to that of the pure system. With increasing d the IN_1 surface tension at triple phase coexistence ($p = p_t$) decreases monotonically to the IN surface tension of the pure system, as shown in Fig. 4.3, where the dimensionless surface tension $\gamma^* = \beta\gamma LD_1$ is plotted. This is expected from an inspection of the phase diagrams as $x_{I,N_1} \to 0$ for increasing d. For the diameter ratio $d = 4.0$ the surface tension at $p = p_t$ is given by $\gamma^*_{IN_1} = 0.209 \pm 0.001$ with the same level of accuracy for all other calculations of the surface tensions. For the long-short mixtures the behavior of the surface tension at the IN_1 interface as a function of length ratio l is very similar. For $l = 3.0$ the surface tension at $p = p_t$ is given by $\gamma^*_{IN_1} = 0.212 \pm 0.001$.

In general, the order parameter and density profiles are shifted with respect to each other. Such a shift can be characterized by the distance $\delta = |z_n - z_S|$ between

the centers z_n and z_S of the density and order parameter profiles, defined by [26]

$$n(z_n) = \frac{n_+ + n_-}{2}, \quad S(z_S) = \frac{S_+ + S_-}{2},$$

where $+/-$ indicate asymptotic bulk values. A nonzero shift δ reflects the fact that the thickness of the interface is different for rods of different orientations. For monodisperse rods it was found that $\delta = 0.45L$ [26]. For binary mixtures δ can be determined for each component separately. For thin-thick mixtures with $d = 4.0$ the IN_1 interface at triple phase coexistence shows $\delta_{thin} = 0.35L$ and $\delta_{thick} = 0.55L$. For long-short mixtures with $l = 3.0$ the effect is similar for the short rods ($\delta_{short} = 0.37L_1$) and much more pronounced for the long rods ($\delta_{long} = 1.54L_1$, i.e., $\delta_{long} \simeq 0.51L_2$).

The profiles of $S_\sigma(z)$ and $n_\sigma(z)$ at N_1N_2 interfaces are also monotonic. For the diameter ratio $d = 4.0$ at $p = p_t$ the interface thickness is given by $t/L = 0.592$ and the surface tension $\gamma^*_{N_1N_2} = 0.019 \pm 0.001$, which is an order of magnitude smaller than $\gamma^*_{IN_1}$. Upon the approach of the critical point $t/L \to \infty$ and the surface tension vanishes. For $d > 4.0$ the surface tension $\gamma^*_{N_1N_2}$ (at $p = p_t$) increases approximately linearly with d as shown in Fig. 4.3.

The biaxiality is found to be small in both the IN_1 and the N_1N_2 interfaces. In Fig. 4.4 we present the profiles $\Delta_\sigma(z)$ of the triple point IN_1 and N_1N_2 (inset) interfaces of the thin-thick mixture with $d = 4.0$, as well as that of the IN_2 interface to be discussed later. The marked curves represent $\Delta_2(z)$ (thick rods), the unmarked ones $\Delta_1(z)$ (thin rods). Figure 4.4 reveals that $|\Delta_\sigma(z)| < 0.017$ in the IN_1 interface, and $|\Delta_\sigma(z)| < 4 \cdot 10^{-4}$ in the N_1N_2 interface. Such small biaxialities indicate that the expansion of Eq. 4.8, truncated at $M = 1$, is accurate for calculating $\Delta_\sigma(z)$, while a truncation at $M = 0$ yields accurate tensions and density profiles. In fact, we checked that the difference between the tensions based on uniaxial ($M = 0$) and biaxial ($M = 1$) profiles falls within the numerical accuracy, i.e., it is less than 1%. Numerical data for the IN_1 interface are consistent with that of Ref. [27, 44]. Even though the magnitude of $\Delta_\sigma(z)$ is small, it is interesting to consider the structure of the profiles in some more detail. The first observation we make is that $\Delta_\sigma(z) > 0$ (< 0) at the isotropic (nematic) side of the IN_1 interface for both species $\sigma = 1, 2$. This indicates that rods at the I-side of the interface have a (small) preference for splay in the XY-plane, whereas those at the N_1 side tend to "stick" through the interface (into the I side). A similar effect exists in the N_1N_2 interface, but now both species have an opposite tendency (see inset): the thin rods splay in the XY plane at the N_1 side, whereas the thick ones "stick" through, and vice versa at the N_2 side. Recall, however, that these effects are small.

4.4.2 IN_2 interfaces

The IN_2 interfaces exist, for $d > 3.8$, in a pressure regime $p_{thick} < p < p_t$. The properties of the IN_2 interfaces depend strongly on the pressure difference with the triple-point (IN_1N_2 phase coexistence). The surface tension of the IN_2 interface

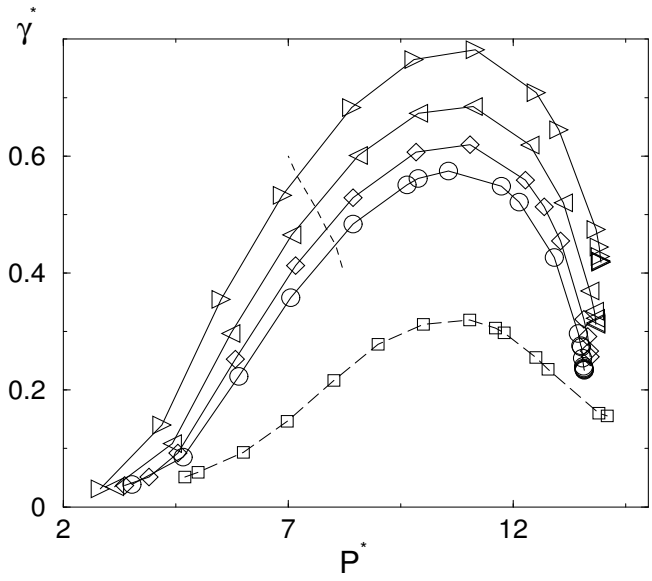

Figure 4.5: Dimensionless surface tension $\gamma^*_{IN_2} = \beta\gamma_{IN_2}LD_1$ of IN_2 interfaces as a function of dimensionless pressure $p^* = \beta pL^2D_1(\pi/4)$ for different diameter ratio $d = 4.0(\circ)$, $4.2(\diamond)$, $4.5(\triangleleft)$, $5.0(\triangleright)$ of thin-thick mixtures. The dashed line indicates the pressure of maximum fractionation. The data for $d = 3.0(\square)$ are included for comparison.

shows a non-monotonic dependence on the bulk pressure p. It develops a maximum, which is several times larger than a linear interpolation between the tension of the two pure systems, as shown in Fig. 4.5. It turns out that the non-monotonic character of $\gamma_{IN_2}(p)$ is related to the fractionation at the IN_2 coexistence, i.e., a larger composition change through the interface leads to a larger interfacial tension. However, the surface tension which corresponds to the pressure of maximal bulk fractionation (indicated by the dashed line in Fig. 4.5) is lower than the maximum of $\gamma_{IN_2}(p)$. The maximal interface stiffness grows with species diameter ratio d as the composition difference between I and N_2 phases increases (see Fig. 4.1). We have also compared the maximal surface tensions for different orientations of the director ($\hat{n} \perp \hat{z}$ and $\hat{n} \parallel \hat{z}$) in several thin-thick mixtures and found the geometry $\hat{n} \perp \hat{z}$ to be thermodynamically stable, i.e., $\gamma_{\hat{n}\perp\hat{z}} < \gamma_{\hat{n}\parallel\hat{z}}$ by at least a factor of two.

The relatively large surface tension of a mixture of rods compared to that of the pure systems of its components may well be an explanation for the relatively large tensions that were measured in suspensions of cellulose [47], which are known to be very polydisperse. This remains to be investigated in detail, however.

The dimensionless undersaturation $\epsilon = 1 - p/p_t$ is a convenient measure of the pressure difference with the triple point. For $0.01 < \epsilon < 0.5$ the profiles of the order parameters $S_\sigma(z)$ and the density of the thick component $n_2(z)$ are smooth and

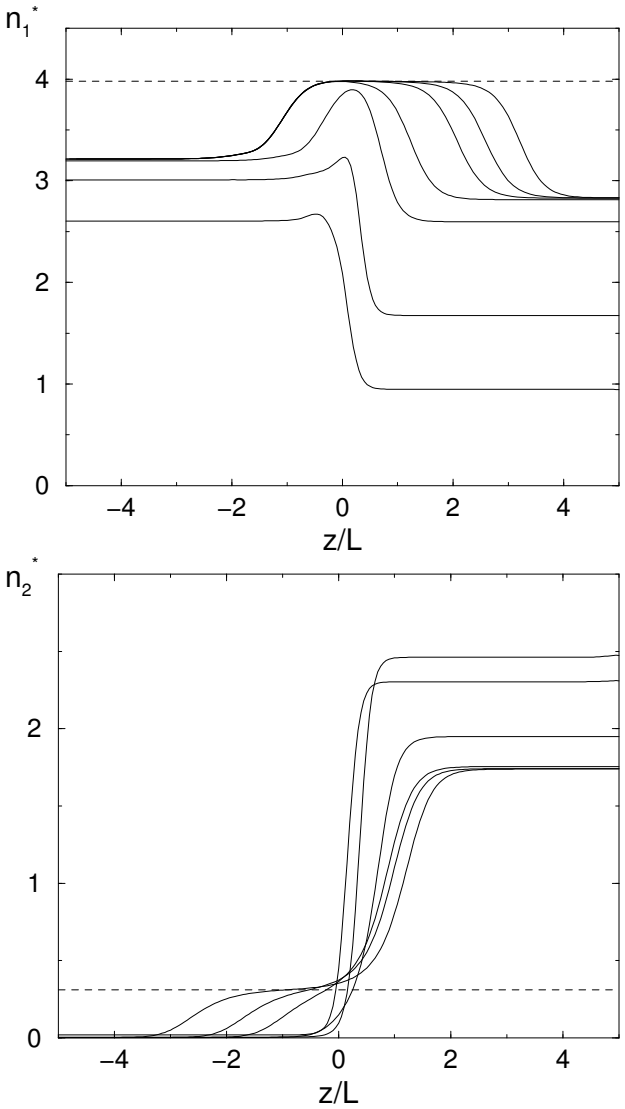

Figure 4.6: Density profiles of the thin rods $n_1^*(z)$ (a) and the thick rods $n_2^*(z)$ (b) in the IN_2 interface for diameter ratio $d = 4.0$ at triple point undersaturations $\epsilon = 1 - p/p_t = 0.29, 0.1, 0.01, 5 \times 10^{-4}, 1.3 \times 10^{-4}, 2.5 \times 10^{-5}$. The bulk I/N_2 phase is at $z \to -\infty/\infty$. The dashed lines $n_1^* = 3.977$ and $n_2^* = 0.312$ represent the bulk density of thin (thick) rods in the triple point N_1 phase. These profiles indicate the formation of a wetting N_1 film in the IN_2 interface.

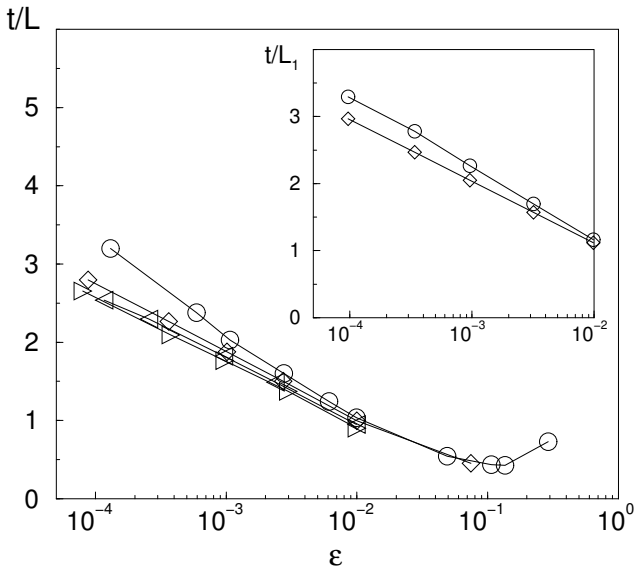

Figure 4.7: Thickness t/L as a function of the undersaturation $\epsilon = 1 - p/p_t$ from the triple point pressure p_t for diameter ratios $d = 4.0(\circ), 4.2(\diamond), 4.5(\triangleleft), 5.0(\triangleright)$ of thin-thick mixtures. The inset shows the film thickness t/L_1 for long-short mixtures with length ratio $l = 3.0(\circ), 3.1(\diamond)$.

monotonic, whereas $n_1(z)$ shows an accumulation of thin rods at the isotropic side of the interface. This effect becomes more pronounced for small undersaturation, i.e., $\epsilon \to 0$, when a film of the nematic phase N_1 appears in the IN_2 interface. Note that the N_1 phase is a metastable bulk phase for any $\epsilon > 0$, so the film thickness is finite. For $d = 4.0$ several profiles $n_1(z)$ and $n_2(z)$ for different values of ϵ are presented in Fig. 4.6, which clearly shows the film formation when $\epsilon \to 0$.

The asymptotic densities at $z \to \pm\infty$ are those of the coexisting I and N_2 bulk phases (at the corresponding ϵ). Using translational invariance of the interface between the bulk phases, we have shifted the profiles with respect to each other such that their IN_1 interfaces coincide. This shows that the local density of thin (thick) rods in the growing film remains constant, and exactly corresponds to the thin (thick) -rod density of the bulk triple point phase N_1 (indicated by the dashed lines in Fig. 4.6). The same identification can be made for all d (or l for long-short mixtures) as well as for the order parameter profiles $S_\sigma(z)$.

The biaxiality of the IN_2 interface was found to be small. A typical profile for thin-thick binary mixture with $d = 4.0$ at $\epsilon = 5 \cdot 10^{-4}$ is presented in Fig. 4.4. The IN_2 biaxiality profile can be considered as a composition of the (earlier discussed) IN_1 and N_1N_2 profiles which is expected as the thickness of the wetting N_1 film is larger than L.

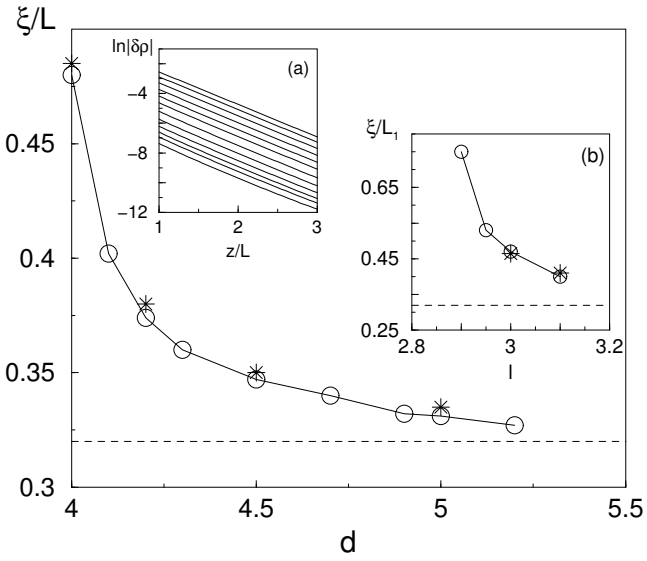

Figure 4.8: Correlation length for rods in the triple-point N_1 phase of thin-thick mixtures as a function of diameter ratio d, determined from adsorption ($*$) analysis (Eq. 4.11) and from density asymptotics ($\circ$) (Eq. 4.12). Inset (a) shows $\ln|\delta\rho(z,\theta)|$ for several values of θ at the N_1 side of the IN_1 interface for $d = 4.0$. Inset (b) displays the correlation length (in units of length of short rods L_1) for long-short mixtures as a function of length ratio l. The dashed lines indicate the correlation length for rods in the N phase of the monodisperse hard-rod fluid.

For all explored mixtures the thickness of the interface t/L (or the adsorption) was found to diverge logarithmically with $\epsilon \to 0$ as shown in Fig. 4.7. For short-ranged interactions one expects, on the basis of mean-field theory [14], that

$$t = -\xi \ln(\epsilon) + C, \tag{4.11}$$

where C is an irrelevant constant offset, and ξ is the correlation length of the phase that forms the wetting film. This implies that the bulk correlation length ξ_{N_1} of the wetting N_1 phase can be determined from the slope of the logarithmic growth of t/L in Fig. 4.7.

The asterisks ($*$) in Fig. 4.8 show the resulting values of ξ_{N_1} as a function of d. These can be compared to the correlation length that one can extract from the asymptotic decay of the one-particle distributions $\rho_\sigma(z,\hat{\omega})$ of the triple-point IN_1 interface into the bulk N_1 phase. This decay can best be analyzed in terms of the deviation from the N_1 bulk density $\delta\rho_\sigma(z,\hat{\omega}) = \rho_\sigma(z,\hat{\omega}) - \rho_\sigma^{N_1}(\hat{\omega})$, which we find to decay as

$$\delta\rho_\sigma(z,\hat{\omega}) = A_\sigma(\hat{\omega}) \exp(-z/\xi_{N_1}), \quad z \to \infty, \tag{4.12}$$

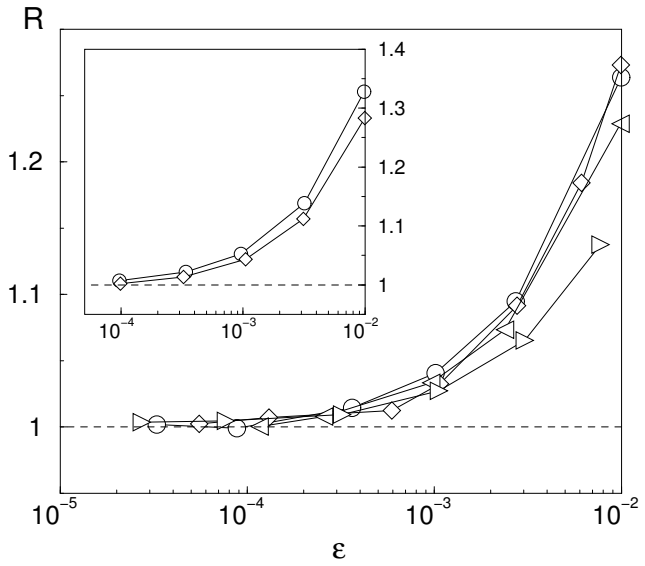

Figure 4.9: Surface tension ratio R [see Eq. (4.13)] as a function of the triple point undersaturation ϵ for diameter ratio $d = 4.0(\circ), 4.2(\diamond), 4.5(\triangleleft), 5.0(\triangleright)$. The inset shows the same quantity for long-short mixtures $l = 3.0(\circ), 3.1(\diamond)$.

where the only species and orientation dependence is in the decay amplitude $A_\sigma(\hat{\omega})$, i.e., the decay (correlation) length ξ is one and the same for all species and orientations. Such a "decay-law", with a single correlation length, is well-known in mixtures of simple liquids [35]. The form (4.12) is illustrated for $d = 4.0$ at $p = p_t$ in the inset (a) of Fig. 4.8, where all curves (representing different θ's) are parallel on a logarithmic scale. The correlation length follows from the (common) slope of these curves, and is marked by $(\circ)$ in the main figure. The agreement with the values of ξ_{N_1} obtained from the logarithmic growth of the interface thickness is clearly good. The inset (b) of Fig. 4.8 shows the similar dependence of the bulk correlation length of the triple-point N_1 phase in the case of long-short mixtures, i.e., as a function of the length ratio l of the two rod species, using the same symbols.

In order to verify the thermodynamic condition of complete wetting, $\gamma_{IN_2} = \gamma_{IN_1} + \gamma_{N_1N_2}$ at the triple-point pressure $p = p_t$, we determine the ratio of surface tensions

$$R(\epsilon) = \frac{\gamma_{IN_2}(\epsilon)}{\lim_{p \downarrow p_t}(\gamma_{IN_1} + \gamma_{N_1N_2})}, \tag{4.13}$$

shown in Fig. 4.9.

For all diameter ratios d considered here, $\lim_{\epsilon \to 0} R(\epsilon) = 1$, which implies a vanishing contact angle. This constitutes the thermodynamic proof of complete triple-point wetting in all thin-thick hard-rod mixtures with $d \geq 4$. For mixtures of long-short

rods the behavior of $R(\epsilon)$ is the same, as shown in the inset of Fig. 4.9. A mean-field analysis of the asymptotic behavior of the surface tension ($\epsilon \to 0$) in the case of complete wetting shows that [14]

$$R(\epsilon) - 1 \sim \epsilon^{2-\alpha} \tag{4.14}$$

with the critical exponent $\alpha = 1$. Analysis of the results in Fig. 4.9 gives $\alpha = 1.00 \pm 0.05$ which can be considered as a consistency test of the present mean-field calculations.

4.5 Summary and discussion

In this Chapter we have studied free interfaces in binary mixtures of hard rods of either different diameters or different lengths within Onsager's second virial functional. We focused on diameter ratios $d > 3.8$ (and length ratios $l > 3.0$), for which the bulk phase diagram exhibits an IN_1N_2 triple point, and restricted attention to the case where $\hat{n} \perp \hat{z}$, with $\hat{n}$ the bulk nematic director and $\hat{z}$ the interface normal. This is the thermodynamically most favorable geometry.

We have determined the behavior of the surface tensions of IN_1, N_1N_2 and IN_2 interfaces between coexisting isotropic and nematic phases as a function of the bulk pressure and/or the diameter ratio d or the length ratio l. The tension γ_{IN_1} is always very close to the tension of the pure fluid of thin (or short) rods, and $\gamma_{N_1N_2}$ varies from zero at the consolute N_1N_2 point to values as large as γ_{IN_1} at the triple point for $d \simeq 4 - 5$. The thickness of the IN_1 and N_1N_2 interfaces are always of the order of the lengths of the rods, except close to the N_1N_2 consolute point, of course. The surface tension γ_{IN_2} is found to change non-monotonically with pressure, exhibiting a maximum close to (but not at) that pressure where the bulk fractionation is maximal. This maximal surface tension is considerably larger than that of the pure systems of the components, typically by a factor of order 3-5. The biaxiality was found to be very small in all cases, similar to the findings of Chapter 3 and Refs. [27, 44] for the one-component case. Perhaps the most interesting finding is the phenomenon of complete triple-point wetting of the IN_2 interface by an N_1 film. The thickness of this film is found to diverge as $-\xi \ln(1 - p/p_t)$ when $p \to p_t$, with ξ the correlation length of the bulk N_1 phase, p_t the triple-point pressure, and $p < p_t$ the pressure. The triple-point wetting phenomenon is confirmed by the numerical value of the surface tensions, which satisfy $\lim_{p \uparrow p_t} \gamma_{IN_2}(p) = \gamma_{IN_1}(p_t) + \gamma_{N_1N_2}(p_t)$. Such a complete wetting scenario was found for all diameter ratios $3.9 < d < 5.2$ and length ratios $2.9 < l < 3.1$ studied here. We expect that this finding will also hold for more extreme ratios $d > 5.2$ and $l > 3.1$, which are more difficult to analyze numerically because of the pronounced nematic ordering of the triple-point N_2 phase.

The predicted phenomenon of triple-point wetting may well be observable in the experimental system of bare and PEG-coated fd virus particles [43] mentioned in the Introduction of this Chapter. We hope that this work stimulates further experimental activities in this direction.

Another interesting direction for future theoretical work would be to consider isotropic-nematic interfaces of polydisperse mixtures, e.g. extending the theory for bulk systems developed in Ref. [48]. For suspensions of length-polydisperse cellulose experimental measurements of the surface tension have been performed [47], and show that the surface tension is much larger than that of a pure system of rods. It is tentative to speculate that the fractionation effect that is also present in binary systems may explain this increase of the tension. We hope to address this question in future work.

Chapter 5

Phase behavior and interfacial properties of nonadditive hard-rod mixtures

Within the Onsager theory we study bulk phase diagrams and free planar isotropic-nematic interfaces of nonadditive binary mixtures of thin and thick hard rods. For species of the same type the excluded volume is determined only by the shape of the particles, whereas for dissimilar rods it is taken to be larger (smaller) then for the pure hard rods. Such a nonadditivity enhances (reduces) fractionation at isotropic-nematic (IN) coexistence and may induce (suppress) a demixing of the high-density nematic phase into two nematic phases of different composition (N_1 and N_2). Studies of interfaces show an increase of the surface tension with fractionation at the IN interface, and complete wetting of the IN_2 interface by the N_1 phase upon approach of the triple point coexistence. In all explored cases bulk and interfacial properties of the nonadditive mixtures exhibit a striking similarity with the properties of additive mixtures of larger diameter ratio.

5.1 Introduction

In his paper about the isotropic-nematic (IN) transition in a solution of monodisperse rod-like particles, Onsager briefly discussed a possible extension of his results to polydisperse systems [11]. Since then, a large amount of work has been devoted to the study of the influence of polydispersity on the phase behavior of hard-rod fluids. Even the simplest mixtures of rods of two different types exhibit rather nontrivial phase diagrams. In addition to the pure isotropic and nematic phases of various composition and regions of their coexistence, the high-density nematic phase can demix (and possibly remix) into two nematic phases (N_1 and N_2) of different composition. The

reason behind the IN transition in binary mixtures is the same as in a monodisperse hard-rod fluids, namely, a competition between orientational entropy and entropy of packing [11, 33]. In contrast, the nematic-nematic demixing does not involve changes in excluded volume (i.e. packing entropy), but rather a competition between orientational entropy and entropy of mixing [37]. Another interesting feature is that for sufficiently large size disparity, the two distinct nematic phases do not remix even at arbitrary high pressure [49].

In general, it is rather difficult to compare these theoretical findings with experiments. Although rod-like particles can be chemically synthesized in various ways [33], typically their size distribution is mono/bidisperse only to a first approximation. By contrast, suspensions of virus particles (TMV, fd) are characterized by a high degree of monodispersity, and are therefore attractive model systems, despite some complicating factors like high surface charge and/or flexibility. Recently several experimental methods to modify the length or the diameter of these viruses have been developed [50]. This opens the possibility to form binary mixtures of a well-defined bidispersity in these systems. In particular, one of the methods is based on altering the effective diameter of the fd-virus by coating it with the polymer PEG [43]. Studies of such binary mixtures of thin and thick rods have revealed coexistence regions of the isotropic and different nematic phases (IN_2 and IN_1), as well as a nematic-nematic coexistence region (N_1N_2) and an IN_1N_2 triple point [51]. Although experiments have confirmed the theoretical predictions regarding the general structure of the phase diagram (see Fig. 4.1 in Chapter 4), one of the experimental findings turns out to be in sharp contrast with the theory. According to the results of Refs. [40, 52], also briefly presented in Chapter 4, mixtures of thin (with diameter D_1) and thick (D_2) rods of equal length L and the diameter ratio $d = D_2/D_1 < 3.8$, exhibit a spindle-like IN coexistence without any nematic-nematic demixing. In the interval $3.8 < d < 4.29$ the single nematic phase demixes into two nematic phases N_1 and N_2 of different composition, which nevertheless remix back at sufficiently high total density (pressure) in the system. Finally, for $d \geq 4.29$ the N_1N_2 phase coexistence remains stable at arbitrary high pressure. Experiments, however, show a broad N_1N_2 coexistence for a diameter ratio as small as $d \sim 3.5$, as well as an almost constant fractionation at the IN coexistence, which is theoretically expected for $d < 2.5$. This suggests to look for some additional factors altering the phase behavior of the mixture.

Possible explanations for the quantitative differences between the experimental phase diagrams and those of the hard-rod mixtures may well be due to the charged nature and the flexibility of the virus particles. However, these effects may be approximately taken into account via introduction of effective hard-core diameters. It is well known, for instance, that the effective diameter of a charged rod can be written as a sum of its hard-core diameter and a term proportional to the Debye-screening length of the suspending medium [53]. For this reason it may yet be possible to approximately describe the system as a hard-rod mixture. However, since the effective rod diameter is determined by soft interactions, different diameters can be assigned to interactions between different species. Such a nonadditivity of the interactions can

be quantified as follows. Whereas the distance of closest approach of the axes of two unlike parallel rods is given by $\frac{1}{2}(D_1 + D_2)$ for additive interactions, it is written as $\frac{1}{2}(D_1 + D_2)(1+\alpha)$ in the case of nonadditive interactions with a so-called nonadditivity parameter α. Studies of the interactions between polymer coated walls [54] as well as studies of the phase behavior of binary mixtures of "hairy" hard rods [55] show that nonadditivity is a relevant factor in these systems. Hence it is not unreasonable to explore an effect of nonadditivity in the present type of systems as well.

Although the microscopic origin of nonadditivity is ultimately based on the more ($\alpha > 0$) or less ($\alpha < 0$) efficient packing of the mixture compared to the pure species, we do not attempt here to calculate α from a microscopic theory. Instead we consider α as a phenomenological parameter of the theory, and investigate its consequences. Of course, this does not imply that all effects of electrostatic interactions, flexibility, etc. are modelled properly now.

Our first goal is to construct bulk phase diagrams of such nonadditive mixtures. Since the methods of analysis turn out to be the same as in studies of the additive binary mixtures of thin and thick rods (see Chapter 4), we also explore the structure of the planar interfaces that exist between the coexisting bulk phases in nonadditive mixtures. As before, we focus on the calculation of both thermodynamic and structural properties of these interfaces. The main thermodynamic quantity of interest is the surface tension γ, and the structural properties we will investigate are the profiles of the density and the order parameters. We will see that interfacial as well as bulk properties of nonadditive mixtures exhibit similarities with those of additive mixtures of thin and thick rods of a more extreme diameter ratio.

This Chapter is organized as follows. In Sec. 5.2 we introduce the Onsager-like functional and the basic Euler-Lagrange equations. In Sec. 5.3 we solve these equations for bulk geometries, and analyze the structure of a few typical bulk phase diagrams. In Sec. 5.4 we briefly quote some changes in a method to solve the Euler-Lagrange equation for interface geometries of binary mixtures, and study IN_1, N_1N_2 and IN_2 interfaces, the latter in particular in the vicinity of the bulk IN_1N_2 triple point. A summary and some discussion of the results will be presented in Sec. 5.5.

5.2 Density functional and method

Consider a fluid of hard cylinders of two different species $\sigma = 1, 2$ of diameter D_σ and equal length L ($D_\sigma/L \to 0$) in a macroscopic volume V at temperature T and chemical potentials μ_σ. Let $\mathbf{r}$ denotes the center-of-mass coordinate of a rod and $\hat{\omega}$ the orientation of the long axis. The interactions between the $\sigma\sigma'$-pair of rods with coordinates $q = \{\mathbf{r}, \hat{\omega}\}$ and $q' = \{\mathbf{r}', \hat{\omega}'\}$ are characterized by a hard-core potential, which is the simple contact potential for rods of the same species ($\sigma = \sigma'$), whereas for unlike rods ($\sigma \neq \sigma'$) it corresponds to interactions between hard rods of diameter $(1 + \alpha)D_1$ and $(1 + \alpha)D_2$. In other words, the distance of closest approach between two parallel rods of different diameters is $\frac{1}{2}(1 + \alpha)(D_1 + D_2)$. The parameter α determines the nonadditivity of the interactions, and for $\alpha = 0$ our

model reduces to the purely additive mixture of thin and thick hard rods, studied in Chapter 4.

Within the second virial approximation and in the absence of external potentials, the grand potential functional $\Omega[\{\rho_\sigma\}]$ of the one-particle distribution functions $\rho_\sigma(\mathbf{r},\hat{\omega})$ can be written [11, 33] as

$$\begin{aligned}\beta\Omega[\{\rho_\sigma\}] &= \sum_\sigma \int dq\rho_\sigma(q)\Big(\ln[\rho_\sigma(q)L^2D_\sigma]-1-\beta\mu_\sigma\Big)\\ &\quad -\frac{1}{2}\sum_{\sigma\sigma'}\int dqdq' f_{\sigma\sigma'}(q;q')\rho_\sigma(q)\rho_{\sigma'}(q'),\end{aligned} \tag{5.1}$$

with $\beta=(k_BT)^{-1}$ the inverse temperature, and $f_{\sigma\sigma'}(q,q')$ the Mayer function, which equals -1 if the rods overlap and vanishes otherwise. Since we consider the limit $D_\sigma/L\to 0$ for any σ, the relative shape disparity of rods is characterized by the ratio $d=D_2/D_1$ of the diameters and the value of the nonadditivity α.

The minimum conditions $\delta\Omega[\{\rho_\sigma\}]/\delta\rho_\sigma(q)=0$ on the functional lead to the set of nonlinear integral equations

$$\ln[\rho_\sigma(q)L_\sigma^2D_\sigma]-\sum_{\sigma'}\int dq' f_{\sigma\sigma'}(q;q')\rho_{\sigma'}(q')=\beta\mu_\sigma \tag{5.2}$$

to be solved for the equilibrium distributions $\rho_\sigma(q)$. These equations are identical to the Euler-Lagrange equations for additive rods mixtures, considered in Chapter 4 (Eqs. (4.2)). Therefore, we can directly apply the method developed there. However, the structure of the bulk phase diagram depends now on the value of the nonadditivity parameter α, and has to be determined first.

Since the bulk distribution functions of the isotropic and nematic phase are translationally invariant, i.e., $\rho_\sigma(\mathbf{r},\hat{\omega})=\rho_\sigma(\hat{\omega})$, we can reduce Eq. (5.2) to

$$\ln[\rho_\sigma(\hat{\omega})L_\sigma^2D_\sigma]+\sum_{\sigma'}\int d\hat{\omega}' E_{\sigma\sigma'}(\hat{\omega},\hat{\omega}')\rho_{\sigma'}(\hat{\omega}')=\beta\mu_\sigma, \tag{5.3}$$

with $E_{\sigma\sigma'}$ the excluded volume of a pair of cylinders of species σ and σ' given by

$$\begin{aligned}E_{\sigma\sigma'}(\hat{\omega},\hat{\omega}') &= -\int d\mathbf{r}' f_{\sigma\sigma'}(\mathbf{r},\hat{\omega};\mathbf{r}',\hat{\omega}')\\ &= L^2(D_\sigma+D_{\sigma'})(1+\alpha(1-\delta_{\sigma,\sigma'}))|\sin\varphi|\end{aligned} \tag{5.4}$$

in terms of the angle φ between $\hat{\omega}$ and $\hat{\omega}'$, i.e., $\varphi=\arccos(\hat{\omega}\cdot\hat{\omega}')$. Note that additional $O(LD^2)$ terms are being ignored in Eq. (5.4), in line with the needle limit ($D_\sigma/L\to 0$) of interest here. Given the linear dependence of the excluded volume on D_σ, one can see that

$$E_{12}(\hat{\omega},\hat{\omega}')=\frac{1}{2}(E_{11}(\hat{\omega},\hat{\omega}')+E_{22}(\hat{\omega},\hat{\omega}'))(1+\alpha). \tag{5.5}$$

In some sense, α plays a similar role in the present context as the so-called χ - parameter in the Flory theory of polymer solutions on a lattice, where demixing is driven by direct unfavorable nearest neighbor interaction between unlike species as compared to that between like species.

Details of the numerical schemes of solving Eq. (5.3) have been discussed in Chapter 4. Here we use a nonequidistant θ-grid of $N_\theta = 30$ points $\theta_i \in [0, \pi/2]$, where $1 \leq i \leq N_\theta$, in order to find the bulk distributions $\rho_\sigma(\theta_i)$. Coexistence of different phases $\{I, N_1, N_2\}$ is determined by imposing conditions of mechanical and chemical equilibrium.

5.3 Bulk phase diagrams

In Fig. 5.1 we show both pressure-composition (a) and density-density (b) representations of bulk phase diagrams of thin-thick binary mixtures ($L_\sigma = L, D_2 > D_1$) for the diameter ratio $d = 3.5$ at various values of the nonadditivity parameter α. In Fig. 5.1(a) the composition variable $x = n_2/(n_1 + n_2)$ denotes the mole fraction of thick rods (as before $n_\sigma = \int d\hat{\omega}\rho_\sigma(\hat{\omega})$), and $p^* = (\pi/4)\beta p L^2 D_1$ is a dimensionless bulk pressure. Note that $(\pi/4)\beta p_{thin} L^2 D_1 = (\pi/4)\beta p_{thick} L^2 D_2 = 14.045$, i.e., $p_{thick} = p_{thin}/d$, and that the tie-lines connecting coexisting phases are horizontal in the $p - x$ representation of Fig. 5.1(a). This representation is convenient for theoretical analysis, whereas the densities (volume fractions) of thin and thick rods are experimental control parameters [46]. For this reason the same phase diagrams of thin-thick binary mixtures are shown in Fig. 5.1(b) in density-density representation, with $n_1^* = n_1 L D_1^2(\pi/4)$ and $n_2^* = n_1 L D_2^2(\pi/4)$ being the dimensionless bulk number densities of thin and thick rods, respectively. In this representation the tie-lines, indicated by the dotted lines, are no longer horizontal.

The structures of the bulk phase diagrams for various α show a striking similarity with the bulk phase diagrams of additive binary mixtures of thin and thick hard rods, presented in Chapter 4 (see Fig. 4.1). At low pressures (or low densities) the phase diagrams show an isotropic (I) phase, and at higher pressures (or densities) one ($\alpha < 0.07$) or two ($\alpha \geq 0.07$) nematic phases (N_1 and N_2). For $\alpha < 0.07$ the phase diagram is spindle-like, and the only feature is a strong fractionation at coexistence, such that the nematic phase is relatively rich in thick rods and the isotropic phase in thin ones. Although the nonadditivity modifies the fractionation gap, the reason behind it remains the same: the relatively large excluded volume in interactions of the thick rods makes them more susceptible to orientational ordering [22, 23, 40]. As a general tendency, the fractionation at isotropic-nematic coexistence becomes stronger for increasing α.

For $\alpha > 0.06$ the bulk phase diagram develops nematic-nematic ($N_1 N_2$) coexistence in a pressure regime $p > p_t$, with p_t the triple-point pressure. Using the simple Gaussian ansatz for one-particle distribution functions, one can demonstrate that the packing entropy does not play a role in nematic demixing in our system, similar to the case of additive mixtures [37]. Although it is known that the functional form of

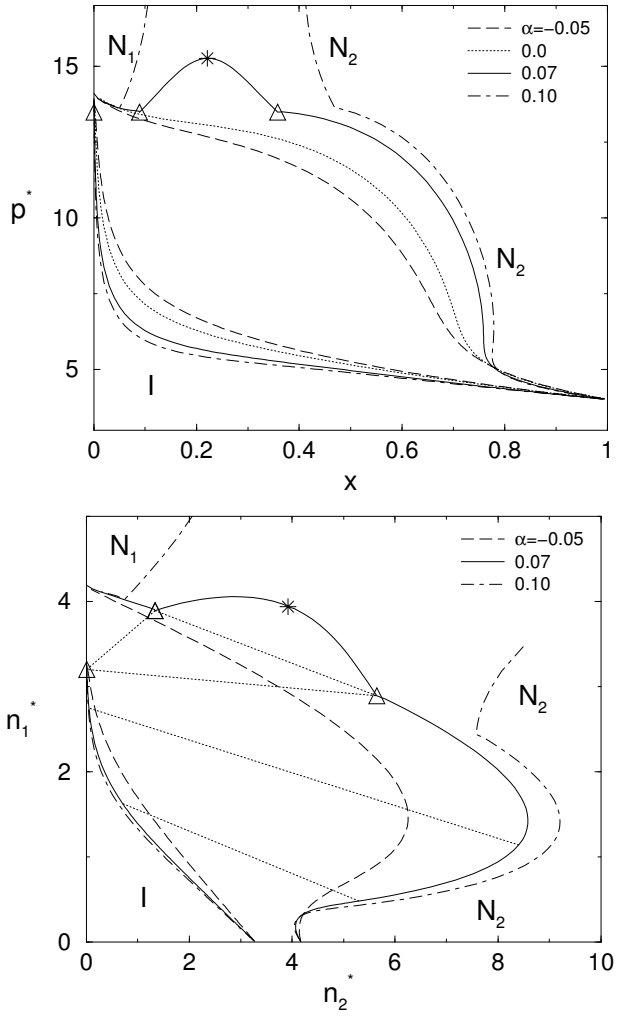

Figure 5.1: (a) Bulk phase diagrams of binary thin-thick mixtures (diameter ratio $d = 3.5$) for different nonadditivity parameter α in the $p - x$ representation, with $p^* = (\pi/4)\beta p L^2 D_1$ the dimensionless pressure, and x the mole fraction of the thicker rods. We distinguish the fully symmetric isotropic phase (I) and orientationally ordered nematic phases (N_1 and N_2). For the nonadditivity parameter $\alpha = 0.07$ the IN_1N_2 triple phase coexistence is marked by ($\triangle$), and the N_1N_2 critical point by ($*$). (b) The same phase diagrams in density-density representation, where $n_1^* = n_1 L D_1^2(\pi/4)$ and $n_2^* = n_2 L D_2^2(\pi/4)$ are the dimensionless bulk number densities of thin and thick rods, respectively. The tie-lines connect coexisting state points.

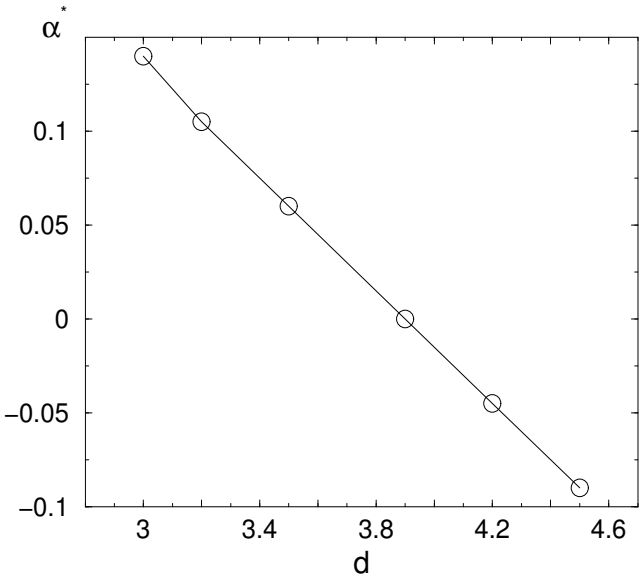

Figure 5.2: Nonadditivity parameter α^* at which the consolute point and triple point coincide for various values of the diameter ratio d. For mixtures, characterized by $\alpha(d) < \alpha^*(d)$ the N_1N_2 demixing is not detected.

$\rho_\sigma(\hat{\omega})$ is not Gaussian even at high densities, an analysis of the exact high-density distribution functions confirmed such a mechanism of nematic demixing [40]. On this basis we assume it to be valid at arbitrary high pressure in our system, and expect the structure of the bulk phase diagrams to be similar to those of additive mixtures. In particular, for $\alpha = 0.07$ nematic remixing is observed at a sufficiently high pressure, as illustrated in Fig. 5.1. The consolute point, at which the density and composition difference between the coexisting nematic phases vanishes, is indicated by $(*)$. Limitations of the numerical scheme, explored in Chapter 7, do not allow to determine whether or not such remixing takes place for larger α. However again, in analogy with additive mixtures, one might expect that the critical values of α and d, at which the nematic demixing becomes stable at arbitrary high densities, exist [40]. Whether this is true, remains to be seen in future work.

In order to characterize the amount of nonadditivity in the excluded volume interactions which leads to significant structural modification of the phase diagram, we explore various thin-thick mixtures of different α and d, and determine the value of α^* at which the pressure of the nematic-nematic consolute point and the triple point pressure coincide. Results of our studies are presented in Fig. 5.2. For $\alpha < \alpha^*$ (at fixed d) the N_1N_2 phase separation is not detected. It is evident that in the interval $d \in [3.5, 4.2]$ even a small nonadditivity $|\alpha| < 5 - 7\%$ may induce or suppress the N_1N_2 demixing transition. This correlates nicely with the experimentally observed

nematic demixing at $d = 3.5$, which cannot be explained by the additive hard-core interactions. The linearity of the function $\alpha^*(d)$ within the explored range of α reflects the linearity of the excluded volume $E_{12}(\hat{\omega}, \hat{\omega}')$ in terms of d and α.

Direct comparison of the bulk phase diagrams of the nonadditive mixture with $d = 3.5$ and $\alpha = 0.07$ and the additive mixture with $d = 4.0$ (presented in Fig. 4.1) shows close values of the fractionation gap at the N_1N_2 coexistence. Further evidence for similarity of these systems in the high density regime will be demonstrated in studies of their interfacial properties.

5.4 Interfaces

Studies of the free planar interfaces between various coexisting bulk phases are also performed in direct analogy with interfacial studies of additive mixtures. We focus on the nonadditive thin-thick mixture characterized by $d = 3.5$ and $\alpha = 0.07$. The expressions for the excluded volume (Eq. 5.4) can be directly used in the $x - y$ integrated kernels $K^{ij}_{\sigma\sigma'}(z - z', \hat{\omega}, \hat{\omega}')$, defined in Eq. (4.7), needed in the study of planar interfaces. Using an equidistant z -grid of $N_z = 200$ points in the interval $z \in [-5L, 5L]$, and corresponding bulk distributions $\rho_\sigma(\theta_i)$ as boundary conditions, we solve (see Eq. (4.9))

$$\beta\mu_\sigma = \ln[\rho_\sigma(z, \theta)L^2_\sigma D_\sigma] + \sum_{\sigma'} \int dz' d\theta' \sin\theta' \mathcal{K}^{00}_{\sigma\sigma'}(z - z', \theta, \theta')\rho_{\sigma'}(z', \theta'), \qquad (5.6)$$

in order to determine uniaxially symmetric nonuniform distributions $\rho_\sigma(z, \theta_i)$.

The IN_1 and N_1N_2 interfaces are found to be smooth and monotonic, in the sense that the profiles of the nematic uniaxial order parameters $S_\sigma(z)$ and the densities $n_\sigma(z)$ change monotonically from the bulk values in the I (N_1) phase to those in the N_1 (N_2) phase. The value of the correlation length $\xi_{N_1} = 0.49 \pm 0.02$ of the bulk N_1 phase at the triple-phase coexistence (as well as ξ_I and ξ_{N_2} for the I phase and the N_2 phase, respectively) can be extracted from the asymptotic decay of the one-particle distributions $\rho_\sigma(z, \theta)$ to their bulk values, according to Eq. (4.12).

The properties of the IN_2 interfaces depend strongly on pressure difference with the triple point (IN_1N_2 phase coexistence). As it is demonstrated in Fig. 5.3, the surface tension of the IN_2 interface shows a non-monotonic dependence on the bulk pressure p, which is related to the fractionation at the IN_2 coexistence. Upon increase of the nonadditivity, the surface tension $\gamma^*_{IN_2}(p)$ grows, again indicating that α plays a role similar to the diameter ratio d. For comparison we have included $\gamma^*_{IN_2}(p)$ for an additive thin-thick mixture with $d = 4.0$.

The microscopic thickness of the interface t is defined as $t = |z_+ - z_-|$ where $z_\pm$ are solutions of $n_1'''(z) = 0$, and a prime denotes differentiation with respect to z. As this equation has a set of solutions in every interfacial region, we choose for $z_\pm$ the outermost ones, i.e., the ones nearest to the bulk phases. This criterion provides a single measure for the thickness of both monotonic and non-monotonic profiles, with

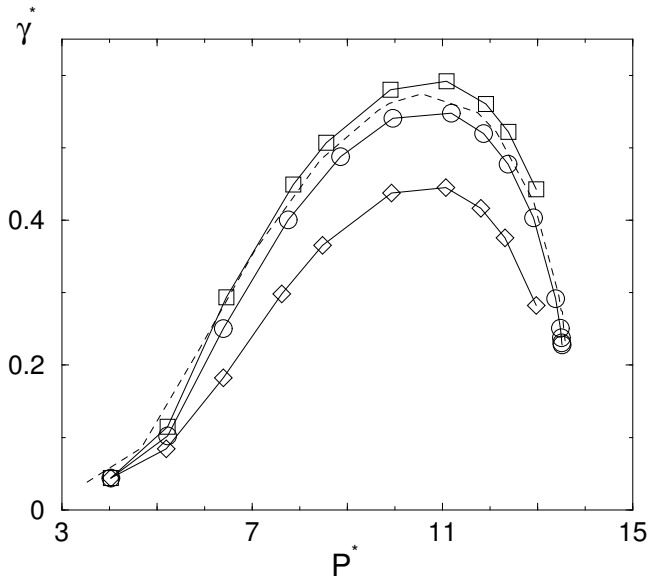

Figure 5.3: Dimensionless surface tension $\gamma^*_{IN_2} = \beta\gamma_{IN_2}LD_1$ of IN_2 interfaces as a function of dimensionless pressure $p^* = \beta pL^2D_1(\pi/4)$ for thin-thick mixtures with diameter ratio $d = 3.5$ and different values of nonadditivity $\alpha = 0.0$ ($\diamond$), 0.07 ($\circ$) and 0.1($\Box$). The dashed line indicates $\gamma^*_{IN_2}(p^*)$ for the additive thin-thick mixture of diameter ratio $d = 4.0$.

and without a thick film in between the asymptotic bulk phases at $z \to \pm\infty$. As we have discussed in Chapter 4, thin rods have a smaller excluded volume and a non-vanishing concentration in both coexisting phases, so their density is a convenient representation of structural changes within the interface. The interfacial width for the one-component IN interface is, with the present definition, given by $t/L = 0.697$.

The thickness of the IN_2 interface was found to diverge upon approach of the triple-point pressure p_t. This can be seen in Fig. 5.4, where t/L is plotted as a function of the dimensionless undersaturation $\epsilon = 1 - p/p_t$, which is a convenient measure of the pressure difference with the triple point. The nature of the film can be analyzed from the density profiles $n_1(z)$ of the IN_2 interface (or equivalently $S_\sigma(z)$, or $n_2(z)$). In Fig. 5.5 the profiles of $n_1(z)$ are shown at several values of the undersaturation ϵ. The asymptotic densities at $z \to \pm\infty$ in Fig. 5.5 are those of the coexisting I and N_2 bulk phases (at the corresponding ϵ). For $\epsilon \to 0$ value $n_1(z)$ in the film approaches the density of thin rods of the bulk triple point N_1 phase, indicated by the dashed line in Fig. 5.5. However, the undersaturation $\epsilon = 10^{-4}$ is yet too large to be in the asymptotic thick-film regime. The same identification can be made for $n_2(z)$ and $S_\sigma(z)$, and on this basis we conclude that the complete wetting phenomenon under consideration is complete triple point wetting of the free IN_2 interface by the N_1 phase. The similarity with complete wetting of the IN_2

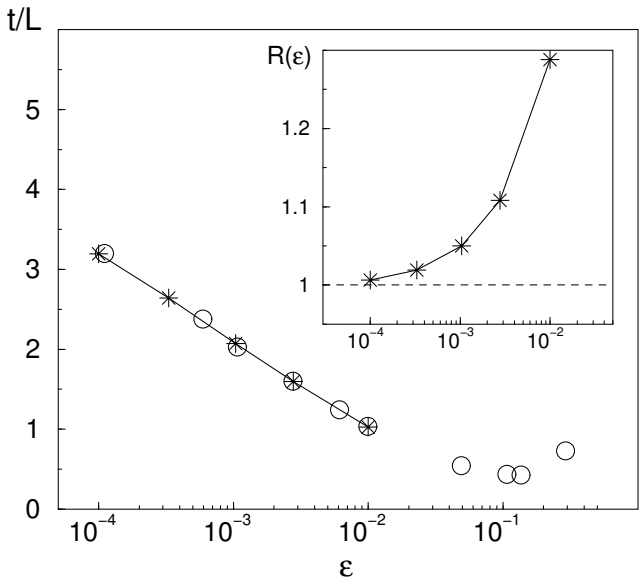

Figure 5.4: Thickness t/L as a function of the undersaturation $\epsilon = 1 - p/p_t$ from the triple point pressure p_t for thin-thick mixtures with diameter ratio $d = 3.5$ and nonadditivity $\alpha = 0.07$ $(*)$. For comparison we show thickness of the IN_2 interface of the additive mixtures for $d = 4.0$ $(\circ)$. The inset shows the surface tension ratio R [see Eq. (5.7)] as a function of the triple point undersaturation ϵ.

interface by the N_1 phase in additive thin-thick mixture with $d = 4.0$ is again rather striking, as is clear from Fig. 5.4, where the thickness of the IN_2 interface for additive rods is indicated by $(\circ)$.

Since one expects, for the short-range interactions of interest here, that the thickness of the complete wetting N_1 film in the IN_2 interface diverges as $t \sim -\xi_{N_1} \ln \epsilon$ for $\epsilon \to 0$ [45], the value of the correlation length of the bulk N_1 phase can be extracted, $\xi_{N_1} = 0.49 \pm 0.02$, which is consistent with the earlier determined value from decay of $\rho_\sigma(z, \theta)$ into the bulk N_1 phase.

The analysis of the structural properties of the IN_2 interface can be complemented by studies of the relative difference in surface tension (see Eq. (4.13))

$$R(\epsilon) = \frac{\gamma_{IN_2}(\epsilon)}{\lim_{p \downarrow p_t}(\gamma_{IN_1} + \gamma_{N_1 N_2})}, \tag{5.7}$$

as presented in the Inset in Fig. 5.4. It is clear that upon approach of triple-point coexistence $\lim_{\epsilon \to 0} R = 1$, which implies a vanishing contact angle. This provides the thermodynamic proof of complete triple-point wetting. The ϵ-dependence of R again reveals that $\epsilon = 10^{-4}$ is too large to be in the asymptotic thick-film regime.

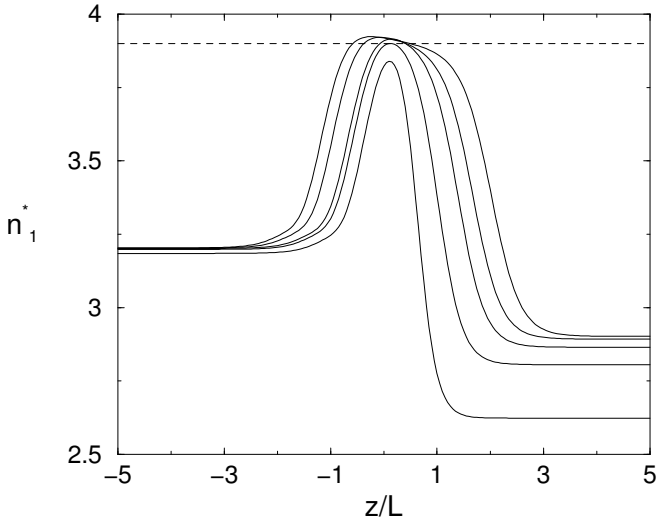

Figure 5.5: Density profiles of the thin rods $n_1^*(z)$ in the IN_2 interface for diameter ratio $d = 3.5$ and nonadditivity $\alpha = 0.07$ at triple point undersaturations $\epsilon = 1 - p/p_t = 10^{-2}, 10^{-2.5}, 10^{-3}, 10^{-3.5}, 10^{-4}$. The bulk I/N_2 phase is at $z \to -\infty/\infty$. The dashed line $n_1^* = 3.977$ represents the bulk density of thin rods in the triple point N_1 phase. These profiles indicate the formation of a wetting N_1 film in the IN_2 interface.

5.5 Summary and discussion

In this Chapter we have explored the bulk phase diagrams and the interfacial properties of the nonadditive mixtures of thin and thick hard rods. Nonadditivity of the rod interactions was introduced in order to explain recent experimental results on phase behavior of the binary mixtures of bare and PEG-coated fd viruses. It reflects the possible variation of the effective hard-core diameter of virus particle interactions between the same and distinct species. As it is illustrated in Fig. 5.1, a small amount of nonadditivity $\alpha > 0$ can stabilize the nematic-nematic phase coexistence, even if it is metastable for the additive mixture with the same diameter ratio. However, such a nematic demixing is always accompanied by an enhanced fractionation at the isotropic-nematic coexistence, which stays in sharp contrast with experimental findings. Therefore, further studies of various effects associated with flexibility and surface charge of virus particles are required, as well as additional experimental results.

The bulk phase diagrams of nonadditive binary mixtures show a large similarity with those of the additive mixtures of larger diameter ratio, which is related to the linear dependence of the rod-rod excluded volume on both parameters. This conclusion is also valid for interfacial phenomena. Similar to the interfaces between different bulk

phases in additive mixtures, the IN_1 and N_1N_2 interfaces are smooth and monotonic, whereas the IN_2 interface exhibits complete wetting by the N_1 phase upon approach of the triple phase coexistence. The complete triple-point wetting scenario was confirmed by (i) the logarithmic divergence of the thickness of the N_1 film with vanishing undersaturation, and (ii) the surface tension ratio $\lim_{\epsilon\to 0} R = 1$. Such a similarity between properties of additive and nonadditive mixtures may represent a significant difficulty to distinguish these in experiments.

Chapter 6

Ordering near a "soft" wall

Within the Zwanzig model we explore the thermodynamic properties of a fluid of monodisperse hard rods in contact with a model substrate represented by a hard wall with a short-ranged attractive or repulsive "tail". The attraction enhances the orientational ordering near the wall in both isotropic and nematic phases, and shifts the transition from uniaxial (U) to biaxial (B) symmetry in the isotropic surface layer to lower chemical potentials, whereas the wetting properties of the substrate remain similar to those of the pure hard wall. The soft repulsion reduces the density in the surface layer, which leads to a shift (or even suppression) of the UB transition, and to strong modification of the wetting properties. At the WI interface one always finds a wetting transition at a sufficiently large strength of the repulsion, whereas a drying transition at the WN interface is observed only for sufficiently long-ranged potentials.

6.1 Introduction

It is well known that the structure of a liquid-crystalline material is significantly modified by the presence of a substrate or an interface [13]. Several major effects can be distinguished: (i) the interaction of the liquid crystal molecules with the substrate leads to the formation of a boundary layer with an ordering different from the bulk; (ii) close to bulk phase transitions such a layer can be transformed into a wetting film of another (yet metastable) bulk phase; (iii) for orientationally ordered bulk phases, the orientation of the director can be fixed by the substrate/interface. These phenomena have been extensively studied near the bulk transition from the disordered isotropic (I) to the orientationally ordered nematic (N) phase. Although the structures of the surface phase diagrams for various limiting surfaces can be determined within the Landau-de Gennes formalism, the role of the specific intermolecular interactions in these surface phenomena remains unclear and requires studies on the level of simple molecular models.

As we have briefly discussed in Chapter 1, studies of model fluids of hard rods allow to quantify the role of short-ranged repulsive interactions in ordering phenomena in bulk and at interfaces. The Onsager model [11] explains successfully the bulk IN phase transition in hard-rod fluids, and its various extensions were applied in studies of bulk phase behavior of binary [33] and polydisperse mixtures [48], semiflexible polymers [56], discs, etc. In contrast, the surface properties of hard-rod fluids are understood rather poorly since the coupling between orientational and translational degrees of freedom of a rod, essential for inhomogeneous systems, brings significant complexity into the model. Up to now studies of surface phase behavior have been performed for a few cases only. For the free IN interface the orientation of the nematic director parallel to the interface was found to be thermodynamically stable [26, 29], and for binary mixtures complete wetting of the IN interface near the triple point by the second nematic phase was predicted [57]. For both systems the one-particle distribution function was found to be essentially uniaxially symmetric (with only a small biaxiality) even in the interfacial region where the translational symmetry is broken [27, 52]. At the same time, the biaxial symmetry was found to be thermodynamically favorable for the interfacial layer of a bulk I phase (close to the bulk IN transition) in contact with a hard wall, and some evidence of complete wetting by the nematic phase of the wall-isotropic (WI) interface was provided by theory [34] and simulations [58]. Other studies concentrated on properties of a hard-rod fluid in contact with a "penetrable" wall which restricts only the translational degrees of freedom of the rods [59]. It was shown that such a wall favors homeotropic anchoring of the nematic director, and the WI interface exhibits complete wetting by the homeotropically aligned nematic phase upon approach to the IN coexistence [29, 60]. The common feature of all these studies is that the chosen wall potential does not allow to control the amount of surface nematic order, in contrast with the Landau-de Gennes models.

A way to overcome this limitation was proposed in a recent study of the surface properties of a hard-spherocylinder fluid in contact with a model substrate, composed of a "penetrable" wall and a short-ranged repulsive or attractive tail [60]. Several wetting transitions and a transition from homeotropic to planar anchoring were observed at different strengths of the wall potential. This is expected, since the wall with the attractive tail favors homeotropic alignment of the nematic director, and for the strong repulsive tail it changes to planar. It is of interest to perform a similar analysis for a substrate which consists of a hard wall and a short-ranged attractive/repulsive tail. Since the substrate potential is characterized by some amplitude (or contact value) and decay length it is interesting to investigate the surface phase behavior as a function of these parameters. In this Chapter we explore the effect of both parameters.

Since studies of surface properties of a fluid of Onsager hard rods is rather difficult numerically, we consider a simpler model fluid of Zwanzig hard rods with a restricted number of allowed orientations [61]. It was demonstrated that this model exhibits a strong first-order IN transition in the bulk [61], and the orientation of the nematic

director parallel to the IN interface was found to be thermodynamically favorable [62], similar to the fully continuous rods. In contact with a hard wall the WI interface is completely wet by the N phase upon approach of the IN coexistence, whereas the WN interface remains partially wet [62]. Although some limitations of the Zwanzig model are known (see Chapter 7 and Refs. [63, 64]), we adopt this model for the present study for reasons of its simplicity.

This Chapter is organized as follows. In Sec. 6.2 we introduce a grand potential functional for a system of Zwanzig hard rods in an arbitrary external potential. Properties of a bulk Zwanzig fluid and the fluid in contact with a structureless hard wall are briefly discussed in Sec. 6.3. In Sec. 6.4 we describe the phase behavior of the Zwanzig rod fluid in contact with a composite wall. We classify various surface phenomena in terms of the potential parameters and construct generic surface phase diagrams. A discussion of the findings will be presented in Sec. 6.5.

6.2 Density functional and method

Consider an inhomogeneous fluid of rectangular hard rods of length L and diameter D ($L \gg D$) in a macroscopic volume V at temperature T and chemical potential μ. The rod orientations are restricted to the three mutually perpendicular directions $\hat{n}_i, i = \{1, 2, 3\}$ representing $\hat{x}$, $\hat{y}$, $\hat{z}$, respectively, whereas the position $\mathbf{r}$ of the center of mass of a rod is continuous. The grand potential functional of the fluid in an external potential $V_i(\mathbf{r})$ with the one-particle distribution functions $\rho_i(\mathbf{r})$ can be written as

$$\begin{aligned} \beta\Omega[\rho] &= \sum_{i=1}^{3} \int d\mathbf{r} \rho_i(\mathbf{r}) \Big(\ln[\rho_i(\mathbf{r})\nu] - 1 - \beta\mu + \beta V_i(\mathbf{r}) \Big) \\ &- \frac{1}{2} \sum_{i,j=1}^{3} \int d\mathbf{r} d\mathbf{r}' f_{ij}(\mathbf{r};\mathbf{r}') \rho_i(\mathbf{r}) \rho_j(\mathbf{r}'), \end{aligned} \tag{6.1}$$

where $\beta = (k_B T)^{-1}$ is the inverse temperature, ν is the rod's thermal volume, and $f_{ij}(r; r')$ is the Mayer function of hard rods with orientations $\hat{n}_i$ and $\hat{n}_j$ and center-of-mass coordinates $\mathbf{r}$ and $\mathbf{r}'$, which equals -1 if the rods overlap and vanishes otherwise. In Eq. (6.1) we adopt the second virial approximation for the grand potential functional $\Omega[\rho]$. In contrast with the freely rotating needles [11], the higher virial terms are important in the Zwanzig model [61]. However, although their inclusion affects the IN bulk phase coexistence densities and order parameters significantly, it does not change the phenomenology of the transition. For this reason, and for reasons of numerical simplicity, we restrict attention here to the second virial approximation.

The minimum conditions $\delta\Omega[\{\rho\}]/\delta\rho_i(\mathbf{r}) = 0$ lead to the set of nonlinear integral equations

$$\beta\mu = \ln[\rho_i(\mathbf{r})\nu] + \beta V_i(\mathbf{r}) - \sum_j \int d\mathbf{r}' f_{ij}(\mathbf{r};\mathbf{r}') \rho_j(\mathbf{r}') \tag{6.2}$$

to be solved for the equilibrium distribution $\rho_i(\mathbf{r})$. Once determined, it can be inserted into the functional to obtain the equilibrium value of the grand potential

$$\beta\Omega = \frac{1}{2}\sum_i \int d\mathbf{r}\rho_i(\mathbf{r})\Big(\ln[\rho_i(\mathbf{r})\nu] - 2 - \beta\mu + \beta V_i(\mathbf{r})\Big). \tag{6.3}$$

Note that $\Omega = -pV$ for a bulk system in a volume V, with $p = p(\mu, T)$ the pressure. In the presence of a planar surface or interface of area A we have $\Omega = -pV + \gamma A$ with $\gamma = \gamma(\mu, T)$ the surface or interface tension.

We restrict our attention to planar substrates with $V_i(\mathbf{r}) = V_i(z)$, where z is the distance of the center of mass of a rod to the substrate. We assume translational invariance in the $x - y$ plane, $\rho_i(\mathbf{r}) = \rho_i(z)$, which allows to further simplify the Euler-Lagrange Eqs. (6.2) [62]

$$\begin{aligned}
\beta\mu &= \ln[\rho_1(z)\nu] + \beta V_1(z) + 2\rho_2(z)L^2D + 2\bar{\rho}_3(z)L^2D,\\
\beta\mu &= \ln[\rho_2(z)\nu] + \beta V_2(z) + 2\rho_1(z)L^2D + 2\bar{\rho}_3(z)L^2D,\\
\beta\mu &= \ln[\rho_3(z)\nu] + \beta V_3(z) + 2\bar{\rho}_1(z)L^2D + 2\bar{\rho}_2(z)L^2D,
\end{aligned} \tag{6.4}$$

with the averaged densities

$$\bar{\rho}_i(z) = \frac{1}{L}\int_{z-L/2}^{z+L/2} dz'\rho_i(z'). \tag{6.5}$$

For convenience we set $\nu = L^2D$; this is merely a gauge for the chemical potential.

We solve Eqs. (6.4) iteratively for a given external potential $V_i(z)$ and fixed chemical potential μ. In all numerical calculations we use an equidistant z-grid of 40 points per L. Convergence is assumed when the relative difference between the results of iteration j and $j + 1$ is smaller then 10^{-10} for all values of z in the grid. Such a high accuracy is required to avoid dependencies of the results of the calculations on the initial guesses. Some additional checks were performed with 80 points per L, which gave virtually identical results.

The results of the calculations can be conveniently represented in terms of several dimensionless order parameters: the total number density

$$c(z) = \sum_{i=1}^{3} \rho_i(z)L^2D, \tag{6.6}$$

the nematic order parameter

$$s(z) = \frac{\rho_3(z) - \frac{1}{2}(\rho_1(z) + \rho_2(z))}{\rho_1(z) + \rho_2(z) + \rho_3(z)}, \tag{6.7}$$

and the biaxiality

$$\Delta(z) = \frac{\rho_1(z) - \rho_2(z)}{\rho_1(z) + \rho_2(z) + \rho_3(z)}. \tag{6.8}$$

Clearly, as the number of order parameters is equal to the number of components of the one-particle distribution function $\rho_i(\mathbf{r})$, Eqs. (6.4) can be expressed in terms of $c(z), s(z), \Delta(z)$ [62].

6.3 Bulk and hard-wall behavior

A homogeneous bulk ($V_i(\mathbf{r}) \equiv 0$) fluid of Zwanzig hard rods exhibits a strong first-order $I - N$ phase transition [61] similar to the system of fully continuous rods [11], although the origin of the nematic state is significantly modified by the orientational discretization [63, 64]. A straightforward numerical calculation yields, in accordance with Zwanzig's original results, values of the isotropic and nematic bulk densities at coexistence $c_I = 1.258$, $c_N = 1.915$, the nematic order parameter $s_N = 0.915$, the bulk pressure $\beta p_{IN} L^2 D = 2.313$, and the chemical potential $\beta\mu_{IN} = 0.8087$. The bulk values of the one-particle distribution function ρ_i are used in all subsequent interfacial calculations as a boundary condition at $z \to +\infty$.

The behavior of a fluid of Zwanzig hard rods in contact with a structureless planar hard wall, described by the potential

$$V_i^{hw}(\mathbf{r}) = \begin{cases} \infty & |z| < 0 \quad (i = 1, 2), \\ & |z| < L/2 \quad (i = 3), \\ 0 & \text{otherwise}, \end{cases} \tag{6.9}$$

has also been studied in detail [62]. For an isotropic bulk phase of density c_b (and chemical potential $\beta\mu = \ln c_b + 4c_b/3$) in contact with the wall a continuous surface phase transition from uniaxial to biaxial local symmetry occurs at $c_{b,UB} = 1.03$ ($\beta\mu_{UB} = 0.307$), quite below the bulk $I - N$ phase transition [62,65]. Upon approach of the IN coexistence ($\mu \uparrow \mu_{IN}$) the surface biaxial film grows smoothly into a thick nematic film with the director parallel to the wall. The excess adsorption

$$\Gamma(\mu) = \frac{1}{L} \int_0^\infty dz (c(z) - c_b) \tag{6.10}$$

diverges logarithmically ($\Gamma \sim -(\xi_N/L) \ln \epsilon$) as a function of undersaturation $\epsilon = (1 - c_b/c_I) \to 0$, which corresponds to complete wetting of the wall-isotropic fluid interface by a nematic film [62]. Here ξ_N is the correlation length of the bulk nematic phase at $\beta\mu = \beta\mu_{IN}$. Young's relation between the surface tension at wall-isotropic, wall-nematic and isotropic-nematic interfaces at coexistence $\gamma_{WI} = \gamma_{WN} + \gamma_{IN}$ also confirms the complete wetting scenario. From the dependence of Γ on the undersaturation we determine the $\xi_N/L = 0.350 \pm 0.002$, which sets the length scale relevant for studies of wetting phenomena at the wall-isotropic fluid interface.

One can also determine the correlation length ξ of the bulk phase by considering the decay of an inhomogeneity into the homogeneous bulk, since

$$\rho_i(z) - \rho_i(\infty) \sim \exp[-z/\xi]. \tag{6.11}$$

By considering, for instance, the free planar IN interface at $\mu = \mu_{IN}$, one obtains the correlation length of the isotropic phase, ξ_I, and that of the nematic phase, ξ_N, by the analysis of the decay at both sides of the IN interface. This analysis reproduces the value of ξ_N as given above within the numerical accuracy, and yields $\xi_I/L = 0.540 \pm 0.002$. These length scales are important for the subsequent studies of soft walls.

6.4 "Soft" wall

The surface phase behavior of a fluid of Zwanzig hard rods becomes significantly more complex when the substrate is characterized not only by the hard wall potential $V_i^{hw}(z)$, but also by some additional short-range potential, which controls the density of rods close to the substrate. Physically it may represent an interaction of a rod with a polymer layer grafted to the wall, or some electrostatic interactions at the wall-fluid interface. For the present study we avoid further discussion of its microscopic origin, and consider an external potential $A\exp[-\kappa(z+\delta_{i3}l)]dl/L$ acting on every rod segment dl at a separation l $(-L/2 \le l \le L/2)$ from the center of mass z of the rod of orientation i, with δ_{ij} the Kronecker delta. We explore the generic properties of the surface phase diagram as a function of the "contact" potential A and the decay constant κ.

The potential of the composite wall is described by

$$\begin{aligned} V_i(\mathbf{r}) &= V_i^{hw}(\mathbf{r}) + \frac{A}{L}\int_{-L/2}^{L/2} dl \exp[-\kappa(z+\delta_{i3}l)] \\ &= \begin{cases} A\exp[-\kappa z] & z > 0, \quad i = 1,2, \\ A\exp[-\kappa z]\dfrac{\sinh(\kappa L/2)}{(\kappa L/2)} & z > \frac{L}{2}, \quad i = 3, \\ \infty & \text{otherwise.} \end{cases} \end{aligned} \tag{6.12}$$

Our primary interest is in the parameter regime $\beta A \le 10$, since larger values of βA correspond essentially to a shift of the hard wall along the z-axis.

Figure 6.1 shows the surface phase diagrams of a fluid of Zwanzig hard rods at chemical potential μ in contact with the composite wall with (a) $\kappa L = 2$ and (b) $\kappa L = 6$. Since the bulk IN transition occurs at $\mu = \mu_{IN}$, one might distinguish the cases where the substrate is in contact with the isotropic bulk phase ($\mu < \mu_{IN}$), and with the nematic bulk phase ($\mu > \mu_{IN}$).

6.4.1 $\mu < \mu_{IN}$

For sufficiently low values of μ the equilibrium distribution functions $\rho_i(z)$ are uniaxial ($\rho_1(z) = \rho_2(z)$, $\Delta(z) \equiv 0$) with respect to the wall normal for any A and fixed κ. This uniaxial (U) symmetry breaks at $\mu \ge \mu_{UB}(A)$, such that the profile becomes biaxial (B) close to the wall ($\rho_1(z) \ne \rho_2(z)$, $\Delta(z) \ne 0$). The chemical potential of the

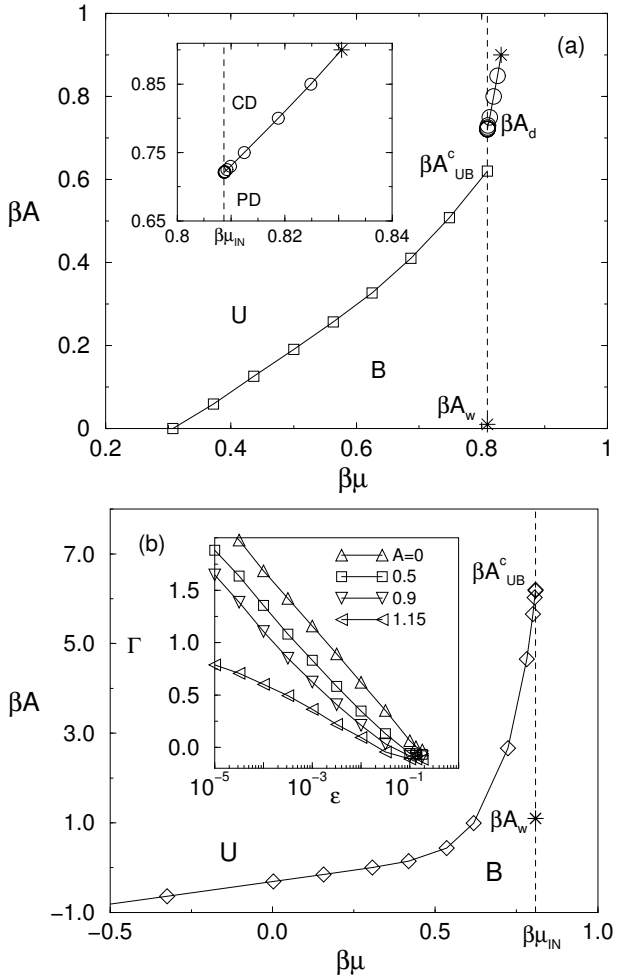

Figure 6.1: Surface phase diagrams of a Zwanzig hard-rod fluid in contact with a soft wall (see Eq. (6.12)) as a function of the amplitude βA and chemical potential $\beta\mu$. The range of the soft potential is rather long in (a), $\kappa L = 2.0$, and much shorter in (b), $\kappa L = 6.0$. In both (a) and (b) we distinguish a uniaxial (U) and biaxial (B) phase for $\mu < \mu_{IN}$, and a wetting transition ($*$) at $\mu = \mu_{IN}$ that separates complete wetting of the wall by a nematic film at $A < A_w$ from partial wetting $A > A_w$. In (a) we also see a predrying line at $\mu > \mu_{IN}$ and a drying transition at $\beta\mu = \beta\mu_{IN}$, that separates complete drying by an isotropic film at $A > A_d$ from partial drying $A < A_d$. The inset in (a) magnifies the predrying line, and that in (b) illustrates the logarithmic divergence of the adsorption Γ with undersaturation $\epsilon = 1 - c_b/c_I$ at $A < A_w$.

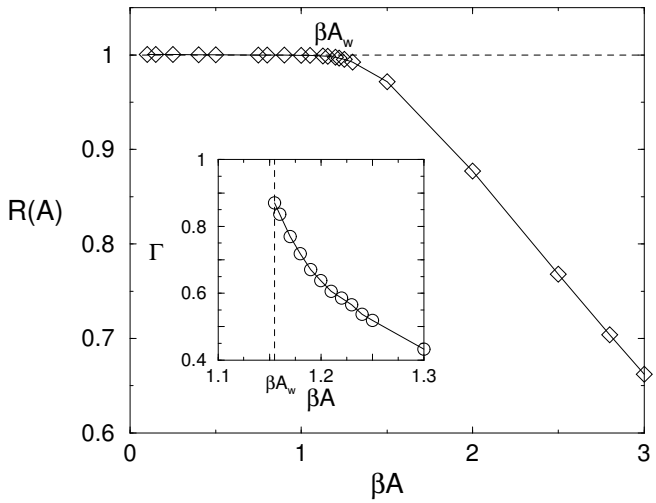

Figure 6.2: Characteristic function $R(A)$ of the relative surface tension difference at the WI and WN interfaces, defined in Eq. (6.13). At $\beta A_w = 1.15$ we have $R(A_w) = 1$, i.e. at $A = A_w$ the wetting transition occurs. The inset shows the dependence of the excess adsorption Γ as a function of the amplitude βA at $\beta\mu = \beta\mu_{IN}$.

UB transition, $\mu_{UB}(A)$, depends on the amplitude βA of the substrate potential, and it shifts towards the bulk phase coexistence μ_{IN} for increasing A. For $\beta A = \beta A^c_{UB}$ the UB transition coincides with the bulk IN transition, such that $\mu_{UB}(A^c_{UB}) = \mu_{IN}$. This implies that an isotropic bulk fluid ($\mu < \mu_{IN}$) in contact with a wall with $A > A^c_{UB}$ is uniaxially symmetric, even upon approach of $\mu \to \mu_{IN}$. We find $\beta A^c_{UB} = 0.62$ for $\kappa L = 2$, and $\beta A^c_{UB} = 6.20$ for $\kappa L = 6$. The UB transition is found to be continuous for all investigated combinations of κL and βA. This is consistent with the findings of Ref. [62], where the case $\beta A = 0$ (hard-wall) was considered.

The shape of the UB-line in the $\mu - A$ representation is essentially linear for $\kappa L = 2$, and exhibits a rather steep increase when $\mu \to \mu_{IN}$ for $\kappa L = 6$. This can be understood by realizing that the shorter range of the potential for $\kappa L = 6$ has a relatively strong effect on rods parallel to the wall ($i = 1, 2$), which gives rise to steep density gradients in the vicinity of the wall. By contrast, for longer-ranged potentials the external field essentially shifts the (local) chemical potential close to the wall from μ to $\mu + A$, such that $\mu_{UB} \simeq \mu_{UB}(0) + A$. This is indeed what we find numerically for small (and even negative) values of A. Apparently the range of the potential with $\kappa L = 2$ is long enough to be in this low-A regime almost up to $A = A^c_{UB}$.

In the regime $A \geq A^c_{UB}$ it is impossible to grow a nematic film in between the wall and the isotropic fluid. In fact, we find that the adsorption Γ remains finite upon approach of $\mu \to \mu_{IN}$ in the regime $A > A_w$, with $\beta A_w = 1.15$ for $\kappa L = 6$, and $\beta A_w = 0.01$ for $\kappa L = 2$. This implies that a nematic film (with some biaxial

character) of finite thickness occurs upon approach of the bulk IN transition if $A_w < A < A_{UB}^c$, i.e. we have partial wetting (PW) of the wall-isotropic (WI) interface. However, for $A < A_w$ the adsorption diverges (logarithmically) as the undersaturation $\epsilon = (1 - c_b/c_I) \to 0$ (see inset in Fig. 6.1), and hence the WI interface shows complete wetting (CW) by the nematic phase. The wetting transition for $\mu = \mu_{IN}$ at $A = A_w$ is a first order transition, as can be seen from the Inset of Fig. 6.2, where the adsorption at saturation is finite for $A > A_w$, and infinite for $A < A_w$. The existence of a wetting transition at $A = A_w$ follows also from the study of the interfacial tensions obtained by the evaluation of the minimum value of the functional, see Eq. (6.3). We consider the ratio

$$R(A) = \frac{\gamma_{WI}(A) - \gamma_{WN}(A)}{\gamma_{IN}}, \tag{6.13}$$

where $\gamma_{WI}(A)$ and $\gamma_{WN}(A)$ are the tensions of the WI and WN interface, respectively, both at $\mu = \mu_{IN}$, and where the $\beta\gamma_{IN}LD = (2.8027 \pm 0.0001) \times 10^{-2}$ is the surface tension of the free planar IN interface. In Fig. 6.2 we show $R(A)$ for $\kappa L = 6$. It can be seen that $R(A) \equiv 1$ (with relative accuracy of 10^{-3}) if $\beta A < \beta A_w = 1.15$, and $R(A) < 1$ if $A > A_w$. This is clear thermodynamic evidence for a transition from partial to complete wetting at $A = A_w$. A similar study for $\kappa L = 2$ shows that $\beta A_w = 0.01$. One expects, for reasons of continuity, that a first-order wetting transition is accompanied by a first-order prewetting transition, from a finite thin to a finite thick film. Unfortunately, we have not been able to find this prewetting transition, despite considerable efforts. We speculate that its critical point is too close to the wetting transition to be detected.

6.4.2 $\mu > \mu_{IN}$

We now consider the nematic bulk phase in contact with the substrate, described by Eq. (6.12). Intuitively, one could expect that for sufficiently large βA rods in the surface layer are characterized by the low-density isotropic distribution. Whether or not such an isotropic layer becomes macroscopic at coexistence, i.e. whether orientational drying of the WN interface by an isotropic film takes place, depends on the difference between the surface tensions of the WI and WN interfaces. In particular, it is known that for $\beta A = 0$ (the hard wall) only partial drying takes place, i.e. the adsorption remains finite as $\mu \downarrow \mu_{IN}$ [30]. Therefore, the search is for the possibility of a drying transition upon increasing βA.

Our numerical results for $\kappa L = 6$ show that Γ remains finite for any $\beta A < 10$. For $\beta A \geq 10$ the density of rods close to the hard wall ($z = 0$) is so small, that its position can be shifted to some $z = z_0 > 0$ without affecting the profiles $\rho_i(z)$ significantly, while the effective amplitude is reduced from A to $A \exp[-\kappa z_0]$. We can conclude that the soft potential with $\kappa L = 6$ is so short-ranged that for any value of βA the hard-wall ($\beta A = 0$) result of partial drying is obtained upon approach of coexistence.

The situation is more interesting for the "softer" case $\kappa L = 2$, where we do find a drying transition at $A = A_d$, with $\beta A_d = 0.72$. When $\mu \downarrow \mu_{IN}$ partial drying is

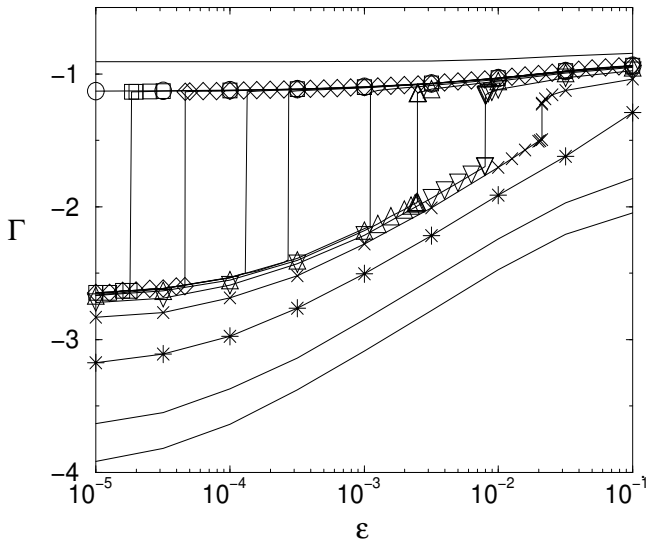

Figure 6.3: Excess desorption $\Gamma(\epsilon)$ at the interface between a nematic phase and the "soft" wall ($\kappa L = 2$) as a function of oversaturation $\epsilon = c_b/c_N - 1$ for different values of A. The desorption varies continuously for $\beta A \leq 0.72$ ($\circ$) and for $\beta A \geq 1.0$ ($*$), whereas for $0.72 < \beta A < 1.0$ it exhibits a discontinuous jump, corresponding to the predrying line ($\beta A = 0.7211$ ($\Box$), 0.7212 ($\diamond$), 0.73 ($\triangle$), 0.75 (∇) and 0.85 ($\times$)). The vertical lines connect coexisting points at the predrying line. The continuous upper curve is for $\beta A = 0.65$, and the two lowest ones for $\beta A = 1.5$ and $\beta A = 2.0$.

observed for $A < A_d$, and complete drying by an isotropic film for $A > A_d$. Studies of the excess desorption $\Gamma(\epsilon)$ as a function of oversaturation $\epsilon = c_b/c_N - 1$ with respect to the IN coexistence for various amplitudes of the wall potential are presented in Fig. 6.3. At low values of the contact potential ($\beta A \leq 0.72$) the desorption remains almost constant upon approach of the IN coexistence. Calculations show that $R(A) > -1$ in this regime, therefore one can conclude that partial drying of the WN interface takes place. The behavior changes qualitatively for $0.72 < \beta A < 0.95$, where $\Gamma(\epsilon)$ exhibits a discontinuous change at some oversaturation $\epsilon > 0$. For $\beta A \simeq 0.95$ the jump of the desorption takes place at $\epsilon = 5 \cdot 10^{-2}$, and its magnitude is (vanishingly) small. For decreasing βA the jump increases and shifts to smaller oversaturations. Finally, at $\beta A = \beta A_d \simeq 0.72$ the jump diverges and occurs at $\epsilon \to 0$. At higher values of the contact potential ($\beta A \geq 1.0$) the desorption grows continuously upon approach of coexistence. Studies of the surface tension difference at coexistence show that $R(A) = -1.000 \pm 0.001$ for all $A > A_d$, which is consistent with a complete drying of the WN interface by an intervening isotropic film. However, an analysis of the profiles of the total density $c(z)$, the nematic order parameter $s(z)$ and the biaxiality $\Delta(z)$, as presented in Fig. 6.4 for $\beta A = 0.73$, shows that the thickest film considered

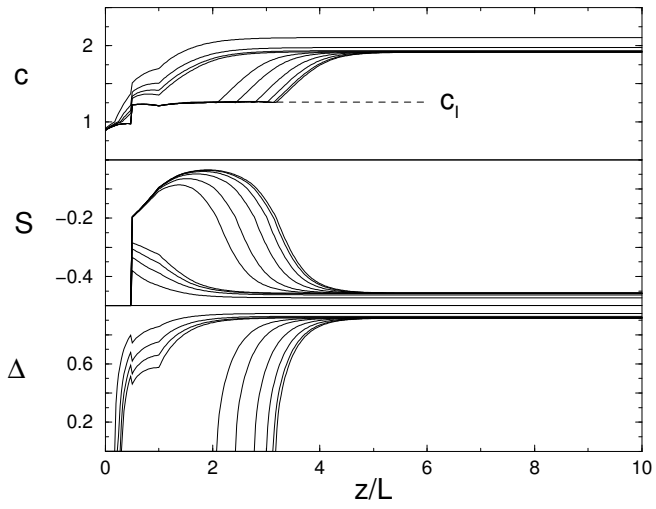

Figure 6.4: Profiles of density $c(z)$, uniaxial order parameter $s(z)$ and biaxial order parameter $\Delta(z)$ for $\beta A = 0.73$, $\kappa L = 2$ for various values of ϵ, ranging from $\epsilon = 10^{-1}$ for the thinnest film to $\epsilon = 10^{-5}$ for the thickest film. Coexistence of a thin and thick film - the predrying transition - occurs at $\epsilon = 10^{-2.6}$.

($\epsilon = 10^{-5}$) is such that $s(z) \neq 0$, whereas $\Delta(z) = 0$ and $c(z) = c_I$ in the film. This implies that the asymptotic limit $\epsilon \to 0$ has not been reached yet, and explains why the regime of logarithmic growth of Γ with ϵ cannot properly be identified in Fig. 6.3. We expect, however, on the basis of the trends of the profiles, that for sufficiently small ϵ the wall will be wet completely by an isotropic film, characterized by $s(z) = 0$, $\Delta(z) = 0$, and $c(z) = c_I$ for a macroscopically large interval of z. It turns out to be difficult to demonstrate this numerically, because the relatively long range of the potential and the small values of ϵ require rather extended and fine spatial grids. The finite desorption jump off coexistence ($\epsilon > 0$) is associated with the predrying transition that ends in a predrying critical point at $\beta A \simeq 0.95$ and $\epsilon = 0.05$. This point is indicated by $(*)$ in Fig. 6.1(a). The regime of approximate scaling of density profiles (associated with a shift of the hard wall and a renormalization of the contact potential) at large A is observed already at $\beta A \geq 1.5$.

6.4.3 $\mu = \mu_{IN}$

So far we have discussed the surface behavior of a fluid of Zwanzig hard rods in contact with a "soft wall" upon approach of the IN coexistence from the isotropic or nematic side. However, since the wetting transitions are defined at coexistence, one can compare the structures of the surface phase diagram for various $\{\kappa, A\}$ at $\mu = \mu_{IN}$. Our analysis is primarily based on the behavior of the relative surface

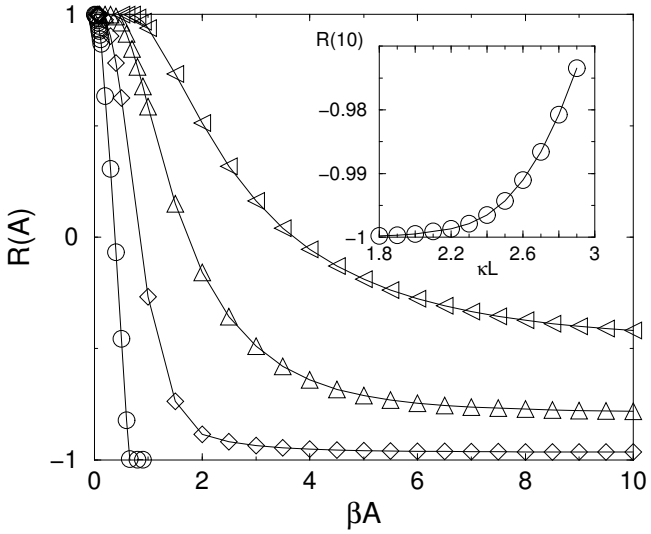

Figure 6.5: Relative surface tension difference $R(A)$ (Eq. (6.13)) as a function of the dimensionless amplitude βA of the wall potential for $\kappa L = 2.0$ ($\circ$), 3.0 ($\diamond$), 4.0 ($\triangle$), 5.0 (∇). The inset shows $R(\beta A = 10.0)$, i.e. in the scaling regime, as a function of κL.

tension difference $R(A)$. Studies of divergencies of the surface excess adsorption require data over several decades of $\epsilon \to 0$, which often represent significant numerical difficulties.

In Fig. 6.5 we illustrate the behavior of the function $R(A)$ at $\mu \simeq \mu_{IN}$ for several values of κL. As follows from Eq. (6.13), complete wetting (drying) of the WI (WN) interface by the nematic (isotropic) phase corresponds to $R(A) = 1$ (-1). Wetting of the WI interface by the nematic phase is observed for all values of κ at sufficiently small βA. This is expected since the pure hard wall in contact with the isotropic phase shows complete wetting behavior [62]. In contrast, complete drying of the WN interface occurs only at sufficiently small values of the inverse decay length κL, i.e. for relatively long-ranged potentials. Physically this can be understood on basis of the following arguments. For any fixed κL an increase of βA leads to higher density gradients close to the wall, and therefore to higher values of the WN surface tension. However, at sufficiently large βA one enters the scaling regime where a further increase of the contact potential leads to a uniform shift of the density profiles in the z-direction, without modification of the surface tension. Therefore, a critical value of $\kappa_c L$ exists, at which the drying transition appears. One can determine $\kappa_c L$ from an analysis of the relative surface tension difference $R(A)$ at sufficiently high A (in the scaling regime), e.g. $\beta A = 10$. As it is clear from the inset of Fig. 6.5, $\kappa_c L \simeq 2.2$, and for larger values of the inverse decay length the WN interface is only partially wet by the isotropic phase ($R(A) > -1$).

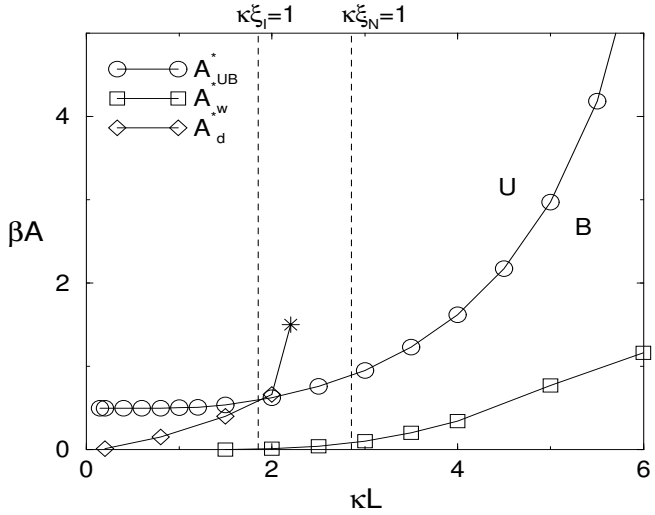

Figure 6.6: Generic surface phase diagram for a fluid of Zwanzig hard rods at the IN coexistence in contact with the "soft" wall (Eq. (6.12)) in terms of the amplitude of the wall potential βA and its decay length κL. Solid lines correspond to the wetting ($\square$), drying ($\diamond$), and the UB ($\circ$) transitions. End point on the line of the drying transitions is indicated by ($*$). The dashed lines indicate values of the bulk correlation length $\xi_N/L = 0.35$ ($\xi_I/L = 0.54$) in the nematic (isotropic) phase.

All our findings are summarized in Fig. 6.6, which represents the generic surface phase diagram in the $\beta A - \kappa L$ representation for a fluid of Zwanzig hard rods at IN coexistence ($\mu = \mu_{IN}$) in contact with the "soft" wall. We distinguish lines of the wetting ($\square$) and drying ($\diamond$) transitions, of which the properties have been already discussed above. In addition, the line of the wetting transitions approaches a linear behavior at sufficiently large κL. This is associated with the fact that for steep potentials density variations within the decay length of the potential are rather small, and can be neglected. Therefore, its contribution to the grand potential is proportional to $(\beta A/L)c(0)\int dz \exp[-\kappa z] = (\beta A/\kappa L)c(0)$. Since the wetting transition for large κL occurs at similar values of the surface free energy, $(\beta A/\kappa L)c(0) = \text{const}$, and $\beta A \sim \kappa L$.

The UB transition ($\circ$) at the WI interface occurs for all κL. It also takes place at the WN interface in the thick isotropic wetting film, i.e. below the intersection of the lines of the drying and the UB transitions. Note that when κ^{-1} becomes smaller than the bulk isotropic (nematic) correlation length ξ_I (ξ_N), the growth of the wetting film is determined by ξ_I (ξ_N). However, this does not introduce any additional structure into the surface phase diagram. For large κL the UB line shows an exponential divergence $\beta A \sim \exp[\kappa L]$, associated with the renormalization of the contact potential in the scaling regime $\beta A = \beta A_0 \exp[\kappa L z_0/L]$.

6.5 Discussion and outlook

We have explored the surface phase behavior of a fluid of Zwanzig hard rods in contact with a substrate composed of a hard wall and an additional short-ranged repulsive or attractive tail. Such a simple potential can effectively control the degree of the nematic (isotropic) order close to the wall, leading to a rich surface phenomenology.

The observed surface phase transitions correspond either to the symmetry changes in the thin surface layer (UB transition) or to the appearance of macroscopically thick (wetting) films of another bulk phase. The UB transition occurs at the WI interface for all attractive and relatively weak repulsive potentials, regardless the nature of the I fluid (bulk phase or metastable thick wetting film in between the substrate and the bulk N phase) in contact with the substrate. The origin of the UB transition lies in the competition between orientational entropy and entropy of packing in a $2D$ plane parallel to the substrate. This is particularly clear for the pure hard wall, where it occurs at $z \to 0$. Since in this case $V_i(z) = 0$ and $\bar{\rho}_3(z) \to 0$ (see the first two Eqs. (6.4)), the UB transition is directly related to the $2D$ bulk IN transition. An attraction to the substrate does not modify this behavior, since the plane at $z = 0$ remains effectively uncoupled from the bulk, and in the uniaxial (U) phase $\rho_{1,2}(0) > \rho_{1,2}(z)$, i.e. the UB transition still takes place at $z = 0$. The added repulsion induces non-monotonic changes of $\rho_{1,2}(z)$ in the U phase, and therefore changes the position of the plane of the UB transition to some $z > 0$. However, the continuous nature of the transition remains. Since $V_1(z) = V_2(z)$ and the averaged density of the third component $\bar{\rho}_3(z)$ reduce the value of the chemical potential in the plane of the UB transition (see Eqs. (6.4)), for sufficiently high βA it becomes unfavorable to increase the amount of ordering in any plane close to the wall (at $\mu \leq \mu_{IN}$), i.e. the UB transition becomes suppressed.

Wetting phenomena at substrates with an attractive potential are found to be similar to the wetting of the hard wall. In particular, the WI interface becomes completely wet by the N phase upon approach of $\mu \uparrow \mu_{IN}$, and the WN interface remains partially dry as $\mu \downarrow \mu_{IN}$. The situation changes for repulsive substrates. Even weak repulsions with a relatively long range increase the WI (WN) surface tension strongly, which results in a wetting (drying) transition. In the explored range of parameters $0.2 \leq \kappa L \leq 6$ and $0 \leq \beta A \leq 10$ the wetting transition has been observed in all cases, whereas for relatively steep (short-ranged) potentials the drying transition does not occur. This can be explained by the shift of the hard wall position to some z_0, since the transformation $\beta A \exp[-\kappa z] = \beta A \exp[-\kappa z_0] \exp[-\kappa(z - z_0)] = \beta A_0 \exp[-\kappa(z - z_0)]$ does not modify $\rho_i(z)$ significantly, provided βA_0 is sufficiently large. Therefore, for steep potentials the density profiles are similar to the profiles of a weakly repulsive substrate with a renormalized contact strength A_0 and the hard wall located at z_0.

In all studied cases the wetting transitions are found to be of first order since the excess wall adsorption exhibits a discontinuous jump at the transition point. However, it turns out to be impossible to determine the locations of the associated prewetting

line. The drying transitions are also found to be of first order. The associated prewetting lines have been detected, and are rather long.

Our findings add some perspective to the results of Ref. [60], where the wetting properties of a fluid made up of hard spherocylinders of a length-to-breadth ratio $L/D = 5$ were explored on a model substrate, which consists of a "penetrable" wall (the exclusion boundary condition over the molecular centers of mass) and an attractive or repulsive tail. Such a model incorporates implicitly the possibility of the "anchoring" transition, since the pure "penetrable" wall ($\beta A = 0$) prefers homeotropic alignment of the nematic director $\hat{n}$, and for large βA it switches into planar orientation. Therefore, for large βA the substrate can be modelled as a hard wall with a repulsive tail. However, since only a single value of κ was explored in Ref. [60], only complete wetting by the planar N phase of the WI interface was found, and wetting transitions were not identified. Whether or not they exist remains to be seen in future work.

Chapter 7

Relation between Onsager and restricted-orientation models

We explore models of hard-rod fluids with a finite number of allowed orientations, and construct their bulk phase diagrams within Onsager's second virial theory. For a one-component fluid, we show that the discretization of the orientations leads to the existence of an artificial (almost) perfectly aligned nematic phase, which coexists with the (physical) nematic phase if the number of orientations is sufficiently large, or with the isotropic phase if the number of orientations is small. Its appearance correlates with the accuracy of sampling the nematic orientation distribution within its typical opening angle. For a binary mixture this artificial phase also exists, and a much larger number of orientations is required to shift it to such high densities that it does not interfere with the physical part of the phase diagram.

7.1 Introduction

Understanding the phase behavior of colloidal suspensions of rod-like particles requires an accurate description of their microscopic properties. Fluids of hard rods may be considered as the simplest systems on which the models incorporating particle orientational degrees of freedom can be tested [33,46]. One of the exact theoretical results dates back to Onsager [11] who analyzed the transition from a uniform isotropic phase to an orientationally ordered nematic phase in a fluid of monodisperse hard needles. As it was demonstrated in Chapter 2, he derived a nonlinear integral equation for the orientation distribution function, a key quantity of the theory, which is constant in the isotropic phase and peaked about the director in the nematic phase. He circumvented the problem of explicitly calculating the nematic orientation distri-

bution function (ODF) by adopting a variational Ansatz, which later was checked numerically to be rather accurate [33].

The generalization of the Onsager model to binary mixtures of rods showed the possibility of strong fractionation [21, 22] and even nematic-nematic demixing at sufficiently high density, driven by a competition between orientation entropy and ideal mixing entropy [23,36,37]. The functional forms of ODF's in these studies were either variational Gaussian [21, 37], truncated expansions in Legendre polynomials [22], or numerically determined on an angular grid [36] or on a scaled angular grid [23]. In all these cases the focus was on describing the system with a continuum of orientations.

An alternative approach is to study models with a finite number N of allowed orientations while the positions of the centers of mass of the rods remain continuous. Such a model was first proposed by Zwanzig [61], with orientations of a rod to be restricted to $N = 3$ mutually perpendicular directions $\hat{\omega}_i, i = \{1, \ldots, N\}$. Despite its inability to resolve the orientational structure of the one-particle distribution function in any detail, the model does exhibit a bulk IN transition. Later it has been applied successfully to explore wetting phenomena near a single hard wall and in a slit [62], and phase diagrams of polydisperse systems [66, 67]. The main advantage of such discrete models in comparison with the continuous ones is their computational simplicity. The combination of spatial inhomogeneity and/or polydispersity with a continuum of orientations is numerically rather demanding, and the computational effort can be reduced significantly by discretizing the orientations [26, 44, 66]. The hope has, of course, always been that with an increase of the number of allowed orientations one would smoothly approach the continuum limit. Here we show that this is *not* the case.

The possibility of a continuous interpolation between the results for the discrete models on the one hand and Onsager-like solutions on the other has first been questioned by Straley [64] in studies of models with dodecahedral ($N = 6$) and icosahedral ($N = 10$) symmetries. He concluded that they do not trend towards the continuum solution due to the single allowed orientation within the typical opening angle ($\approx \pi/9$) of the nematic distribution at coexistence. Unfortunately, one cannot proceed the sequence of models with $N = 3, 6, 10$ any further, since a larger fully symmetric set of orientations on the unit sphere does not exist. In order to be able to study the effect of discretizing the allowed orientations we give up part of the symmetry of the set, and this allows to connect continuous and discrete models. We apply this method not only to a one-component system of rods, but also to binary mixtures, which may be considered as the simplest polydisperse systems.

This Chapter is organized as follows. In Sec. 7.2 we derive the grand potential functional for a model with a discrete number of allowed rod orientations from the Onsager functional. We calculate bulk equations of state for specific orientational sets, and determine the number of orientations required to resemble the continuous Onsager solution. In Sec. 7.3 we apply the method to construct bulk phase diagrams of binary mixtures of thin and thick rods. We demonstrate that their structure can be modified significantly due to orientational discretization. A summary and some discussion of results will be presented in Sec. 7.4.

7.2 Monodisperse rods

Consider a fluid of hard rods of length L and diameter D ($L \gg D$) in a macroscopic volume V at temperature T and chemical potential μ. The "Onsager" grand potential functional $\Omega[\rho]$ of the one-particle distribution function $\rho(\hat{\omega})$ can be written, within second virial approximation, as [11]

$$\beta\Omega[\rho(\hat{\omega})] = \int d\hat{\omega}\rho(\hat{\omega})\Big(\ln[\rho(\hat{\omega})\nu] - 1 - \beta\mu\Big) + \frac{1}{2}\int d\hat{\omega}d\hat{\omega}' E(\hat{\omega},\hat{\omega}')\rho(\hat{\omega})\rho(\hat{\omega}'), \tag{7.1}$$

where $\beta = (k_B T)^{-1}$ is the inverse temperature, ν is the rod's thermal volume, and $E(\hat{\omega},\hat{\omega}')$ is the excluded volume of rods with orientations $\hat{\omega}$ and $\hat{\omega}'$. The function $\rho(\hat{\omega})$ is normalized as $n = \int d\hat{\omega}\rho(\hat{\omega})$, with n the bulk number density (which depends on $\beta\mu$). The minimum condition $\delta\Omega[\rho(\hat{\omega})]/\delta\rho(\hat{\omega}) = 0$ on the functional leads to the nonlinear integral equation

$$\ln[\rho(\hat{\omega})\nu] + \int d\hat{\omega}' E(\hat{\omega},\hat{\omega}')\rho(\hat{\omega}') = \beta\mu, \tag{7.2}$$

to be solved for the equilibrium distribution $\rho(\hat{\omega})$.

Models with a discrete number N of allowed rod orientations can be derived systematically from the continuous model (7.1) by dividing the unit sphere into solid sectors $\Delta\hat{\omega}_i, (i = 1,\ldots,N)$ around vectors $\hat{\omega}_i$, and fixing the rod density $\rho(\hat{\omega}) = \rho(\hat{\omega}_i)$ within each sector as well as the excluded volume $E(\hat{\omega},\hat{\omega}') = E(\hat{\omega}_i,\hat{\omega}_j)$ for every pair of sectors. The grand potential functional $\Omega[\rho_i]$ of such an "orientationally discretized" fluid with density distribution $\rho_i = \rho(\hat{\omega}_i)\Delta\hat{\omega}_i$ and the excluded volumes $E_{ij} = E(\hat{\omega}_i,\hat{\omega}_j)$ is

$$\beta\Omega[\rho_i] = \sum_{i=1}^{N}\rho_i\Big(\ln[\rho_i\nu] - 1 - \beta\mu\Big) + \frac{1}{2}\sum_{i,j=1}^{N}E_{ij}\rho_i\rho_j - \sum_{i=1}^{N}\rho_i\ln\Delta\hat{\omega}_i \tag{7.3}$$

with normalization $n = \sum_{i=1}^{N}\rho_i$ and $\Delta\hat{\omega}_i$ being the volume of the solid sector $\Delta\hat{\omega}_i$. The last term in Eq. (7.3) represents the contribution to the grand potential Ω due to the discretization procedure, i.e. it shows the intrinsic difference between continuous and discrete models. For a homogeneous distribution of vectors $\hat{\omega}_i$ on the unit sphere and $\Delta\hat{\omega}_i = \Delta\hat{\omega}$ (i.e. for the models with $N = 3, 6$ and 10 [64]), it trivially shifts the chemical potential $\beta\mu_d = \beta\mu + \ln\Delta\hat{\omega}$, which does not have any consequence for the solutions ρ_i at a fixed n, and for the thermodynamics of the isotropic-nematic transition. However, when $\Delta\hat{\omega}_i$ is not the same for all i, it acts as an external orientational field that tends to favor the larger sectors over the smaller ones. This becomes explicit if we consider the Euler-Lagrange equations that corresponds to the

discrete functional (or equivalently the analog of Eqs. (7.2))

$$\ln[\rho_i \nu] + \sum_{j=1}^{N} E_{ij}\rho_j = \beta\mu + \ln \Delta\hat{\omega}_i, \tag{7.4}$$

now to be solved for ρ_i. Note that the equation of state $p = p(n, T)$ does not pick up an additional term from the discretization,

$$\beta p = n + \frac{1}{2}\sum_{j=1}^{N} E_{ij}\rho_i\rho_j, \tag{7.5}$$

but the distributions ρ_i to be inserted into it *do* depend on the discretization.

Further discussion requires a specification of the set of allowed orientations $\hat{\omega}_i, i = 1, \ldots, N$ and the associated solid sectors $\Delta\hat{\omega}_i$. Unfortunately, it is impossible to cover a surface of the unit sphere completely by equal regular spherical M-polygons, where M indicates the number of polygon's sides (only 5 Platonic solids exist). But the symmetries of the function $\rho(\hat{\omega})$ can be explicitly included into the set of vectors $\hat{\omega}_i$ in order to simplify the problem. For the present study we fix the $\hat{z}$-axis of the coordinate system to be parallel to the nematic director $\hat{n}$ and assume uniaxial symmetry of the function $\rho(\hat{\omega}) = \rho(\theta)$, with $\theta = \arccos(\hat{\omega} \cdot \hat{n})$ the angle between $\hat{\omega}$ and $\hat{n}$. The azimuthal angle is denoted by ϕ, and hence we characterize a vector $\hat{\omega} = (\sin\theta\cos\phi, \sin\theta\sin\phi, \cos\theta)$ by the angles θ and ϕ. The "up-down" symmetry of the nematic phase reduces the orientational space to half the upper-hemisphere, i.e. $\theta \in [0, \pi/2]$ and $\phi \in [0, \pi]$. As we do not expect any azimuthal symmetry breaking we restrict attention to N_ϕ uniformly distributed values for ϕ for every allowed θ. We consider a uniform distribution of N_θ polar angles $\theta \in [0, \pi/2]$, i.e.

$$\begin{aligned}(\theta_k, \phi_l) &= \Big(\frac{\pi(k-1)}{2(N_\theta - 1)}, \frac{\pi(l-1)}{N_\phi - 1}\Big), \\ k &= 1, \ldots, N_\theta, \quad l = 1, \ldots, N_\phi,\end{aligned} \tag{7.6}$$

as well as a uniform distribution of N_θ values of $\cos\theta \in [0, 1]$, i.e.

$$\begin{aligned}(\theta_k, \phi_l) &= \Big(\arccos\Big[1 - \frac{k-1}{N_\theta - 1}\Big], \frac{\pi(l-1)}{N_\phi - 1}\Big). \\ k &= 1, \ldots, N_\theta, \quad l = 1, \ldots, N_\phi\end{aligned} \tag{7.7}$$

The solid sectors $\Delta\hat{\omega}_i$ are determined by bisecting the angles between the vector $\hat{\omega}_i$ and its nearest neighbors, and the corresponding volumes are given by $\Delta\hat{\omega}_i = \int_{\Delta\hat{\omega}_i} \sin\theta d\theta d\phi$, such that $\sum_i \Delta\hat{\omega}_i = 4\pi$.

Figure 7.1 shows the dimensionless pressure $p^* = \beta p L^2 D$ as a function of the dimensionless bulk density $n^* = nL^2D$ for the grid (7.6) with different N_θ and $N_\phi = 5$. The plateaux (of the solid lines) correspond to the isotropic-nematic coexistence,

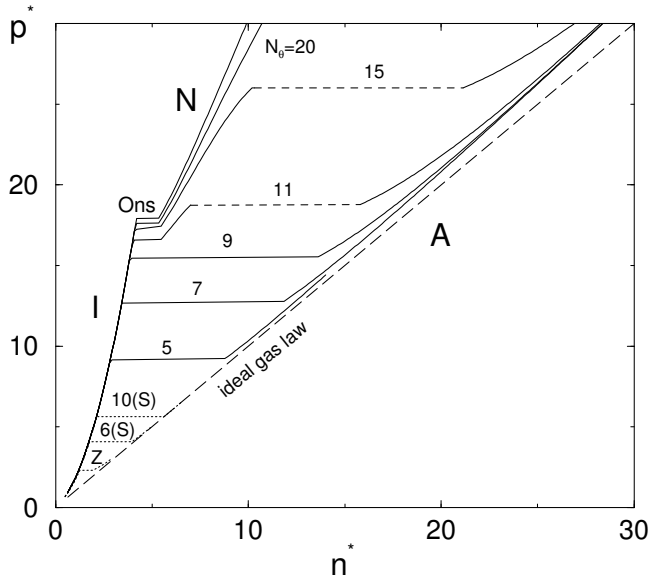

Figure 7.1: Equation of state for models with different number of allowed polar angles N_θ. Positions of the phase transitions are indicated by the horizontal lines. The continuous Onsager solution (Ons) can be reproduced in the present density interval with $N_\theta \geq 50$. The dotted lines correspond to equations of state for the Zwanzig (Z), dodecahedral (6S) and icosahedral (10S) models [64]. The dashed horizontal lines correspond to a spurious nematic-nematic ($N - A$) transition due to poor discretization of the allowed orientations.

obtained by equating pressure and chemical potential in the two phases. For $N_\theta \leq 9$ the transition occurs between the isotropic phase (I) and an (almost) perfectly aligned nematic phase (A) with pressure close to the the ideal gas pressure. Note that such grids correspond to a single θ within the "Onsager" opening angle, i.e. $0 \leq \theta_1 \leq \pi/18 < \theta_2$. As soon as $0 \leq \theta_1 < \theta_2 \leq \pi/18$, or $N_\theta > 9$, the distribution function $\rho(\theta)$ at isotropic-nematic coexistence starts to converge to the continuous solution. These results are in full agreement with the previous explanation of Straley [64]. Equations of state for the model (7.7) are very similar to Fig. 7.1 but start to resemble an Onsager-like distribution function for $N_\theta > 80$ due to the poor sampling of $\hat{\omega}_i$ near the nematic director. Equations of state for the Zwanzig ($N = 3$), dodecahedral ($N = 6$) and icosahedral ($N = 10$) models were calculated using the original formulations [64], and are included for comparison. Our results for $N_\theta \leq 9$ seem to converge well to these existing results.

For $N_\theta > 20$ the pressure of the high-density nematic phase clearly demonstrates a linear dependence on the bulk density, i.e. $\beta p(n) \sim n$. With increasing N_θ it gradually approaches a limiting scaling behavior $\beta p(n) = 3n$, established for the continuous Onsager solution by means of a scaling argument [49].

The discretization of the rod's allowed orientations shows the existence of an "artificial transition" from a less-ordered nematic phase (N) to a near-perfectly aligned phase (A) for $N_\theta > 9$, as indicated by the dashed horizontal lines in Fig. 7.1. It occurs due to the same competition between excluded volume and orientational entropy as in the IN transition, and puts an additional constraint on the description of the nematic bulk state by restricted-orientation models. Below we argue that it has important consequences for discrete models of (polydisperse) hard-rod mixtures, where separation into nematic phases with different composition occurs at sufficiently high densities.

7.3 Binary mixtures

Consider a binary mixture of thin (D_1) and thick (D_2) hard rods of equal length L and the diameter ratio $d = D_2/D_1 = 4$ in a macroscopic volume V at temperature T and chemical potentials μ_1 and μ_2, respectively. The "Onsager" grand potential functional for this system can be written as [33]

$$\beta\Omega[\{\rho_\sigma(\hat{\omega})\}] = \sum_{\sigma=1}^{2} \int d\hat{\omega}\rho_\sigma(\hat{\omega})\Big(\ln[\rho_\sigma(\hat{\omega})\nu] - 1 - \beta\mu_\sigma \Big) + \frac{1}{2} \sum_{\sigma,\sigma'=1}^{2} \int d\hat{\omega}d\hat{\omega}' E_{\sigma,\sigma'}(\hat{\omega};\hat{\omega}')\rho_\sigma(\hat{\omega})\rho_{\sigma'}(\hat{\omega}'), \tag{7.8}$$

with normalization $n_\sigma = \int d\hat{\omega}\rho_\sigma(\hat{\omega})$. It is known from previous Chapters and Refs. [40,52,57] that the bulk phase diagram of this system exhibits (i) strong fractionation at isotropic-nematic ($I - N_2$) coexistence, (ii) nematic-nematic ($N_1 - N_2$) coexistence ending in a consolute N_1N_2 point at sufficiently high pressure, and (iii) an IN_1N_2 triple point. The discrete version of this model follows directly from (7.3) as

$$\beta\Omega[\{\rho_{\sigma i}\}] = \sum_{\sigma=1}^{2}\sum_{i=1}^{N} \rho_{\sigma i}\Big(\ln[\rho_{\sigma i}\nu_\sigma] - 1 - \beta\mu_\sigma \Big) + \frac{1}{2} \sum_{\sigma\sigma'=1}^{2}\sum_{i,j=1}^{N} E_{\sigma i;\sigma' j}\rho_{\sigma i}\rho_{\sigma' j} - \sum_{\sigma=1}^{2}\sum_{i=1}^{N} \rho_{\sigma i} \ln \Delta\hat{\omega}_i \tag{7.9}$$

with the densities $\rho_{\sigma i} = \rho_\sigma(\hat{\omega}_i)\Delta\hat{\omega}_i$, the excluded volumes $E_{\sigma i;\sigma' j} = E_{\sigma\sigma'}(\hat{\omega}_i, \hat{\omega}_j)$ and the normalization of number densities $n_\sigma = \sum_{i=1}^{N} \rho_{\sigma i}$.

Figure 7.2 shows the phase diagrams for discrete systems in the $p^* - x$ representation with the dimensionless pressure $p^* = \beta p L^2 D_1$ and the mole fraction of thick rods $x = n_2/(n_1 + n_2)$, for several orientational grids (7.6) with $N_\theta = 11$ (a), 20 (b), 30 (c), 50 (d) and $N_\phi = 10$. Note that all four discretizations are such that they reproduce the physical "Onsager"-like $I - N$ transition at $x = 0$ and $x = 1$, at pressures $p^* \approx 17.7$ and 4.4, respectively. However, the existence of the artificial aligned

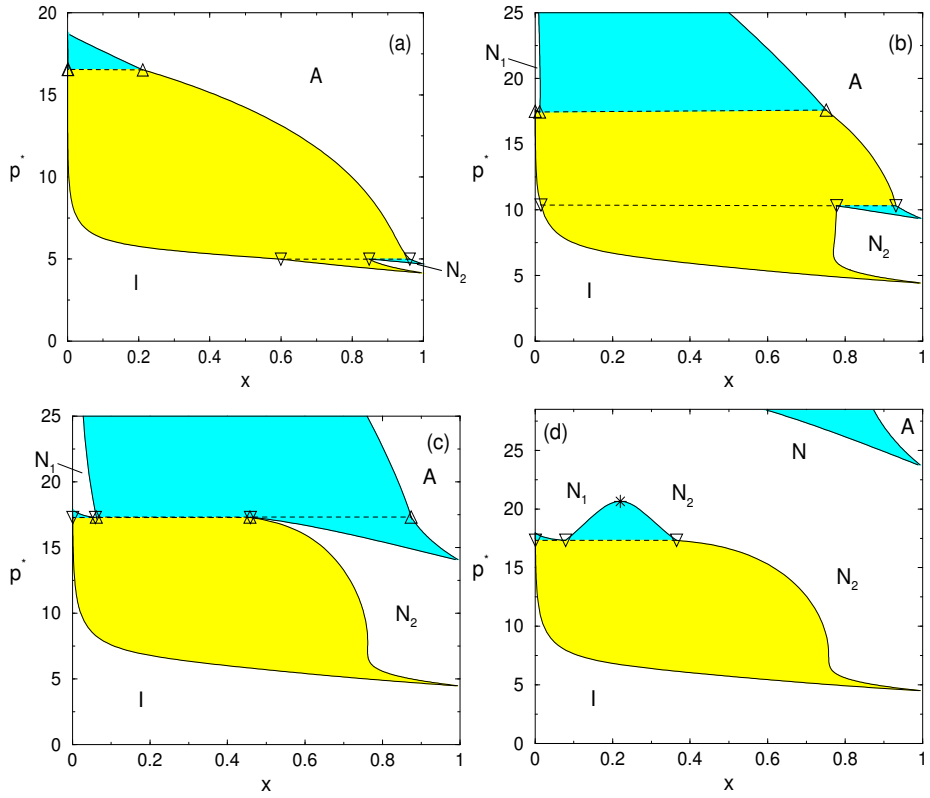

Figure 7.2: Bulk phase diagrams of a binary thin-thick mixture of hard rods (diameter ratio $D_2/D_1 = 4.0$, equal length $L \gg D_2$), in the pressure-composition representation, with p^* the dimensionless pressure and x the mole fraction of the thicker rods. We distinguish the low-pressure isotropic phase (I), high-pressure nematic phases (N_1 and N_2), aligned phase A, upper ($\triangle$) and lower (∇) triple phase coexistence and an $N_1 - N_2$ critical point ($*$). The grey regions, enclosed by the binodals, denote the two-phase regimes, and the tie lines that connect coexisting phases, are horizontal.

nematic phase A gives rise to spurious $I - A$, $N_1 - A$ and $N_2 - A$ phase equilibria, where I, N_1 and N_2 are the physical isotropic and nematic phases. (For the coarsest discretization with $N_\theta = 11$ (Fig. 7.2(a)) the N_1 phase is stable in a very narrow region beyond the resolution of the picture.) Upon refining the discretization from $N_\theta = 11$ the IN_2A triple point (∇) shifts to higher pressures, and combines with the IN_1A triple point ($\triangle$) at $N_\theta = 30$ (Fig. 7.2(c)) to form the physical IN_1N_2 triple point (now denoted by ∇) and an artificial N_1N_2A triple point ($\triangle$) at slightly higher pressure. Further grid refinements to $N_\theta = 50$ yields the physical phase diagram with an IN_1N_2 triple point and N_1N_2 consolute point as in Ref. [40], but with a spurious

$N - A$ coexistence at pressures beyond the "physical" part of the phase diagram. At these pressures one does not distinguish N_1 and N_2 nematic phases, but the single nematic phase denoted by N here.

7.4 Summary and discussion

We have explored the connections between continuous and restricted orientation models of monodisperse and binary hard-rod fluids (in the Onsager "needle" limit $L \gg D$). The main finding is that a discretization of the orientations leads to the existence of a nonphysical almost perfectly aligned nematic phase (A) at high densities. If the discretization is coarse, i.e., the number of allowed orientations is small, then the A phase can coexist with the isotropic phase (I), and at sufficiently fine discretization with the nematic phase N. We also found that the continuum limit requires a finer orientation grid for a mixture than the one-component fluid.

In order to reduce the number of discrete orientations in binary mixtures, we have explored several models with a nonuniform discretization of the angular space. In particular, the physical phase diagram of binary mixtures of thin and thick rods with $d = 4.0$ can be reproduced with $N_\theta = 30$ if $2N_\theta/3$ points are uniformly distributed in the interval $[0, \pi/4]$ and the remaining $N_\theta/3$ points in $[\pi/4, \pi/2]$. Note that this does not remove the conceptual problem, it rather shifts the problem to identifying correlations between the structure of the phase diagram and the employed numerical grids. However, this procedure can be tedious, e.g. for interfacial problems or highly polydisperse fluids, since studying these correlations involves the calculation of complete phase diagrams. Nevertheless we used and checked this scheme ourselves in studies of free planar interfaces of binary hard-rod mixtures in the Chapters 3, 4 and Refs. [52, 57].

Clearly, the results are strongly influenced by the adopted limit $L \gg D$, but we would expect similar effects, although weaker, for a finite L/D ratio. An additional interesting issue concerns the importance of all virial coefficients in the Zwanzig model, even in the Onsager limit $L \gg D$. As the second virial theory is exact for freely rotating needles [11], one can try to relate an increase in the number of virial coefficients necessary to recover the Onsager limit to the decrease of the number of allowed orientations. This issue requires studies of models with higher order virial coefficients, which are far from trivial and beyond the scope of this work.

The findings of the present Chapter could be relevant for the study of inhomogeneous and/or polydisperse fluids of rods, which are computationally more demanding and hence impose the use of a rather coarse grid of orientations in order to be tractable and practical. It shows that care must be taken with such rather coarse grids, since they can give rise to an artificial, discretization-induced aligned nematic phase.

Bibliography

[1] C. Wetter, "Die Flussigkristalle des Tabakmosaikvirus", Biologie in unserer Zeit **3**, 81 (1985).

[2] A. Galindo et al., J. Chem. Phys. **119**, 5216 (2003).

[3] P.G. de Gennes, J. Prost, *The Physics of Liquid Crystals*, Clarendon Press, Oxford, 1993.

[4] S. Chandrasekhar, *Liquid Crystals*, Cambridge Univ. Press, Cambridge, 1977, 1992.

[5] G.R. Luckhurst, G.W. Gray (Eds.), *The Molecular Physics of Liquid Crystals*, Academic Press, New York, 1979.

[6] P.J. Collings, J.S. Patel (Eds.), *Handbook of Liquid Crystal Research*, Oxford Univ. Press, Oxford, 1997.

[7] G. Friedel, Ann. Phys. **18**, 273 (1922).

[8] L.J. Yu, A. Saupe, Phys. Rev. Lett. **45**, 1000 (1980).

[9] S. Singh, Phys. Rep. **324**, 107, 2000.

[10] F.C. Bawden, N.W. Pirie, J.D. Bernal, and I. Fankuchen, Nature **138**, 1051 (1936).

[11] L. Onsager, Ann. N.Y. Acad. Sci. **51**, (1949) 627 .

[12] J.P. Hansen and I.R. McDonald, *Theory of Simple Liquids*, Acad. Press, London, 1986.

[13] B. Jérôme, Rep. Prog. Phys. **54**, 391 (1991).

[14] M. Schick, in *Liquids at Interfaces*, edited by J. Charvolin et al. (Elsevier, Amsterdam, 1990), p. 415.

[15] H.B. Callen, *Thermodynamics : an introduction to the physical theories of equilibrium thermostatics and irreversible thermodynamics*, Wiley, New York, 1975.

[16] R. van Roij, *"Soft Condensed Matter"*, Lecture notes, Utrecht University, 2001.

[17] B. Mulder, *"Density Functional Theory"*, Lecture notes.

[18] R. Evans, in *Liquids at Interfaces*, edited by J. Charvolin et al. (Elsevier, Amsterdam, 1990), p. 4.

[19] J.P. Straley, Mol. Cryst. Liq. Cryst. **24**, 7 (1973).

[20] D. Frenkel, J. Phys. Chem. **91**, 4912 (1988).

[21] Th. Odijk and H.N.W. Lekkerkerker, J. Phys. Chem. **89**, 1272 (1985).

[22] H.N.W. Lekkerkerker, Ph. Coulon, R. Van Der Haegen, and R. Deblieck, J. Chem. Phys. **80**, 3427 (1984).

[23] R. van Roij and B. Mulder, J. Chem. Phys. **105**, 11237 (1996); **109**, 1584 (1998).

[24] R. Holyst and A. Poniewierski, Phys. Rev. A **38**, 1527 (1988).

[25] B.G. Moore and W.E. McMullen, Phys. Rev. A **42**, 6042 (1990).

[26] Z.Y. Chen and J. Noolandi, Phys. Rev. A **45**, 2389 (1992).

[27] Z.Y. Chen, Phys. Rev. E **47**, 3765 (1993).

[28] D.L. Koch and O.G. Harlen, Macromolecules **32**, 219 (1999).

[29] M. Allen, J. Chem. Phys. **112**, 5447 (2000).

[30] R. van Roij, M. Dijkstra, and R. Evans, J. Chem. Phys. **113** 7689 (2000).

[31] M.S. Al-Barwani and M.P. Allen, Phys. Rev. E **62**, 6706 (2000).

[32] A.J. McDonald, M.P. Allen, and F. Schmid, Phys. Rev. E **63**, 010701 (2001).

[33] G.J. Vroege and H.N.W. Lekkerkerker, Rep. Prog. Phys. **55**, (1992) 1241.

[34] A. Poniewierski and R. Holyst, Phys. Rev. A **38**, 3721 (1988).

[35] R. Evans, R.J.F. Leote de Carvalho, J.R. Henderson, and D.C. Hoyle, J. Chem. Phys. **100**, 591 (1994).

[36] T.M. Birshtein, B.I. Kolegov, and V.A. Pryamitsyn, Polym. Sc. U.S.S.R **30**, 316 (1988).

[37] G.J. Vroege and H.N.W. Lekkerkerker, J. Phys. Chem. **97**, 3601 (1993).

[38] R. van Roij and B. Mulder, Phys. Rev. E **54**, 6430 (1996).

[39] M. Dijkstra and R. van Roij, Phys. Rev. E **56**, 5594 (1997).

[40] R. van Roij, B. Mulder and M. Dijkstra, Physica A **261**, 374 (1998).

[41] R. Sear and G. Jackson, J. Chem. Phys. **103**, 8684 (1995).

[42] P.C. Hemmer. Mol. Phys. **96**, 1153 (1999).

[43] K. Purdy and S. Fraden, private communication.

[44] K. Shundyak and R. van Roij, J. Phys.: Condens. Matter **13**, 4789 (2001).

[45] R. Evans, Adv. Phys. **28**, 143 (1979).

[46] S. Fraden, in *Observation, Prediction and Simulation of Phase Transitions in Complex Fluids*, edited by M. Baus *et al.* (Kluwer, Dordrecht, 1995), p. 113.

[47] W. Chen and D.G. Gray, Langmuir **18**, 633 (2002).

[48] P. Sollich, J. Phys.: Condens. Matter **14** R79 (2002).

[49] R. van Roij and B. Mulder, Europhys. Lett. **34**, 201 (1996).

[50] Z. Dogic and S. Fraden, Phil. Trans. R. Soc. Lond. A **359**, 997 (2001).

[51] see the web-page of K.Purdy, http://people.brandeis.edu/ krp/future.html

[52] K. Shundyak and R. van Roij, Phys. Rev. E **68**, 061703 (2003).

[53] A. Stroobants, H.N.W. Lekkerkerker, and Th. Odijk, Macromolecules **19**, 2232 (1986).

[54] M. Muthukumar and J.-S. Ho, Macromolecules, **22**, 965 (1989).

[55] H. Menzel. In J.C. Salamone, editor, *Polymer Materials Encyclopedia*, p. 2916. CRC Press, Boca Raton, FL, 1996.

[56] A.N. Semenov and A.R. Kokhlov, Sov. Phys. Usp. **31**, 988 (1988).

[57] K. Shundyak and R. van Roij, Phys. Rev. Lett. **88**, 205501 (2002).

[58] M. Dijkstra, R. van Roij, and R. Evans, Phys. Rev. E **63**, 051703 (2001).

[59] M.P. Allen, Mol. Phys. **96**, 1391 (1999).

[60] D. de las Heras, L. Menderos and E. Velasco, Phys. Rev. E **68**, 031709 (2003).

[61] R. Zwanzig, J. Chem. Phys. **39**, 1714 (1963).

[62] R. van Roij, M. Dijkstra and R. Evans, Europhys. Lett. **49**, 350 (2000).

[63] K. Shundyak and R. van Roij, accepted for PRE and cond-mat/0311505.

[64] J.P. Straley, J. Chem. Phys. **57**, 3694 (1972).

[65] L. Harnau and S. Dietrich Phys. Rev. E **65**, 021505 (2002).

[66] N. Clarke, J.A. Cuesta, R. Sear, P. Sollich and A. Speranza, J. Chem. Phys. **113**, 5817 (2000).

[67] Y. Martinez-Raton and J.A. Cuesta, J. Chem. Phys. **118**, 10164 (2003).

Samenvatting

Een van de meest gebruikte klassificaties voor materie is de indeling in drie verschillende toestanden: vast, met vaste vorm en inhoud; vloeibaar, met vast volume, maar met de vorm van het vat; gasvormig, zonder vaste vorm of volume. Ondanks het grove karakter geeft deze klassificatie de fundamentele symmetrieën aan en karakteriseert ze de structuur van die toestanden op atomair niveau: Ordening op korte en lange afstanden is typisch voor kristallen, terwijl het ontbreken van orde op lange afstanden in combinatie met een quasi-kristallijne ordening op korte afstanden typisch is voor vloeistoffen. Een vrijwel ongecorreleerde structuur karakteriseert gassen. Het idee om met behulp van symmetrieën verschillende toestanden van materie te onderscheiden staat centraal in de moderne fysica.

Specifieke symmetrieën kunnen worden geassocieerd met de verdeling van de posities van atomen of moleculen, maar ook met orientaties van magnetische momenten in magneten, met de lading van aangeslagen toestanden in halfgeleiders, met eigenschappen van golffuncties van electronen in supergeleiders, etc. In dit proefschrift beschouwen we eigenschappen van materialen waarvan de bouwstenen anisotrope staafachtige objecten zijn. De symmetieën van de toestanden worden vastgelegd door de verdeling van de posities en de orientaties van de deeltjes. Behalve de gebruikelijke gas-, vloeistof- en kristalfasen, blijken deze materialen een heel scala aan toestanden te hebben met verschillende orientatie- en/of gedeeltelijke positieordening. Deze toestanden worden mesofasen (mesomorfe of mesogene fasen) genoemd, of *vloeibaar kristallijn*.

Vloeibare kristallen (Eng: 'Liquid crystals' (LC's)) zijn een soort tussentoestand tussen de volledig ongeordende vloeistof en het volledig geordende kristal. De symmetrieën van de mesofasen kunnen worden geklassificeerd aan de hand van rotatie- en translatievrijheidsgraden. Volgens de nomenclatuur die oorspronkelijk werd voorgesteld door Friedel [7] kunnen de vloeibaar kristallijne fasen van staafachtige moleculen verdeeld worden in twee verschillende types: nematisch en smectisch. De nematische fase is de eenvoudigste fase, waarin de moleculen (gemiddeld) een goed gedefinieerde orientatie hebben, maar geen ordening in posities op lange afstanden. Er bestaat een aantal nematische fasen. Hoewel een isotrope vloeistof (I) plaats- en rotatiesymmetrie heeft, $T(3) \times O(3)$, wordt de rotatiesymmetrie gebroken bij de overgang van de isotrope vloeistof naar de nematische fase (N). In het eenvoudigste geval wordt de

groep $O(3)$ vervangen door een van de uniaxiale symmetriegroepen, D_∞ of $D_{\infty h}$. De nieuwe fase wordt dan de uniaxiale nematische fase genoemd. De gemiddelde orientatie van de moleculen kan worden weergegeven door een eenheidsvector, $\hat{n}$, die de *director* wordt genoemd. Een andere nematische fase, die biaxiaal wordt genoemd, kan zich voordoen als de rotatiesymmetrie van het systeem verder wordt gebroken rond de director $\hat{n}$. Alle bekende biaxiale nematische fasen zijn hetzij mengsels van staaf- of plaatachtige moleculen, hetzij systemen van latvormige deeltjes [8, 9]. Voor de volledigheid beschrijven we hier kort de smectische fase, die gekarakteriseerd wordt door een gelaagde structuur, waarin staafjes in een laag wel orientatie- ordening maar geen positie-ordening vertonen. Voor een uitgebreide klassificatie wordt de geinteresseerde lezer verwezen naar de literatuur [3–6].

De interactie tussen de deeltjes bepaalt de stabiliteit van een vloeibaar kristallijne fase tegen destructieve thermische fluctuaties. Men kan speculeren dat aantrekkende krachten nodig zijn om de ordening op lange afstand, die wordt geobserveerd in nematische en smectische LC's, te behouden. Het blijkt echter dat eigenschappen van sommige mesogene materialen kunnen worden begrepen aan de hand van zuiver afstotende interacties. Suspensies van colloïdale staafachtige deeltjes zijn een voorbeeld van zulke systemen. De eerste experimenten aan zulke systemen zijn gedaan door Bawden, die in 1936 als eerste de overgang tussen isotrope en nematische fasen waarnam in een suspensie van het tobacco mosaic virus (TMV) [10]. De theoretische onderbouwing werd gegeven door Onsager [11], die, uitgaand van een modelvloeistof bestaand uit harde naalden, in staat was om de IN overgang te verklaren aan de hand van een competitie tussen orientatie- en pakkingsentropie, i. e. door middel van een zuiver entropisch mechanisme. In de jaren 1980 bleek uit computer simulaties, en later ook uit theorieën en experimenten (aan TMV suspensies), dat de aanwezigheid van een afstotende interactie met korte dracht tussen staafachtige deeltjes ook verantwoordelijk kan zijn voor de vorming van een smectische fase. Een vergelijkbaar fenomeen doet zich voor in eenvoudige vloeistoffen, waar de structuur grotendeels wordt bepaald door zuiver afstotende interacties [12]. Vanwege de molecuulstructuur en interacties is in het geval van vloeibare kristallen met een lage moleculaire massa de situatie veel gecompliceerder, maar onderzoek aan vloeistoffen bestaand uit harde staven biedt een unieke mogelijkheid om de rol van afstotende interacties in het ontstaan van 'liquid crystal' ordening te kwantificeren.

In veel practische situaties wordt de thermodynamische toestand van een systeem niet alleen bepaald door de thermodynamische variabelen van de bulk, maar ook door de opgelegde randvoorwaarden. In mesogene meterialen kan een aantal belangrijke grensvlakeffecten worden onderscheiden [13]. De interactie van vloeibaar kristallijne deeltjes met een substraat of een grensvlak leidt tot de vorming van een grenslaag met een dikte ξ en een ordening die anders is dan die van de bulk. Als het systeem niet in de buurt van een bulk faseovergang is, is ξ van de orde van een paar molecuullengtes. Maar zodra het systeem in de buurt van een overgang komt, kan zo'n laag een film worden (met een dikte veel groter dan ξ) van een andere (nog metastabiele) bulkfase. Net als bij bevochtiging in andere systemen kan bij nadering tot coexistentie een

onderscheid gemaakt worden tussen volledige of gedeeltelijke bevochtiging, en bij coexistentie tussen kritieke of eerste-orde bevochtiging [14].

In dit proefschrift worden vragen beantwoord over ordening aan grensvlakken in systemen bestaande uit harde staven bij coexistentie van de isotrope en nematische fasen en hun ordening aan simpele modelsubstraten. De indeling is als volgt.

Hoofdstuk 2 geeft wat achtergrond informatie over de relatie tussen statistisch mechanische en thermodynamische beschrijvingen van bulksystemen van harde staven, als mede een introductie tot het asymptotisch exacte Onsager model.

In hoofdstuk 3 wordt onderzoek beschreven aan het eenvoudigste vrije IN grensvlak in een systeem van monodisperse harde Onsager staven. De analyse van dit systeem leidt tot de ontwikkeling van een effectieve methode om de een-deeltjes verdelingsfunctie te bepalen in een inhomogeen systeem.

De beschrijving van onderzoek aan de vrije grenslagen tussen de isotrope en nematische fasen wordt voortgezet in hoofdstuk 4, waar ze worden beschouwd in tweecomponentige mengsels van harde staven. Voor voldoend verschillende vormen van de deeltjes bevat het bulkfasendiagram een tripel punt, waar een isotrope(I) fase bestaat naast twee nematische fasen (N_1 en N_2) met verschillende samenstelling. Voor alle onderzochte mengsels vinden we dat bij nadering tot het tripel punt komplete bevochtiging optreedt van het IN_2 grensvlak door een tussenliggende N_1 film. We berekenen de oppervlaktespanning van het grensvlak tussen de isotrope en nematische fasen en vinden een verrassende toename met het compositieverschil tussen de twee coexisterende fasen.

Deze studies worden aangevuld met een analyse van het bulk- fasengedrag en de grens-vlakeigenschappen van niet-additieve binaire mengsels van dunne en dikke harde staven. De formulering van dit model is gebaseerd op recente experimenten in de groep van Fraden, die het fasengedrag van een mengsel van virusdeeltjes met verschillende diameters heeft onderzocht. In ons model hebben deeltjes van hetzelfde type onderling een harde, afstotende potentiaal, maar is het uitgesloten volume voor verschillende deeltjes groter (kleiner) dan dat van een additief mengsel. Deze niet-additieve eigenschap doet de fractionering toenemen (afnemen) bij coexistentie tussen de isotrope en nematische fasen (IN) en kan ontmenging veroorzaken (tegengaan) van een nematische fase met een hoge dichtheid naar twee nematische fasen met veschillende samenstelling (N_1 en N_2). Analyse van de grensvlakken geeft aan dat aan het IN grensvlak de oppervlaktespanning toeneemt met de fractionering en dat, bij nadering van tripel punt coexistentie, komplete bevochtiging van het IN_2 grensvlak door de N_1 fase optreedt. In alle gevallen is er een grote overeenkomst tussen de bulk- en grensvlakeigenschappen van de niet-additieve mengsels en de additieve mengsels met een grotere verhouding tussen de diameters.

In hoofdstuk 6 beschouwen we de eigenschappen van een monodisperse vloeistof bestaande uit harde staven in contact met een enkele wand (W). Studies van de grensvlakeigenschappen van vloeistoffen van Onsager harde staven stellen ons voor grote numerieke problemen. Daarom beschouwen we een eenvoudigere modelvloeistof bestaande uit harde staven met een beperkt aantal toegestane orientaties. Binnen dit

zgn. Zwanzig model onderzoeken we de thermodynamische eigenschappen van een vloeistof bestaande uit monodisperse harde staven in contact met een modelsubstraat dat wordt beschreven als een harde wand met een aanvullende zachte (exponetieel vervallende) afstotende of aantrekkende potentiaal. De aantrekking doet de ordening van de orientatie toenemen in de buurt van de wand in zowel de isotrope als de nematische fase, en reduceert de chemische potentialen van de overgang van uniaxiale (U) naar biaxiale (B) symmetrie in de oppervlakte laag. Daarentegen blijven de bevochtigings- eigenschappen van het substraat vergelijkbaar met die van een harde wand. De zachte afstoting vermindert de dichtheid in de grensvlaklaag, wat een verandering, of zelfs afwezigheid van de UB overgang tot gevolg heeft, als mede sterke verandering van de bevochtigingseigenschappen. Bij het WI grensvlak vindt men bij voldoend grote afstoting altijd een bevochtigingsovergang. Bij het WN grensvlak treedt daarenten een 'drying' overgang op bij voldoend lange dracht van de repulsie.

In hoofdstuk 7 bekijken we sommige beperkingen van modellen van vloeistoffen van harde staven met een eindig aantal toegestane orientaties. Met behulp van Onsager's tweede viriaaltheorie construeren we bulk-fasendiagrammen. Voor een systeem van identieke staafjes laten we zien dat de discretisatie van de orientatie het ontstaan van een kunstmatige, (bijna) perfect parrallele nematische fase tot gevolg heeft, die coexisteert naast de (fysische) nematische fase als het aantal toegestane orientaties voldoende groot is, of naast de isotrope fase als het aantal orientaties klein is. Voor binaire mengsels bestaat deze kunstmatige fase ook en is een veel groter aantal toegestane orientaties nodig om deze fase naar zulke hoge dichtheden te verschuiven dat het fysische gedeelte van het fasendiagram niet verstoord wordt.

Acknowledgements

It is a difficult task to acknowledge all people who influenced my life during the last four years and contributed, in different ways, to this thesis. I am very grateful to all my friends and colleagues, however, I would like to add some personal words.

I would like to express my sincere gratitude to my thesis advisor Dr. René van Roij. His energy and clear way of thinking were the driving force for me at all stages of research. I have learned from him how to listen quietly to any naive idea, and then probe it with few precise questions. He patiently accepted my excursions into different branches of physics, and always returned me back with the slogan "the work is finished, published". He read every chapter of this thesis a number of times, which finally transformed it from a hardly understandable draft to a readable thesis.

To many sides of scientific life I have been introduced by my promotor Prof.Dr. Matthieu Ernst. His permanent interest to new ideas in physics, and inexhaustible energy in solving various physical problems will certainly stay as one of very good examples for me in the future. I would like to thank him for all his hospitality and help, and it was a pleasure for me to share some of my computer knowledge with him.

I cannot forget to acknowledge my first scientific advisor and teacher Prof.Dr. V.M. Adamyan, who strongly encouraged me to deepen my scientific education. I hope to appreciate his kind support and wise advices in the future.

Discussions with many people led to improvements in this thesis. I am very grateful for their patience and stimulating suggestions, especially to Prof.Dr. Joseph Straley, Prof.Dr. Robert Evans, Prof.Dr. Seth Fraden, Prof.Dr. Henk Lekkerkerker, Prof.Dr. Jan Dhont, Prof.Dr. Bela Mulder, Dr. Paul van der Schoot, Dr. Marjolein Dijkstra, Dr. Gerard Barkema, Dr. Matthias Schmidt, Drs. Kirstin Purdy, Drs. Svyatoslav Savenko, and many others. And I strongly acknowledge Drs. Astrid de Wijn for the dutch translation of the samenvatting.

I am very thankful to Prof.Dr. Wim van Saarloos whose brilliant lectures on pattern formation phenomena had inspired me to go into field of non-equilibrium physics, and who kindly supported my interests in physics of granular matter. Wim helped me to crystalize ideas in terms of a research proposal, and I have deeply appreciated all his suggestions and knowledgable comments.

During these years I have enjoyed scientific discussions with many friends. I am particularly grateful to Prof.Dr. Ricardo Brito, Dr. Jun'ichi Wakou, Dr. Enrico Car-

lon, Dr. Usama Al Khawaja, Dr. Fei Zhou, Dr. Boris Fine, Dr. Vladimir Shevchenko, Dr. Behnam Farid, Dr. André Zvelindovsky, Dr. Patrick Warren, Dr. Paddy Royal, Dr. Bastian Wemmenhove, Dr. Jacco Snoeijer, Dr. Alexander Morozov, and many others.

Life beyond physics in Holland was pretty new (and sometimes complicated) for me. I am very grateful to Liesje Ernst for her help and care in various matters. With many other friends I had the privilege to enjoy the warm and beautiful atmosphere of her house. She introduced me to Jan and Annie Vissers, to whom I am also very indebted for their kind support and help.

I wish to acknowledge kind assistance of Leonie Silkens, who guided me through myriads of administrative papers and questions. I am also very indebted to Biene Meijerman, Geertje Speelman, and Wilma van Egmond, whose precision and sure charm often transformed the difficult problems into simple answers.

I would like to thank the people from the FOM personel department. Their assistance was always effective and timely, I doubt I could solve my numerous problems with foreign police and housing without them.

I am very grateful to all my friends from the Institute for Theoretical Physics, namely Zoltan, Hans, Kevin, Joanna, Marijn, Stefan, Mathijs, Willem, Dennis, Jean Maria, Michiel, Mathijs, Jeroen, Bas, Jani, Masud, Jens, Richard, Rembert, all of you.

Special thanks should also go to my numerous russian friends for being with us all these years: families Gilevich, Ovsyanko, Znamenskikh, Fine, Stepanyan, Ivanovikh, Savenko.

I am very grateful to Helena Petrenko for her permanent support and help in all situations. My world outlook would certainly be very different without her.

I wish to express my deep gratitude to my parents-in-law, Galina Vasiljevna and Yurij Nikolaevich for their help, kind support and everyday interests to our life. And I thanks my father Yevgenij Semenovich for his convinced and constant encouraging to experience new frontiers, and my mother Vera Grigorjevna for her love and putting aside her wishes to joy of mine.

Finally, I would like to thank my wife, Lyudmyla, and son Yury for their love.

Curriculum Vitae

The author of this thesis was born on March 14, 1974 in Odessa, Ukraine. In 1991 he obtained a high school degree (summa cum laude) in Moscow Suvorov Military School, and entered the Faculty of Physics and Astronomy of Odessa State University (OSU). He combined the undergraduate studies with teaching activities for talented high-school students in Odessa Richelieu Lyceum in 1992-1995. In 1996 he was graduated (summa cum laude) from the Department of Theoretical Physics, OSU with diploma work "Quantum scattering on graphs" under guidance of Prof.Dr. V.M. Adamyan. This work had been continued in 1996-1999 under the research project "Quantum scattering on graphs and physics of nanostructures" at the Department of Theoretical Physics, OSU. During this time author also worked as a freelance IT consultant, and he became an IT staff member of the British Embassy in 1999. However, his love for physics (strongly supported by Prof. Adamyan) turned out to be stronger then other interests, and in 2000 he joined Institute for Theoretical Physics, Utrecht University, where he started to work on this PhD project under guidance of Dr. R. van Roij. The author was happy to provide class assistance in courses on "Critical phenomena" with Prof.Dr. H. Knops, "Conformal field theory" with Prof.Dr. J. Ambjorn, and "Thermal Physics" with Dr. M. Dijkstra.